
**Addis Ababa University**
**Addis Ababa Institute of Technology**
**School of Electrical and Computer Engineering**
**Communication Engineering Graduate Program**

---

# Enhancing Spectrum Prediction and Awareness with Deep Learning Approaches

---

*by*

**Bethelhem Seifu Shawel**

A dissertation submitted to the School of Electrical and Computer Engineering in partial fulfillment of the requirements for the degree of **Doctor of Philosophy**

in

Communication Engineering

**Date:** May, 2024

**Addis Ababa University**
**Addis Ababa Institute of Technology**
**School of Electrical and Communication Engineering**
**Communication Engineering Graduate Program**

# Enhancing Spectrum Prediction and Awareness with Deep Learning Approaches

*by*

**Bethelhem Seifu Shawel**

## Approval by Board of Examiners:

| | | |
|---|---|---|
| Chairman, School Graduate Committee | Signature | Date |
| **Dr. -Ing. Dereje Hailemariam**<br>Advisor | Signature | Date |
| **Prof. Sofie Pollin**<br>Advisor | Signature | Date |
| **Dr. Fitsum Assamnew**<br>Internal Examiner | Signature | Date |
| **Dr. Fikreselam Gared**<br>External Examiner | Signature | Date |

# Declaration

I hereby declare that dissertation represents solely my original work and does not incorporate any material from other educational institutions without proper acknowledgement. To the best of my knowledge, it does not contain previously published material by another person without recognition.

**Bethelhem Seifu Shawel**

Signature _____ Date _____

This thesis has been formally submitted for examination under my supervision and endorsement as a university advisor.

## Supervisors

**Dr. -Ing. Dereje Hailemariam**
School of Electrical and Computer Engineering
Addis Ababa Institute of Technology,
Addis Ababa University
Ethiopia

Signature _____ Date _____

**Prof. Sofie Pollin**
Department of Electrical Engineering,
Katholieke Universiteit Leuven
Belgium

Signature _____ Date _____

Addis Ababa, Ethiopia

# Abstract

The growing demand for ubiquitous connectivity and real-time applications has placed significant strain on the finite radio spectrum, making efficient utilization crucial. To address this, static allocation methods must be replaced with real-time spectrum management that ensures optimal sharing, utilization, and management of spectrum bands among multiple users. By building comprehensive Spectrum Awareness (SA) through continuous monitoring and situational understanding of the radio environment and network conditions, and by intelligently predicting spectrum availability and usage through accurate Spectrum Prediction (SP), new opportunities for wireless services can be unlocked, paving the way for the next generation of connected technologies.

In that regard, this PhD thesis aims to enhance SP and SA tasks using Deep Learning (DL) techniques, addressing three primary challenges: achieving accurate long-term spectrum predictions with limited data, understanding spectrum usage across multiple dimensions, and developing robust prediction models to improve accuracy. These challenges are tackled across three network perspectives: Cognitive Radio Networks (CRNs), Mobile Network Operators (MNOs), and Unmanned Aerial Vehicle (UAVs)-assisted networks.

First, long-term spectrum predictability and multi-dimensional analysis are explored for CRNs using a distance-dependent central data fusion center and predictors based on Long Short-Term Memory (LSTM) and Convolutional Long Short-Term Memory (ConvLSTM) networks. These models analyze temporal and spatial dependencies to generate single- and multi-location interpolated spectrum data. Evaluation of prediction performance showed, LSTM models performing best for lower-frequency bands with deterministic Primary Users (PU) patterns, achieving an improvement by 9.7% over the baseline model and a prediction error below 5 dBm for 2.5 hours, using only 75 minutes of past monitoring data. Conversely, ConvLSTM models excel at higher-frequency bands by processing interpolated spectrum maps, yielding approximately a 14% improvement in prediction accuracy. With limited PU knowledge and sparse sensor deployment, increasing the cooperative region provides minimal accuracy gains, with a maximum error probability reduction by 0.15 at 1500 meters coverage radius.

Second, the SP problem for MNOs is tackled using voice and data traffic from Global System for Mobile (GSM) and Long-Term Evolution (LTE) networks as proxies for spectrum utilization. By mapping traffic data to channel utilization and employing DL-based models, spectrum utilization was predicted accurately without direct monitoring. Voice traffic, with its deterministic nature, allowed for pre-mapping before prediction, while LTE data traffic required a post-prediction mapping approach to prevent error propagation. For this prediction task, different DL models based on Convolutional Neural Networks (CNNs) and LSTM were proposed, and their prediction accuracy was assessed using Root Mean Squared Error (RMSE) and Mean Absolute Error (MAE)

at cluster and base station levels. Results revealed that the CNN model excelled in predicting voice channel utilization, improving performance by 26.9% at the cluster level and 36% at the base station level due to its ability to capture temporal patterns. On the other hand, for LTE traffic prediction, the CNN-LSTM hybrid model achieved a 40% improvement in RMSE at the cluster level, effectively managing multivariate data and detecting peak-hour irregularities.

Lastly, for wireless networks with 3D architectures, such as UAV-assisted systems, Spectrum Situational awareness (SSA) is achieved with Volumetric Radio Environment Maps (VREMs) that represent propagation loss across both areal and altitude dimensions. This work introduces two novel DL approaches for constructing the VREMs: the Volume-to-Volume (Vol2Vol) method and the Sliced-VREM method. The Vol2Vol approach directly models 3D data using a 3D-GAN, achieving high accuracy at greater altitudes, with a Structural Similarity Index (SSIM) of 0.9447. On the other hand, the Sliced-VREM method leverages stacked 2D environmental maps and transmitters with an altitude-aware Spider-UNet to efficiently capture altitude dependencies, making it more computationally practical for lower-altitude scenarios. Both approaches demonstrate significant performance improvements over traditional 2D baselines, with MAE reductions of up to 62.9%. Furthermore, preliminary spectrum occupancy maps generated from these VREMs reveal spatial and altitudinal variations, even at low heights of 9 m or less, showcasing their potential to provide actionable insights for dynamic spectrum sharing without relying on extensive monitoring infrastructure.

***Keywords***: Spectrum prediction(SP), Spectrum awareness (SA), Cognitive Radio Networks (CRNs), Long-Term Prediction, Deep Learning, Volumetric Radio Environment Maps (VREM), Traffic-Driven Models, Spectrum Situational Awareness (SSA)

# Acknowledgments

Completing this PhD research has been a deeply enriching journey, filled with opportunities to broaden my horizons in ways I never imagined possible. I am profoundly grateful to my exceptional advisors, supportive colleagues, and loving friends and family for their unwavering support throughout this transformative experience.

I am deeply grateful to my advisors, Dr. -Ing. Dereje Hailemariam and Prof. Sofie Pollin, whose guidance and unwavering support have been invaluable throughout this journey. Dr. Dereje's commitment to consistently offer his time and expertise provided invaluable guidance in the right directions. I am grateful for our biweekly meetings and the countless hours he devoted to discussing ideas, refining methodologies, and addressing challenges. His constant encouragement and belief in my abilities have inspired me to strive for the better and work on this PhD even through difficult times.

Prof. Sofie's unwavering support and openness to assist whenever I faced difficulties or had questions regarding my research were truly invaluable. While empowering me to develop my ideas independently, she also enriched my understanding of the subject matter. The collaborative atmosphere fostered by Prof. Sofie and her research team at KU Leuven not only made my time there enjoyable but also provided me with a profoundly enriching experience that was pivotal for my PhD research.

When I find myself in need of brainstorming or refining my research, my go-to support system is my fellow doctoral students, colleagues friends. I cannot express enough gratitude to Dr. Tsegamlak Terefe and Yonas Yehualaeshet for their invaluable contributions. Our joint research endeavors have been immensely rewarding, enriched by our ongoing feedback discussions. Their insights have not only broadened the scope of my research but have also been instrumental in refining my papers, including this one. I am truly thankful for our collaborative works.

Last but not least, I want to express my deepest gratitude to my family. The unwavering belief my parents have in my potential to achieve greatness has been my daily inspiration. Their

patience, support, and guidance transformed my PhD journey into a meaningful experience, even during countless sleepless nights. I'm immensely thankful for my sister, Helina, and brother, Henock, as well as my bonus sister, Azeb, for being constant sources of joy and light in my life. Their love and encouragement have been my pillars of strength.

***This one is all for you Heliye!***
***Until we meet again, with love always.***

# Contents

# List of Figures

# List of Tables

# List of Abbreviations

| | |
|---|---|
| **2D** | Two-Dimensional |
| **3D** | Three-Dimensional |
| **5G** | Fifth Generations |
| **ABS** | Aerial Base station |
| **AUE** | Aerial User Equipment |
| **B5G** | Beyond Fifth Generations |
| **BL-enc** | Encoder basic layers |
| **BL-dec** | Decoder basic layers |
| **CDRs** | Call Detail Records |
| **CN** | Core Network |
| **CRNs** | Cognitive Radio Networks |
| **CNNs** | Convolutional Neural Networks |
| **ConvLSTM** | Convolutional Long Short-Term Memory |
| **CS** | Circuit Switched |
| **DL** | Deep Learning |
| **DTT** | Digital terrestrial TV |
| **DSS** | Dynamic Spectrum Sharing |
| **DSA** | Dynamic Spectrum Access |
| **GAN** | Generative Adversarial Networks |
| **GBS** | Ground Base Station |
| **GSM** | Global System for Mobile |
| **GUEs** | Ground User Equipment |
| **HAPs** | High Altitude Platforms |
| **I2I** | Image-to-Image |
| **IDW** | Inverse Distance Weighting |
| **IoT** | Internet of Things |
| **KPIs** | Key Performance Indicators |
| **LEO** | Low Earth Orbit |

| | |
|---|---|
| **LoS** | Line of Sight |
| **LTE** | Long-Term Evolution |
| **LAD** | Least Absolute Deviation |
| **LSTM** | Long Short-Term Memory |
| **MAE** | Mean Absolute Error |
| **ML** | Machine Learning |
| **MME** | Mobility Management Entity |
| **MNOs** | Mobile Network Operators |
| **MSE** | Mean Square Error |
| **MSC** | Mobile Switching center |
| **NTNs** | Non-Terrestrial Networks |
| **PU** | Primary Users |
| **PGW** | Packet Data Network Gateway |
| **PS** | Packet Switched |
| **QoS** | Quality of Service |
| **RAB** | Radio Access Bearer |
| **RAN** | Radio Access Network |
| **RE** | Resource Element |
| **PRBs** | Physical Resource Block |
| **REMs** | Radio Environment Maps |
| **RMSE** | Root Mean Squared Error |
| **RSRP** | Reference Signal Received Power |
| **SA** | Spectrum Awareness |
| **SSA** | Spectrum Situational awareness |
| **SP** | Spectrum Prediction |
| **SGW** | Serving Gateway |
| **SI** | Silhouette Index |
| **SME** | Spectrum Management Entity |
| **SNR** | Signal to Noise Ratio |
| **SS** | Spectrum Sensors |
| **SSIM** | Structural Similarity Index |
| **SU** | Secondary Users |
| **SDR** | Software-defined Radios |
| **TNs** | Terrestrial Networks |
| **TCH** | Traffic Channel |

| | |
|---|---|
| **TCH/H** | Half rate TCH |
| **UAVs** | Unmanned Aerial Vehicle |
| **UDP** | Urban Dominant Path |
| **UE** | User Equipment |
| **VREMs** | Volumetric Radio Environment Maps |
| **Vol2Vol** | Volume-to-Volume |

# List of Publications

## Articles in Refereed Journals

[1] **K-Means Clustering Assisted Spectrum Utilization Prediction with Deep Learning Models**. Bethelhem S. Shawel, Frehiwot Bantigegn, Tsegamlak T. Debella, Sofie Pollin, and Dereje H. Woldegebreal. In: Engineering Proceedings . 18:1 (2022), issn: 2673-4591. doi: 10.3390/engproc2022018002. url: https://www.mdpi.com/2673-4591/18/1/2.

[2] **A Multivariate Approach for Spatio-temporal Mobile Data Traffic Prediction**. Bethelhem S. Shawel, Endale Mare, Tsegamlak T. Debella, Sofie Pollin, and Dereje H. Woldegebreal. In: Engineering Proceedings . 18:1 (2022), issn: 2673-4591. doi: 10.3390/engproc2022018010. url: https://www.mdpi.com/2673- 4591/18/1/10.

[3] **A Deep Learning Approach to a Volumetric Radio Environment Map Construction for UAV-Assisted Networks**. Bethelhem S. Shawel, Dereje H. Woldegebreal and Sofie Pollin. In: International Journal of Antennas and Propagation. 2024:9062023 (2024), 16. doi: 10.1155/2024/9062023.

## Articles in Refereed Conference Proceedings

[1] **Deep-learning based Cooperative Spectrum Prediction for Cognitive Networks**. Bethelhem S. Shawel, Dereje H. Woldegebreal and Sofie Pollin. In: 9th International Conference on Information and Communication Technology Convergence: ICT Convergence Powered by Smart Intelligence, (ICTC 2018). 2018. doi: 10.1109/ICTC.2018.8539570.

[2] **Convolutional LSTM-based Long-Term Spectrum Prediction for Dynamic Spectrum Access**. Bethelhem S. Shawel, Dereje H. Woldegebreal and Sofie Pollin. In: 27th European Signal Processing Conference (EUSIPCO 2019). 2019. doi: 10.23919/EUSIPCO.2019.8902956.

# 1 Introduction

## 1.1 Background

In the world of wireless communication, the radio spectrum is a crucial yet limited resource. As bandwidth-intensive wireless services advance and the need for seamless connectivity grows, the demand for more spectrum is significantly increasing. This trend is particularly evident in Fifth Generations (5G) and Beyond Fifth Generations (B5G) networks that are designed to meet various service requirements by relying on diverse frequency bands. For instance, applications requiring broader coverage, such as industrial Internet of Things (IoT), typically operate within lower spectrum bands (Sub-1GHz range). On the other hand, those prioritizing enhanced transmission speeds and reliable connectivity, including mission-critical services and augmented reality, mostly aim at millimeter wave (mmWave) and Tera-Hertz (THz) frequency ranges [1–3].

However acquiring a new spectrum cannot always meet such a wide range of demands, leading to significant challenges in spectrum allocation, congestion, and interference management [4]. To address these challenges, various strategies are considered, ranging from implementing Dynamic Spectrum Sharing (DSS) to embracing innovative network architectures, such as the integration of space-air-ground networks. DSS-enabled access to spectrum is often referred to as the "*real-time adjustment of spectrum use in response to changing circumstances and objectives*" and is critical to maximizing the efficiency of spectrum use. Similarly, terrestrial and non-terrestrial networks coming together in B5G are expected to enable networks to deliver service-aware radio access, leading to better spectrum utilization and reduced congestion [4–6]. Furthermore, incorporating Machine Learning (ML) and Deep Learning (DL) solutions into B5G network design marks a new phase of network intelligence, enabling flexible resource allocation and proactive spectrum management [7–9]. Nonetheless, successfully harnessing these innovative strategies requires complete and real-time and predicted awareness of spectrum use in different dimensions [4, 7].

Spectrum Awareness (SA) aims to provide a comprehensive understanding of how, when, and where spectrum is utilized [10]. It involves monitoring different frequency bands in time and space to detect usage patterns, available frequencies, or "spectrum holes", and potential sources of interference [11]. Incorporating this real-time awareness with prediction capabilities enables networks to plan and allocate resources proactively rather than reactively. Such predictive SA is recognized as a fundamental enabler of intelligent and efficient wireless networks. Its role in optimizing spectrum utilization, enabling advanced spectrum-sharing approaches, and ensuring reliable communication in dynamic environments emphasizes its importance [2]. This can be further highlighted in the context of 5G and beyond Cognitive Radio Networks (CRNs), Mobile Network Operators (MNOs), and Unmanned Aerial Vehicle (UAVs) networks, as follows.

- **Empowering Cognitive Radio Networks:** As critical components of 5G and B5G, CRNs are being designed to ensure enhanced network capacity, flexibility, dynamic spectrum efficiency, as well as the ability to support a multitude of devices, services, and applications with varying Quality of Service (QoS) requirements [12]. Their dynamic and complex nature makes them entirely reliant on spectrum knowledge for their true cognitive ability. Equipped with sensing and predicting capabilities, CRNs can measure and analyze nearby radio environments to dynamically adjust their radio settings and determine the best sharing arrangements. This involves deciding whether to temporarily access the licensed spectrum as Secondary Users (SU) when not in use or to coexist with the Primary Users (PU) without causing interference or congestion [11, 13].

- **Dynamic Spectrum Access for MNOs:** The increasing demand for improved coverage and capacity is driving MNOs to seek intelligent solutions for efficiently utilizing and acquiring new spectrum resources. Dynamic Spectrum Access (DSA) provides MNOs with the ability to access spectrum resources dynamically and opportunistically. Instead of being confined to fixed, pre-allocated spectrum bands, DSA allows MNOs to access unused or underutilized spectrum bands in real-time [14, 15]. One approach to address the growing demand for mobile data services is to dynamically utilize existing spectrum resources across different radio access technologies, such as Long-Term Evolution (LTE)'s carrier aggregation (CA) and DSS of low- and mid-bands (< 3 GHz) for the coexistence of 5G new radio and LTE [16]. Another approach involves spectrum-shared access between multiple MNOs, where temporary spectrum leasing or spectrum pooling is permitted [17, 18]. In both scenarios, MNOs must continuously monitor and develop a comprehensive understanding of their anticipated spectrum utilization. This involves

identifying spectrum bands available for DSA modalities, enabling MNOs to optimize their spectrum usage effectively.

- **Spectrum sharing beyond the plane:** As we enter the era of B5G, it's important to recognize how wireless networks are evolving beyond the traditional Two-Dimensional (2D) network architecture. Integrating aerial networks, such as Unmanned Aerial Vehicle (UAVs), with terrestrial cellular networks revolutionizes spectrum resource utilization by adding an extra dimension [5, 19]. For instance, UAVs operating at higher altitudes enable shared spectrum usage between ground users and UAVs, considering their altitude differences. However, the high mobility of UAVs means that their radio environment characteristics change dynamically over time and in Three-Dimensional (3D) space, posing challenges for spectrum monitoring and joint resource management. This calls for a new approach to SA, incorporating real-time spectrum monitoring and situational awareness, such as understanding radio device mobility and transmission conditions in a complex 3D radio environment [20, 21]. By adopting such approaches, these networks can efficiently and intelligently utilize spectrum resources, ensuring seamless connectivity and minimizing interference.

From CRNs to ground-based networks and airborne domains, real-time and predicted spectrum knowledge is reshaping the landscape of wireless networks. It provides the critical real-time and future understanding of how spectrum is used, allowing for efficient allocation, advanced sharing techniques, and reliable communication in ever-changing environments. This is especially important for 5G and B5G networks with their diverse service demands and need to maximize spectrum usage. However, realizing the full potential of real-time and predicted SA depends on the accuracy and completeness of the information, tailored to the specific requirements of the networks and the sharing modalities. The next section delves deeper into these considerations and explores techniques for building accurate predicted spectrum knowledge.

### 1.1.1 Building a complete spectrum awareness

Deciding which frequency bands to use as an opportunistic user (or SU) which bands to share temporarily as an incumbent or PU relies heavily on accurate monitoring and analysis of

spectrum usage. This primarily involves real-time sensing, done over narrow or wide-bands with a dedicated sensor network or in crowdsource with sensing-enabled devices.

From simple energy-based detection techniques to those that consider the statistical properties of the signal, spectrum sensing schemes help compute energy levels, duty cycles, or other statistical features to determine spectrum occupancy and utilization [22, 23]. A Spectrum database that stores past sensed data, along with details like location and network-related information of PU and SU, and environmental factors can also be combined with spectrum sensing to build comprehensive SA. In this case, real-time sensing offers immediate insights, while the spectrum database provides historical data for further analysis and predictions [11, 23–25].

Complementing real-time sensing, *Spectrum Prediction (SP)* plays an important role in inferring relevant information about the future availability of spectrum opportunities. In doing so, SUs can be more proactive in their approach towards utilizing the available spectrum, reducing the time needed to detect and their energy consumption as well as improving the overall throughput [25, 26]. With an implicit notion of time dependency, statistical or ML/DL techniques can be used to effectively exploit historical data from the spectrum database for modeling spectrum usage patterns and providing sequential predictions [27]. Different SP problems could be addressed by focusing on various spectrum-related parameters such as the status of the spectrum channel as idle or busy *(availability/occupancy)*, the average fraction of time a spectrum channel is being used (*utilization*), or the power level on a specific channel to define channel quality.

The prediction length could be limited to a single next-step forecast or might try to see further into the future, making predictions for multiple steps ahead based on historical data. Depending on how far ahead we want to predict and the level of detail in the data (data resolution), multi-step predictions could be made over short or long time frames. SU rely on predictions to opportunistically detect and utilize the spectrum, adjust its transmission parameters, or vacate licensed spectrum channels in the presence of PU. This requires quick decision-making within seconds or minutes to enhance QoS and minimize interference [26, 28–30]. Conversely, when spectrum sharing is administratively managed, as in spectrum pooling or leasing, bands with longer availability increase the market value of shared spectrum or simplify the technical challenges with coordination and interference management. In these cases, the length of the predicted information is required to be hours or days [31].

Another approach to developing long-term knowledge about spectrum usage is through the

use of Radio Environment Maps (REMs). Enabled by databases, REMs serve as fine-grained digital radio maps that provide extensive and up-to-date information on spectrum availability in large geographical areas and periods [32–34]. In a broader context, REMs encompass all maps populated with data related to radio aspects, such as signal strength, quality, coverage, and propagation characteristics, in different spectrum bands and within a specific geographic region. The strength of REMs lies in their ability to integrate real-world data, such as building layouts, sensed data, terrain features, obstacles, and network configurations, into their visual representation of how spectrum usage varies in different locations [20].

In all cases, whether we constructed REMs or employed prediction techniques to analyze different availability and usage patterns, the achieved accuracy relies on the techniques used. Their ability to exploit large sets of measurement data, extract complex patterns, and incorporate additional information enhances the built spectrum knowledge.

### 1.1.2 Deep learning Models

Over the past few years, DL is increasingly being referred to as the data-driven backbone of the future of wireless networks and is being leveraged to address various challenges and improve performance in different aspects of communication. Its ability to learn complex patterns and representations directly from data has revolutionized many aspects, including signal processing, resource allocation, interference mitigation, spectrum management, and more [8, 35]. In the context of this research, DL's strengths align seamlessly with the demands of SP and SA, addressing challenges in monitoring, predicting, and managing radio spectrum dynamically.

One of the key strengths of DL is its capability to handle sequential data and perform temporal predictions, making it an invaluable tool for tasks like spectrum prediction. Among the architectures designed for such tasks, Recurrent Neural Networks (RNNs), and particularly *Long Short-Term Memory (LSTM)* networks, have significantly simplified retaining information from previous inputs and inferring future knowledge [36, 37]. In this regards, LSTM networks are particularly effective for time-series tasks, such as spectrum occupancy forecasting, where long-term memory is essential to capture usage trends, anomalies, and fluctuations [13, 35].

As specialized RNN architecture, LSTM is designed to handle long-term dependencies by addressing the vanishing or exploding gradient problems found in traditional RNNs. It achieves this through the use of memory cells equipped with input, forget, and output gates. These

gates selectively retain or discard information over extended periods, enabling the network to maintain context and learn relationships over long sequences [38]. Figure 1.1 illustrates the architecture of an LSTM network, where its core functionalities are defined as follows [39]:

$$i_t = \sigma(W_{\chi i}\chi_t + W_{Hi}H_{t-1} + W_{Ci} \odot C_{t-1} + b_i)$$

$$f_t = \sigma(W_{\chi f}\chi_t + W_{Hf}tH_{t-1} + W_{Cf} \odot C_{t-1} + b_f)$$

$$o_t = \sigma(W_{\chi o}\chi_t + W_{Ho}H_{t-1} + W_{Co} \odot C_{t-1} + b_o)$$

$$C_t = f_t \odot C_{t-1} + i_t \odot g(W_{pc}\chi_t + W_{Hc}H_{t-1} + b_c)$$

$$H_t = o_t \odot \hbar(C_t) \tag{1.1}$$

The gating units-input $i_t$, forget $f_t$, and output $o_t$-control the flow of information, while the cell state $C_t$ and hidden state $H_{t-1}$ store and transform data for temporal predictions. Weights $W_x$, $W_H$, and $W_c$, represent input, output, forget, and cell weights, respectively, with biases $b_i$,$b_o$, $b_f$, and $b_c$. The point-wise multiplication operation is denoted by $\odot$.

The selection of activation functions depends on the learning task. For predicting real-valued data, the activation function for cell updates ($g(x)$, and output $\hbar(x)$), is chosen as the Rectified Linear Unit (ReLU) function: *R (x) = max(0,x)*. Gate activation, $\sigma(x)$, use the sigmoid function: $\sigma(x) = (1 + e^{-x})^{-1}$. This setup ensures the LSTM network effectively captures long-term dependencies and enhances predictive accuracy.

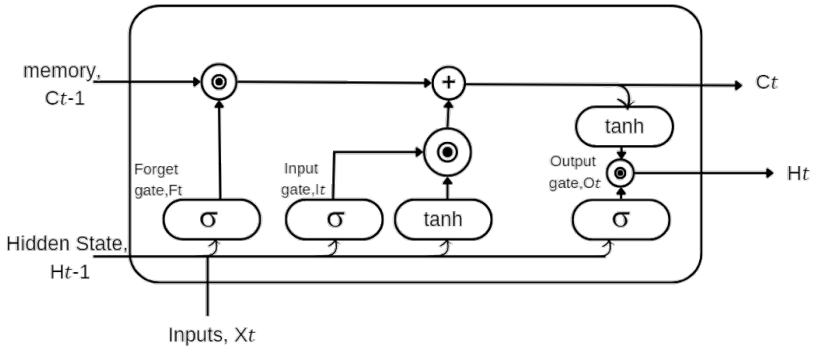


**Figure 1.1:** LSTM network [39].

*Convolutional Neural Networks (CNNs)* is another powerful DL architecture, particularly suited for feature extraction tasks in structured grid-like 1D, 2D, and 3D data [8, 40]. CNNs excel at

automatically learning hierarchical representations of visual data by applying convolutional filters (kernels) across the input data to produce feature maps. This capability enables and simplifies wide range tasks in wireless Communication including signal classification and identification, channel modeling, and spatial data analysis.

Mathematically, the fundamental convolution operation in CNN for an input $X$, output $Y$ and a particular filter $W$ can be expressed as [41]:

$$Y(i) = (X * W)(i) = \sum_j X(j) \cdot W(i,j) \quad \text{(for 1D convolution)} \tag{1.2}$$

$$Y(i,j) = (X * W)(i,j) = \sum_m \sum_n X(m,n) \cdot W(i-m, j-n) \cdot W(i,j) \quad \text{(for 2D convolution)} \tag{1.3}$$

$$Y(i,j,k) = (X * W)(i,j,k) = \sum_m \sum_n \sum_p X(m,n,p) \cdot W(i-m, j-n, k-p) \quad \text{(for 3D convolution)} \tag{1.4}$$

CNNs are versatile in handling data across different dimensions. For 1D data like time series, the network apply 1D convolutions that slide filters along a single dimension $i$, effectively capturing local patterns and temporal dependencies. This allows 1D CNNs to identify trends, seasonalities, and anomalies while processing data in parallel, offering a significant reduction in computation time compared to sequential models like RNNs [42]. For 2D data such as images or spatial maps, CNNs use 2D convolutions that slide $W$ across both height $i$ and width $j$ dimensions [43]. This enables the detection of spatial features, from simple edges to complex structures like shapes and objects [41]. Applications include image classification, object detection, and spectrum map analysis, where each output pixel aggregates localized input information, ensuring effective spatial feature extraction. For 3D data like video frames, volumetric imaging, or spatial-temporal radio maps, CNNs extend convolutional operations to three dimensions [44]. Filters,$W$, slide across height $i$, width $j$, and depth $k$, capturing volumetric features and relationships essential for tasks such as 3D object recognition and video analysis. Across all dimensions, CNNs leverage a weight-sharing mechanism to reduce parameters and offer scalability, allowing seamless adaptation to higher-dimensional data with minimal architectural changes. This makes CNNs powerful tools for feature extraction and analysis in diverse applications.

Although LSTM-based networks have already been proven at handling temporal dependencies in time series data, maintaining structural locality and solving multi-dimensional problems is a challenge. To that aspect, Convolutional Long Short-Term Memory (ConvLSTM) can

come in-handy by combining CNNs and LSTM to learn the multi-dimensional dependencies in sequential data [41]. While maintaining a similar architecture to LSTM, the ConvLSTM consists of convolution layers rather than fully connected layers in the hidden state, gating (input, putout, and forget), and cell units. That means that the input to each LSTM unit is a convolutional feature map, instead of a scalar or vector, and Equation 1.1 is modified as defined in [41] to reflect the convolution operation as:

$$
\begin{aligned}
i_t &= \sigma(W_{\chi_i} * \chi_t + W_{Hi} * H_{t-1} + W_{Ci} \odot C_{t-1} + b_i) \\
f_t &= \sigma(W_{\chi_f} * \chi_t + W_{Hf} * H_{t-1} + W_{Cf} \odot C_{t-1} + b_f) \\
o_t &= \sigma(W_{\chi_o} * \chi_t + W_{Ho} * H_{t-1} + W_{Co} \odot C_{t-1} + b_o) \\
C_t &= f_t \odot C_{t-1} + i_t \odot g(W_{pc} * \chi_t + W_{Hc} * H_{t-1} + b_c) \\
H_t &= o_t \odot \hbar(C_t)
\end{aligned} \tag{1.5}
$$

where $*$ denoting convolution operator.

When considering long-term prediction problem that can be re-framed as a sequential learning task, where multiple lengths of past observation are used to provide multiple-length future prediction, the use of an encoder-decoder structure is essential to maintain the compressed representation of the input data [45]. As the name implies the architecture as illustrated in Figure 1.2 is comprised of two sub-models: an Encoder ($E$) that takes a variable-length sequence an input to provide its compressed representation or state and a Decoder ($D$) that is capable of providing multiple-length target output $Y$ based on the compressed representation [46]. For tasks involving complex sequential data, such as signal reconstruction and network traffic anomaly detection, the encoder-decoder framework proves invaluable by capturing temporal dependencies effectively. Figure 1.2 depicts the recurrent variant of the architecture where $E$ processes sequential inputs $X(t-n:t)$ , leveraging temporal patterns, and the $D$ generates the $X(t+1:t+l)$ predictions iteratively, conditioned on prior outputs. Such structures enable flexible applications, including image-to-image translation and sequential predictions, optimizing feature extraction across time-series tasks [8].

In addition to temporal prediction and feature extraction, DL plays a crucial role in data generation tasks. Generative models, such as Generative Adversarial Networks (GAN) are widely used for this purpose. GANs, in particular, have gained significant attention for their

2 https://medium.com/analytics-vidhya/a-review-of-generative-adversarial-networks-part-1-a3e5757a3dc2

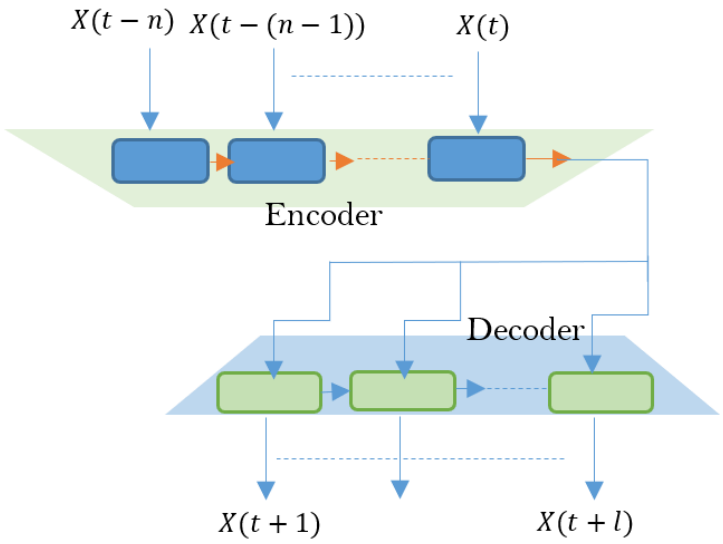


**Figure 1.2:** Encoder Decoder Architecture.

ability to generate realistic synthetic data by pitting two neural networks as illustrated in Figure 1.3 - the generator ($G$) and the discriminator ($D$) - against each other. These networks work by training a $G$ to produce samples that are indistinguishable from real data and letting the $D$ to evaluate its authenticity. This has applications in image synthesis and data augmentation. For instance, testing new wireless network protocols and configurations can be simplified with GAN-augmented data representing various real-world network scenarios, such as varying network loads, interference levels, or environmental factors, without requiring extensive real-world data collection [8].

In general, DL networks and architectures have enabled significant breakthroughs in various domains. From making accurate temporal predictions with LSTMs, extracting meaningful features with CNNs, to generating realistic data with GANs, DL models are redefining possibilities. In the context of this research DL models specifically address challenges such as handling large, complex multidimensional data sets, learning from them efficiently, generating new ones, and making accurate, long-term predictions - crucial for dynamic spectrum management and optimizing network protocols in real-world scenarios.

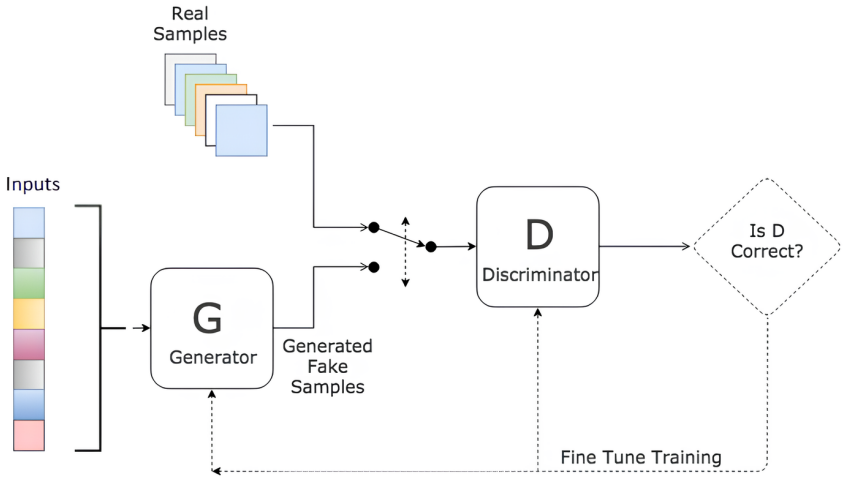


**Figure 1.3:** GAN Architecture.[2]

## 1.2 Motivation

The usage of spectrum channels (or bands) is inherently dynamic due to various factors, such as the diverse technologies and their corresponding service demands, user behavior, and radio environment characteristics, among a few. This dynamicity makes it challenging to accurately understand and predict spectrum availability using conventional methods. Consequently, we have identified three main challenges in this area. These challenges serve as a significant motivation for our research, driving us to develop efficient solutions to better understand the use of spectrum resources in the face of these complexities.

### 1.2.1 Challenge 1: Providing accurate long-term spectrum predictions with limited monitoring spectrum data

SU require accurate spectrum availability information over extended periods for informed decision-making, especially in anticipation of PU' return. However, existing prediction techniques are mostly limited to short-term forecasts, which are inadequate for critical decisions on spectrum sharing, mobility, or channel access adjustments. The lack of extensive and continuous historical spectrum monitoring data, along with the issue of compounding and propagating prediction errors, presents significant challenges in providing accurate long-term predictions [47, 48].

Many sensing devices, particularly those in IoT-CRNs, are often designed with limited processing power and memory, making it difficult for them to perform complex spectrum sensing and continuously store a comprehensive view of the spectrum environment over prolonged duration [22]. This issue worsens when these devices experience signal blockage (shadowing) and fail to detect actual spectrum usage (missed detection), limiting the accuracy of single-point spectrum monitoring [49].

With the reduced quality and availability of monitoring data in such networks, the likelihood of incorrect SP (false alarms) increases. As predictions extend into the future and are made on a slot-by-slot basis, these prediction errors inevitably accumulate and amplify over time, significantly degrading the quality of predicted long-term SA.

### 1.2.2 Challenge 2: Understanding spectrum in multiple dimensions

Understanding how spectrum is utilized across space and time (*spatio-temporal*) is essential for effectively managing resources and meeting the diverse needs of users in dynamic wireless networks. Whether in CRNs or networks assisted by UAVs, user mobility causes their spectrum requirements to change as they move between locations or altitudes. Spatio-temporal SP enables such users to adjust their communication parameters or switch channels seamlessly as they navigate different spatial environments [50, 51].

Moreover, with varying service demand over time and space, traffic patterns and corresponding spectrum usage can fluctuate spatio-temporally. Thus, having a multidimensional understanding allows MNOs to adapt their spectrum resource allocation strategies based on real-time and predicted changes. For instance, a cellular network might allocate more resources to specific areas during peak usage hours or adjust channel selection based on predicted changes in user activity. Considering spectrum as a tradable commodity, MNOs can also leverage this knowledge to determine the sharing arrangement or value of spectrum in different locations and time frames [52].

However, achieving comprehensive and accurate spatio-temporal SP is hindered by various factors, including limited sensing ranges and the dynamic nature of the radio environment [53]. Conventional spectrum sensing techniques, which often utilize fixed and sparsely distributed sensing devices, suffer from limited terrestrial range and are particularly problematic in scenarios involving mobile users or UAVs operating in a 3D space [54]. This makes it challenging

to accurately *fill in* (or interpolate) the unsensed locations and capture a complete picture of spectrum usage across a large geographical area and at higher altitudes. Processing real-time spectrum data from these sensors and predicting the joint spectrum-time-space characteristics at different altitudes also introduces additional overhead and necessitates robust prediction techniques capable of handling the large data volume.

### 1.2.3 Challenge 3: Limitations of prediction models in achieving accuracy and exploring extensive data

When aiming to develop comprehensive SP across various dimensions, models that are capable of capturing both temporal and spatial variations in spectrum usage are necessary to make accurate predictions. Among the most commonly used models for understanding usage patterns and predicting spectrum availability are parametric models, including linear regression, moving average models, Hidden Markov models, and Bayesian inference [9, 26, 35, 55–57]. While these models can provide reasonably "good" predictions, they have inherent limitations related to handling large-scale spectrum data and assumptions about the underlying distribution of the data.

Parametric models, such as linear regression and moving average models, operate under the assumption that the underlying distribution of spectrum data remains constant over time [56]. However, this assumption does not hold true in many real-world scenarios as spectrum usage is by nature a non-stationary process whose characteristics are time-dependent. This leads to challenges for the models in capturing non-stationary patterns or trends and consequently may struggle to provide accurate long-term SP. Moreover, these models may lack the flexibility needed to capture complex and non-linear relationships present in multi-dimensional spectrum data. This limitation can result in poor predictive performance, particularly when the sensed spectrum data has poor Signal to Noise Ratio (SNR).

Although incorporating additional explanatory information and large-scale prior spectrum data can enhance the models' accuracy, addressing limitations associated with long-term memory dependencies and handling large-scale or multiple attributes remains challenging [9]. To that aspect, DL models have gained popularity due to their capability to thrive and improve their likelihood of estimations with self-learning ability on large data [8]. However, the effectiveness

of DL models relies on proper model selection, and the quality and robustness of the data, posing challenges to the accuracy of their analysis.

## 1.3 Literature Review

Given the significance of understanding current spectrum usage trends and anticipating future patterns, a wide array of research has been undertaken in this area. This ranges from spectrum monitoring initiatives to different techniques for analyzing and exploring the spectrum data to gain diverse and accurate predicted insights.

Various spectrum monitoring activities have been done to gather long-term spectrum information at a large geographical scale [58–61]. The government or Industry-driven initiatives often rely on costly and sophisticated sensing devices, limiting their capacity for large-scale monitoring [62, 63]. In contrast, initiatives such as Electrosense[3], RadioSense[4], and RadioHound utilize low-cost, low-power Software-defined Radios (SDR), enabling distributed sensor deployment and wide-area spectrum monitoring [64, 65]. While these SDR-based approaches may have limitations in implementing advanced sensing techniques, they are favored for their ability to conduct large-scale monitoring campaigns. Nevertheless, spectrum monitoring requires a certain fundamental trade-off between frequency resolution and time resolution; not to mention all monitoring endeavors encounter a compromise that impacts either the quality or availability of sensed data concerning duration and coverage area, potentially influencing the accuracy of SA [58].

With the primary goal being identifying future spectrum channel availability, prediction-based spectrum decision-making plays a crucial role in reducing monitoring time and energy consumption in CRNs [26, 55]. Various modeling and prediction techniques have been employed for this purpose, including Hidden Markov Models, Bayesian Inference, regression models, and probabilistic models such as Gaussian Processes [47, 51, 56, 66–69]. Hidden Markov Models represent the spectrum as a series of hidden states and predict future states based on transition probabilities, providing accurate predictions despite the limited statistical models. Bayesian Inference models, on the other hand, are used in uncertain situations, updating information about spectrum occupancy based on prior knowledge and new evidence [70]. On the other

3 https://electrosense.org/
4 https://www.chistera.eu/projects/radiosense

hand, regression models see the prediction problem as a time series forecasting and provide future spectrum values based on past observations, while probabilistic models like Gaussian Processes handle uncertainty in predicting future spectrum occupancy [56, 69]. Recently, neural networks such as LSTM and multilayer perceptrons have also gained popularity in SP for their ability to handle complex patterns and nonlinear relationships in spectrum data [47, 51, 67, 68].

While significant advancements have been made in improving prediction accuracy, there are limited studies on the implications of long-term SP and methods to enhance their quality. The tensor completion approach presented in [68, 71] addresses long-term SP in the presence of missing values and sparse anomalies, demonstrating 24-hour predictions despite the model's limitations in capturing the multi-dimensional nature of spectrum occupancy.

These techniques typically utilize historical data from various spectrum measurement and monitoring campaigns to exploit spectral-temporal correlations observed due to PU's or SU's spectrum usage patterns. However, they are mostly executed locally from a single SU's point of view, meaning predictions are solely based on spectrum sensing data from a single SU [26]. Recognizing the spatial dependency of the radio environment, cooperative SP approaches have been explored to enhance prediction accuracy collaboratively [72]. In centralized cooperative SP, information from multiple SUs or spectrum sensors is combined at a central entity through pre-fusion or post-fusion techniques [57]. In the pre-fusion approach, each SU locally predicts future spectrum availability based on its past information before sending it to the fusion center for combined spectrum decision-making. Conversely, the post-fusion scenario involves multiple SUs sending their spectrum sensing information to be combined and predicted to gain awareness of future spectrum availability.

Similarly, potential benefits of cooperative SP have been evaluated using Hidden Markov Models as a local predictor with both hard (Equal gain combining) and soft (selective combining) collaborative fusion techniques in [66, 73, 74]. Soft fusion, highlighted in [73], improves SP accuracy, albeit with varying performance based on noise level, number of cooperators, and chosen fusion rule. Despite the performance improvements due to cooperation, determining the optimal number of sensors for cooperation remains a critical question. Addressing this, [75] emphasizes the importance of selecting the optimal number of sensors for accurate sensing by analyzing trade-offs between accuracy and overhead based on channel conditions, noise level, and chosen fusion rules. However, further research is needed to generalize these findings beyond specific scenarios and adapt them to the complexities of dynamic sensor networks.

The limitations of both measurement data quality and the overhead associated with deploying large spectrum sensing networks can be mitigated by exploring alternative data sources. While research on understanding spectrum usage directly from network or service-related data is limited, [76] establishes connections between spectrum usage measurements and service congestion. In addressing spectrum scarcity and under-utilization in future mobile networks, [9] proposes a novel strategy based on real-time, data-driven insights and dynamic spectrum allocation algorithms. By leveraging network data diversity, such as cell load, user mobility, and traffic patterns, the approach in the paper utilizes ML/DL to forecast future traffic demands and user locations. Additionally, [77] evaluates the upper limit of required radio resources using network-level data to enhance spectrum usage. However, challenges persist in generalizing findings from specific datasets and incorporating multidimensional and dynamic spectrum changes.

Earlier conventional approaches to single-point spectrum sensing and prediction often overlooked this spatial and temporal dynamism, leading to inefficient utilization and potential interference with existing users in DSS scenarios. Moving beyond these single-point predictions, [50] lays the groundwork for accurate SP by modeling spatial correlations with random fields and spatial statistical analysis. Extracting parameters from diverse real-world measurements, the paper's methodology significantly outperforms traditional occupancy prediction methods in terms of accuracy metrics. However, adapting this success to dynamic environments and managing the computational complexity of parameter estimation requires further investigation [35].

Tackling the complexity of analyzing higher dimensions of data and realizing spectrum usage more clearly can be achieved with REMs [33, 78, 79]. REMs' capability to depict information in a digital radio map form simplifies understanding spectrum usage and availability across wide geographical areas and offers versatile applications. Different spatial interpolation approaches are used to analyze the spatial relation in spectrum data and estimate the values at unobserved locations based on the known values at nearby locations. Inverse Distance Weighting (IDW) and kriging are the most used deterministic and geo-statistical models to provide a complete spectrum occupancy map representation [20, 80–82]. Furthermore, [83] presents spectrum maps constructed by combining tensor completion and prediction to address spectrum data limitation. Despite being dependent on specific network topological and spectrum usage patterns, this approach has achieved superior reconstruction accuracy and prediction performance compared to spatial statistical methods. Another approach, presented in [84], constructs REMs to depict

spectrum usage based on received signal level. This paper addresses the issue of measurement data limitation and how to optimally place sensors for accurate Spectrum map construction. By employing a novel genetic and local search algorithm to optimize sensor placement, the approach significantly improves accuracy compared to random deployment and centralized sensing, particularly in dynamic scenarios.

When more dynamic spectrum environment and 3D network architectures such as in UAV-assisted networks are considered the task of spectrum monitoring and accurate prediction becomes complex. Unlike conventional 2D spectrum sensing approaches the work in [54] leverages UAVs to collect and analyze spatio-temporal data via cooperative sensing that demonstrates a framework for accurate 3D SA. While this framework shows improved performance over traditional methods in terms of detection probability and false alarm rate, real-world challenges remain. [20] is another research that presents 3D spectrum monitoring by prioritizing regions of interest (ROIs) with high spectrum opportunity potential, achieving notable results in accuracy and energy efficiency. However, the use of such dynamic sensing devices and mitigating radio environmental factors require a broader study.

To that, an extended concept of SA called Spectrum Situational awareness (SSA) is introduced as the ability to comprehend the current and future state of the spectrum usage based on knowledge about the network conditions and other factors, including user mobility, location, and change on the radio or propagation environment [21, 53, 85, 86]. Especially when monitoring spectrum data in all dimensions is challenging, having a predefined representation of the radio propagation information is essential as presented in [87]. The paper represents propagation environment modeling to improve spectrum parameter estimation in uncertain environments and enhance SSA.

In conclusion, this literature review highlights various spectrum monitoring approaches and advanced data analysis techniques to understand current spectrum usage trends and predict future patterns. Combining monitoring data from multiple sensors cooperatively and utilizing statistical or ML/DL-based models has been shown to improve prediction accuracy. Despite these advancements, challenges remain in balancing accuracy with the overhead of processing data from widely distributed sensors, integrating alternative data sources, and adapting to dynamic environments. Future strategies involve utilizing diverse network data for additional situational awareness or as an alternative to direct spectrum monitoring data, and using advanced prediction techniques. This extensive body of work underscores the ongoing efforts and future directions necessary to optimize spectrum utilization effectively.

# 1.4 Objectives

## 1.4.1 General Objective

This PhD research aims to improve the accuracy and comprehensiveness of predicted SA in both time and space using DL techniques while considering it from various network perspectives.

## 1.4.2 Specific Objectives

To achieve the main objective, we explored different aspects aligned with the identified challenges. The specific objectives are outlined as follows.

**Investigating challenge 1: Providing accurate long-term spectrum predictions with limited monitoring spectrum data**

- Examine the challenge of long-term SP, spanning hours or days, in various network perspectives, notably in CRNs and MNOs.
- Evaluate the implementation of cooperative prediction with real-time spectrum data.
- Explore the utilization of contextual and situational information regarding spectrum usage to address the limited monitoring data.
- Develop an indirect approach to SP with partial or no spectrum monitoring data.

**Investigating challenge 2: Understanding spectrum in multiple dimensions**

- Investigate and identify methods for providing long-term SP over large geographical areas with sparsely monitoring spectrum data.
- Investigate the challenge of establishing SA from the viewpoint of UAV-assisted networks.
- Explore methods to capture the characteristics of spectrum usage in frequency, time, and space (2D and 3D).

**Investigating challenge 3: Limitations of prediction models in achieving accuracy and exploring extensive data**

- Investigate and propose DL models for long-term predictions.
- Examine DL architectures and models for capturing the multi-dimensional characteristics of spectrum data.
- Propose DL models capable of accurately depicting spectrum usage in the form of maps or images.
- Evaluate the proposed DL models against baselines and alternatives using standard metrics for accuracy and robustness.

## 1.5 Methodology

This research adopts an **iterative methodology**, evolving through phases informed by observations and findings at each step, to systematically address three critical challenges: achieving accurate long-term SP with sparse and limited monitoring data, understanding spectrum utilization or availability in multiple dimensions, and overcoming the limitations of prediction models. Each phase of the research,as summarized in Figure 1.4, builds upon the insights from the previous phase, employing scientific methods of observations, hypothesis formulation, data collection, experimentation, and validation to develop robust solutions.

The research began by observing that long-term SP are highly dependent on the availability and quality of spectrum measurement data. The hypothesis for this phase was that a cooperative SP framework, leveraging centralized data fusion, could mitigate the limitations of sparse spectrum monitoring and improve prediction accuracy. Data for this phase was collected from sparsely distributed sensors in CRNs, capturing temporal patterns of spectrum usage over extended periods and from different location. Using this data, a centralized framework was developed wherein LSTM-based or ConvLSTM-based networks were employed to model temporal dependencies and provide single or multi-location predictions. A Spectrum Management Entity (SME) was introduced to combine data from multiple sensors using a soft fusion technique, addressing data sparsity and improving prediction robustness. The performance of this approach was validated using standard metrics such as Root Mean Squared Error (RMSE)

and Mean Absolute Error (MAE), demonstrating its potential in generating reliable long-term predictions even in sparse monitoring scenarios. As the research progressed, it became evident that the dependence on direct spectrum measurements limited the scalability and applicability of the predictions. This observation led to the second phase, where the research explored the indirect relationship between MNOs traffic data and spectrum utilization. The hypothesis for this phase was that traffic data, such as voice and data volumes, could serve as a reliable proxy for spectrum usage, enabling accurate predictions without the need for direct spectrum measurements. The network-level parameters, including traffic volume, user density, and allocated radio resources, were obtained from MNOs for this phase. By mapping the relationship between traffic patterns and spectrum resource usage and utilizing advanced DL models, such as CNNs and hybrid CNN-LSTM architectures, this approach successfully captured temporal traffic and utilization patterns, enabling accurate long-term spectrum utilization predictions. Clustering techniques, such as k-means, were also used to identify spatial and temporal patterns in the traffic data, enhancing the predictive accuracy across diverse network regions. The proposed models were rigorously evaluated against baseline approaches, with results indicating improvements in prediction accuracy, particularly for regions with high traffic variability.

Recognizing the limitations of two-dimensional analysis in fully understanding spectrum utilization, the research extended to a third phase focusing on 3D situational awareness. The hypothesis here was that incorporating 3D spatial variability into spectrum analysis could provide a more comprehensive understanding of spectrum environments, particularly for UAV-assisted networks. Data for this phase was generated synthetically using advanced simulation tools, accounting for realistic network configurations and environmental factors such as building layouts and UAV placement. Generative models, including 3D-GAN and Spider-UNet architectures, were developed to construct Volumetric Radio Environment Maps (VREMs). These maps captured propagation loss information across three dimensions, integrating altitude and spatial variability to enable enhanced situational awareness. The quality of the constructed maps was validated using Structural Similarity Index (SSIM) and RMSE metrics, showcasing the models' ability to accurately represent complex spectrum environments.

Throughout these phases, the research employed a rigorous validation and refinement process. Standard metrics, such as RMSE, MAE, and SSIM, were used to evaluate model performance across all phases. Comparative analyses against baseline models and ground-truth data were

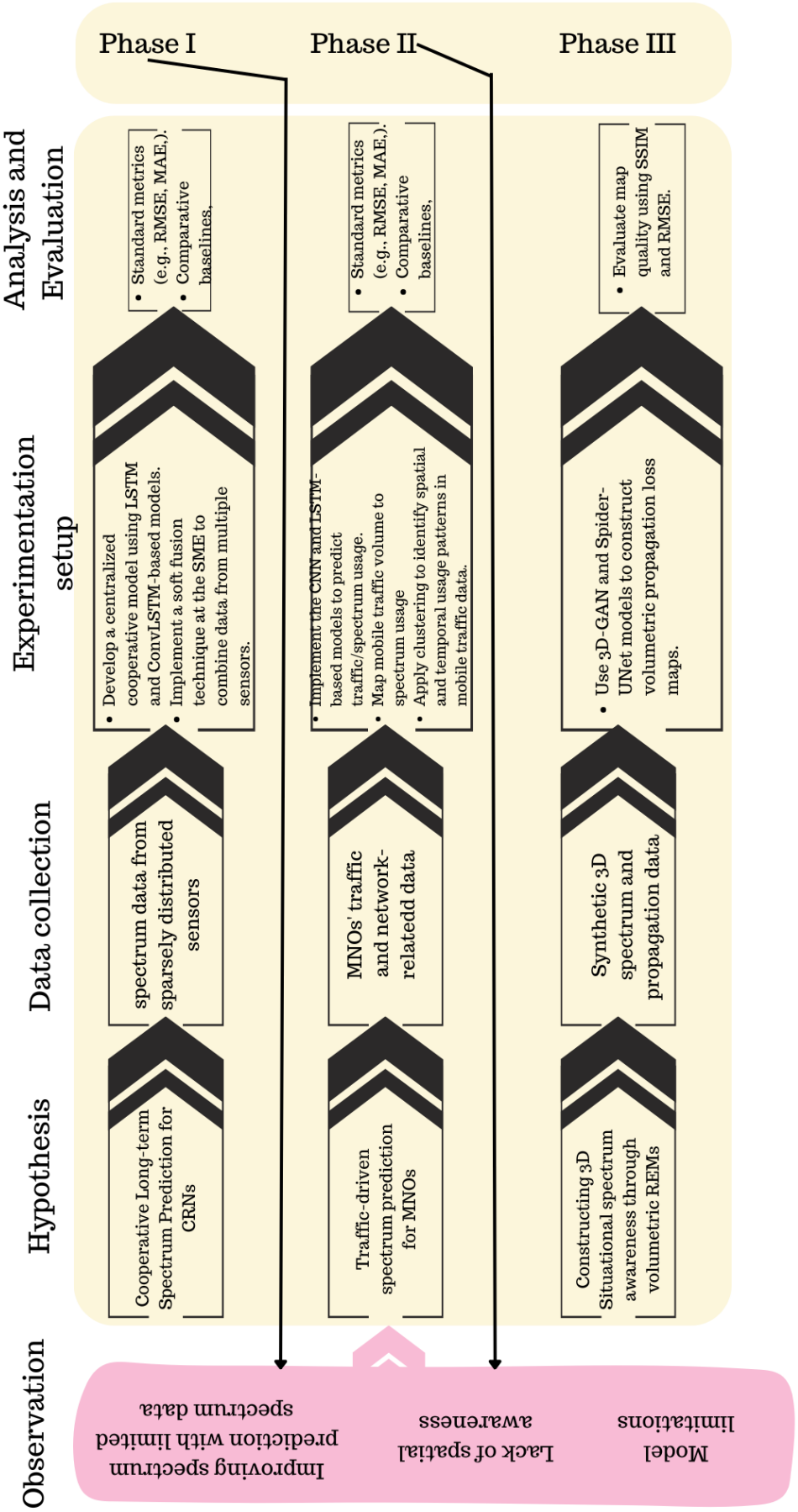


**Figure 1.4:** Research Methodology Flowchart

conducted to quantify improvements. Insights gained from each phase were iteratively used to refine the models, optimize hyperparameters, and adjust training methodologies, ensuring the robustness and scalability of the solutions. This iterative approach not only addressed the identified challenges but also facilitated the development of a comprehensive framework for enhancing predicted spectrum awareness across diverse network scenarios.

## 1.6 Contribution

Through our research, we contribute to the field of predicted and constructed SA by authoring five well-cited and peer-reviewed conference papers and journal articles. Our work extends the existing body of research by addressing key challenges in building accurate SP. Below, we discuss the contributions, highlighting their unique insights.

- **Enhancing Long-Term SP**:
  - The first major contribution is the developing a centralized cooperative prediction framework to improve long-term spectrum predictability. This framework utilizes LSTM-based models with soft fusion techniques to combine data from sparsely distributed spectrum sensors. By fusing data from multiple sensors, this method addresses the challenge of limited monitoring data and enhances prediction accuracy over extended periods, crucial for real-time spectrum management.
  - To tackle the issue of data sparsity and visualizing predicted spectrum map over different locations geographical area , IDW with CNN-based models is used. This method helps to capture spatial correlation of spectrum usage and fill spatial gaps in the spectrum data and extends the prediction capability to larger geographical areas, providing a more complete understanding of spectrum usage across space and time. enabling predictions over a geographic area of up to 4 square kilometers, with an average RMSE reduction of 12% compared to non-interpolated data.
  - The contributed publications, [88] and [89] explore the development and application of this DL-based cooperative framework, demonstrating its effectiveness in predicting spectrum usage in CRNs by utilizing data from multiple sensors deployed in Spain. It also discusses the impact of sparse deployment on prediction accuracy, contributing to a more reliable long-term SP method.

- **Modeling and predicting Traffic-Driven Spectrum Utilization**:
  - The research introduces indirect methods for predicting spectrum utilization by mapping MNOs voice and data traffic volume to spectrum usage. CNNs and hybrid CNNs-LSTM based architectures, are employed to translate real-time aggregated voice and data traffic into actionable SP. Spatial and temporal clustering techniques with k-means, are utilized to analyze and generalize traffic or utilization patterns, enhancing the accuracy of predictions at both cluster and base station levels. This approach reduces reliance on extensive spectrum sensing infrastructures and enables efficient spectrum management at the operator level.
  - **Related Papers:**
    * For voice traffic information obtained from Global System for Mobile (GSM) networks, [90] highlights the effectiveness of the LSTM-based model, achieving a remarkable 36% improvement in prediction accuracy compared to CNN-based models during peak-hour service usage.
    * The data services the spectrum resource utilization was examined for the predicted LTE traffic presented in [91]. The proposed hybrid CNN-LSTM model incorporates multivariate features (such as traffic volume, active users, and allocated resources) that showed improved data traffic prediction accuracy by 40% compared to univariate approaches. The use of k-means clustering further enhanced the prediction by partitioning traffic patterns, reducing RMSE by 8% across temporal clusters.
- **Advancing Spectrum Awareness in 3D Environments:**
  - The novel concept of VREMs was introduced to build situational awareness in 3D wireless network environments and provide the baseline context about complex spectrum environments and radio signal propagation patterns. The map-constructing models developed based on 3D-GAN and Spider-UNet achieved an RMSE below of 15% and SSIM of 0.92, demonstrating high accuracy in constructing volumetric propagation loss maps.
  - As 3D measurement data is not readily available to train the proposed models, a commercial wireless propagation and radio network planning software is used to

simulate actual radio propagation and generate a large set of VREMs data. The simulation took into account the 3D environment geometry and Advanced LTE-based network configuration parameters. This simulated data covering 5 cubic kilometers of a UAVs-assisted network environment was used to validate the models, showing near-perfect propagation loss maps in regions with limited scatterers and an SSIM improvement of 10% over 2D-only models.

  - **Related Paper:** [92] demonstrates the efficacy of these models in constructing VREMs for UAV-assisted networks. The contribution of this works was used to construct coverage map and build preliminary spectrum availability and occupancy awareness at different altitudes.

- **Developing Robust Deep Learning Models for SP:**
  The research introduced a diverse range of advanced DL models to address the complex temporal, spatial, and spectral dependencies inherent in SP problems. LSTM-based models with encoder-decoder architectures effectively captured nonlinear temporal dependencies without relying on predefined assumptions. These models enabled the creation of long-term predictive knowledge of spectrum usage while minimizing error propagation. Incorporating CNN-based models further enhanced the ability to analyze spatial relationships in spectrum and traffic data across multiple locations, providing a more comprehensive understanding of usage patterns. Furthermore, the proposed 3D-GAN facilitated volumetric data reconstruction by leveraging a set of 3D input data. To complement this, the modified altitude-aware Spider-Unet model provided an efficient alternative by sequentially processing volumetric data as sliced 2D image frames, ensuring accurate and computationally efficient 3D data construction.

These contributions collectively advance the state of SP by providing methods for long-term prediction, indirect spectrum modeling, and SSA in complex environments. The results demonstrate the potential of DL techniques to address critical challenges in modern wireless networks, paving the way for more efficient spectrum management and utilization.

## 1.7 Organization

Following the contributions outlined in the previous section, the remaining chapters are structured to address each challenge comprehensively, focusing on the perspectives of the three networks. Jointly presenting our work in [88, 89], Chapter 2 addresses predicting future spectrum availability in the context of CRNs and using data from sparsely distributed sensors to improve the accuracy of long-term forecasting. Chapter 3 focuses on enhancing SP by examining traffic patterns, particularly voice [90] and data traffic [91], and translating them into spectrum requirements for accurate predictions. In Chapter 4, the focus extends beyond traditional SA and SP methods to develop situational awareness of the spectrum environment. This presented our work in [92] for building a knowledge base about the 3D propagation environment for UAV-assisted networks. Finally, Chapter 5 provides the Conclusion and Future Work section, which summarizes the dissertation's key findings and suggests potential directions for future research.

# 2 Cooperative Long-term Spectrum Prediction for Cognitive Radio Networks

## 2.1 Introduction

The concept of CRNs emerged over two decades ago to address the challenges of inefficient spectrum utilization in traditional wireless networks. With spectrum scarcity and static allocation methods that hinder efficiency, CRNs introduced intelligence to network devices. This intelligence enables devices to dynamically access unused spectrum bands opportunistically, adapting to changing environmental conditions and user needs through DSS or DSA[11].

One of the key features of CRNs is spectrum sensing and prediction, which involves detecting and characterizing spectrum usage in real time and for extended periods in the future. This process allows CRN devices, or SUs, to identify available spectrum bands and determine whether they can be used without causing interference to PUs. The cooperative communication among SUs enhances the reliability of their SA and performance by enabling them to share spectrum sensing results and coordinate their actions.

In this chapter, we point out that effectively capturing the long-term temporal pattern of spectrum usage and conducting cooperative SP can be an effective way to improve long-term SP in wireless networks, specifically CRNs. To achieve this, we used real spectrum monitoring data collected from a dedicated sensing network consisting of multiple sensors at different locations. By pooling the measurement data from these sensors and combining it in a centralized cooperative manner with soft fusion, we aimed to improve the accuracy of our predictions and provide interpolated spectrum information. The effectiveness of DSS implemented by the SU is highly dependent on the accuracy and duration of the predicted spectrum availability information. Taking that into account, we introduce two DL models, specifically LSTM- and ConvLSTM-based models, and assess their prediction performance based on factors such as the number of sensing nodes, the quality and length of past measurement data, and the spatial sparsity of the sensing nodes. Furthermore, by using the IDW interpolation method to create a spatially interpolated spectrum map for the second proposed model, it is possible to learn

the joint spectrum-spatial-temporal dependencies observed in the spectrum data and provide predicted spectrum maps for longer-time instances.

Toward that end, this chapter presents our two papers published in peer-reviewed conference proceedings. The papers are listed below.

- Bethelhem. S. Shawel, Dereje. H. Woledegebreal, and Sofie Pollin, *"Deep-learning based Cooperative Spectrum Prediction for Cognitive Networks,"* 2018 International Conference on Information and Communication Technology Convergence (ICTC), Jeju, Korea (South), 2018.
- Bethelhem. S. Shawel, Dereje. H. Woldegebreal and Sofie Pollin, *"Convolutional LSTM-based Long-Term Spectrum Prediction for Dynamic Spectrum Access,"* 2019 27th European Signal Processing Conference (EUSIPCO), A Coruna, Spain, 2019.

## 2.2 Cooperative Long-term Spectrum Prediction Scenarios and System model

### 2.2.1 Cooperative Scenario and System model

To fully utilize the centralized spectrum decision approach, we considered a scenario where a central cloud-based SME is used to analyze and provide long-term SP. As illustrated in Figure 2.1, the SME comprises three components: a database system that is capable of storing historical sensing data, a fusion center for combining or interpolating spatially sparse measurements, and a forecasting and decision unit to provide long-term SP and identify the future availability of the band. Sparsely distributed $M$ SUs that are and $K$ low-power Spectrum Sensors (SS) are connected to a SME for reporting their local measurement. SS are responsible for conducting wide-band spectrum monitoring and providing real-time data on spectrum usage to the SME. The SUs, mwhich may also have sensing capabilities similar to SS, utilize the information from SME to opportunistically access unused spectrum bands without interfering with PUs. When a particular SU wants to access spectrum resources, it requests information from the SME on their status and availability at a particular location or over a certain geographical area. The SME then conducts the predictions based on stored spectrum data and sends the spectrum

decision information to the SU. By continuously monitoring multiple frequency channels, $f$,

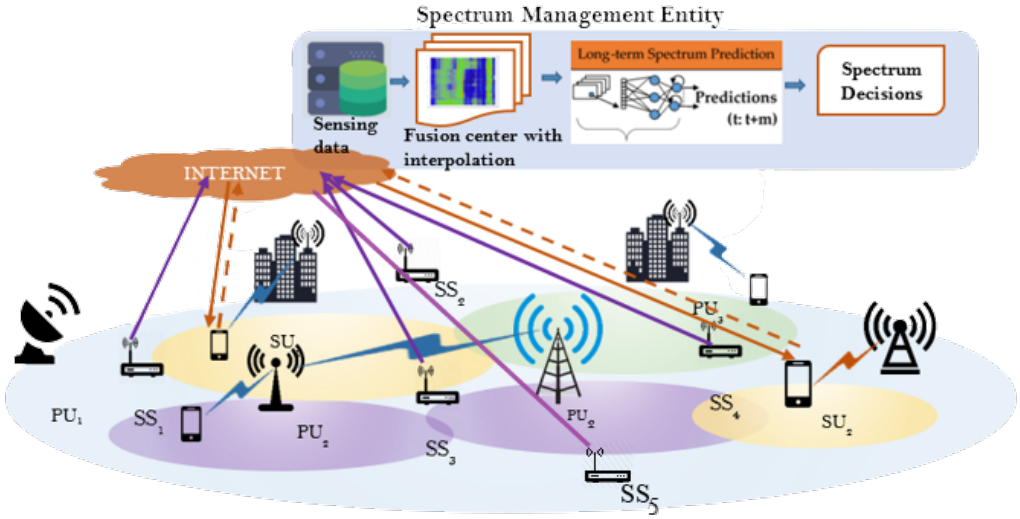


**Figure 2.1:** Cooperative SP system model.

SU and SSs (collectively referred to as the sensing nodes) send the received signal power level ($Pr$, which varies over time) to the SME. The received signal for a particular sensing node at location $i$ in $\mathbb{R}^2$ space is expressed as a time series data with $n$ historical observations as:

$$Pr_i(f, t-n:t) := Pr_i(f, t-n), Pr_i(f, t-n+1), Pr_i(f, t-n+2), \ldots, Pr_i(f, t) \tag{2.1}$$

where $n \in \mathbb{Z}$.

In defining the prediction problem, we considered two scenarios: providing long-term SP at a single location as presented in [88] or for multiple locations in a given area as shown [89]. In both cases, the cooperative long-term SP problem utilizes $Pr_i(f, t-n:t)$ to provide $l$ future SP $\hat{Pr}_i(f, t+1:t+l)$ as:

$$\hat{Pr}_i(f, t+1:t+l) := (Pr_i(f, t+1), Pr_i(f, t+2), Pr_i(f, t+3), \ldots, Pr_i(f, t+l)) \tag{2.2}$$

where $l \in \mathbb{Z}$.

Considering the random placement of sensing nodes and their limited number, we employed the IDW method for both combining and interpolation purposes. IDW is a deterministic method that assumes a stronger correlation among the spectrum data collected from the nearby sensing nodes. It does not require prior information about the characteristics of the measured data set. In IDW, weights are assigned to nearby nodes based on their distance from the location of the SU requesting cooperation. These weights are then used to calculate a weighted average of the spectrum data.

For a given location $i_m$ in $\mathbb{R}^2$, and for $M+K$ collected spectrum measurements from the sensing nodes, we defined a location-aware fusion algorithm as:

$$\underset{\substack{j\leq M+K\\ j\neq m}}{\mathcal{F}}\{Pr_{i_j}(f,t)\} = \sum_{\substack{j\leq M+K\\ j\neq m}} \omega_j * Pr_{i_j}(f,t) \tag{2.3}$$

$$\omega_j = \frac{d_j^{-\beta}}{\sum_{\substack{j\leq M+K\\ j\neq m}} d_j^{-\beta}} \tag{2.4}$$

where $\omega_j$ refers to the weighting coefficient between the location $i_m : \{x_m, y_m\}$ and $i_j : \{x_j, y_j\}$. $d_j$ is the Euclidean distance defined for location $i_m$ concerning each sensing node and $\beta$ is a power parameter also referred to as the distance decay exponent that governs the smoothness of the combination/fusion. $\beta$ is a user-defined parameter that controls the rate at which the influence of nearby points decreases with distance. The value of $\beta$ can range from 0 to infinity, with larger values indicating a faster rate of distance decay. When $\beta$ is set to 0, all spectrum measurements of different sensing nodes within the search radius have equal weights, regardless of their distance from the particular SU. $\beta$ can have an equivalency to the path loss exponent in radio signal propagation, in which the optimal value is generally determined after running a grid search between $(1, 6)$ [93].

Thus, the combined output from fusion center, $\bar{Pr}_{i_m}(f, t-n : t)$, for a given SU $m, m \in M$ located at $i_m$ expressed as:

$$\bar{Pr}_{i_m}(f,t) = \begin{cases} \underset{(j\leq M+K}{\mathcal{F}}\{Pr_{i_j}(f,\bar{t})\}, Pr_{i_m}(f,t)) & if Pr_{i_m}(f,t) \neq 0 \\ \underset{j\leq M+K}{\mathcal{F}}\{Pr_{i_j}(f,t)\} & \text{otherwise} \end{cases} \tag{2.5}$$

where $\mathcal{F}\{\cdot\}$ is the location-aware combing algorithm used in fusion center. If all SUs are in the

sensing phase, then the total number of inputs to the fusion center is equal to $M + K$. However, when some of the SUs temporarily halt their sensing functionality, the number of inputs is less than $M + K$. Considering the latter case, for a particular SU requesting information from the SME without conducting any sensing on its own, this knowledge can be granted by taking the sensing data from its neighboring sensing nodes. This act enables SUs to have SA without continuous sensing, which in turn increases their data transmission time.

Figure 2.2 illustrates the time slot structure we consider for SUs for sensing and non-sensing-driven SA. The time structure consists of three-time blocks, (i) $t_d$, time for data transmission for SU, (ii) $t_p$, time for SME to conduct data fusion and forecasting to provide SUs with decisions on the spectrum availability, and (iii) $t_s$, time for SU to conduct spectrum sensing before requesting cooperative spectrum decision from SME in Figure 2.2 (a) or time for SU to send location information using dedicated control channel in Figure 2.2 (b).

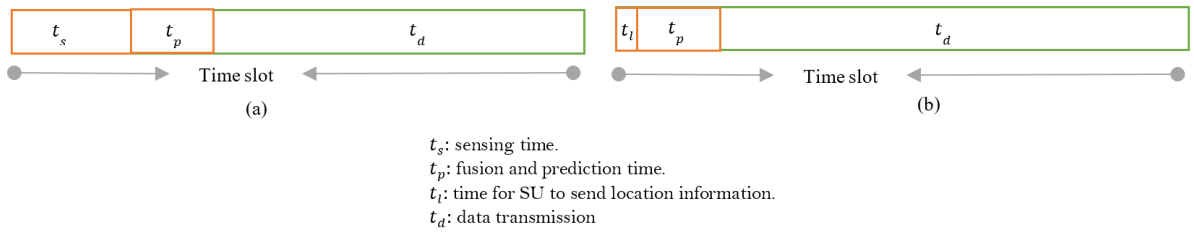


**Figure 2.2:** Time slot structure for SU (a) during the sensing phase, (b) during its non-sensing phase.

Furthermore, under the assumption that the specific spectrum channel, $f$, being occupied is represented by a value of $H_1$ and its availability by a value of $H_0$, error probability for cooperative spectrum availability detection is defined as [57]:

$$\mathcal{P}d_i(f,t) = \mathcal{P}\{\hat{P}r_i(f,t) \geq \lambda | H_0\} \tag{2.6}$$

where $\hat{P}r_i(f,t)$ is the predicted received signal at the j-th location in $\mathbb{R}^2$ space and $\lambda$ is the energy threshold used to determine occupancy for a particular channel $f$. $\lambda$ is set based on the sensing nodes noise floor at $f$ and margin added to ensure that the signal from a PU can be distinguished from the noise. For calibrated noise floor, a common practice is to set the $\lambda$ around -85 dBm to -75 dBm (where the threshold is 10-20 dB above the noise floor) [64].

### 2.2.2 Cooperative Spectrum Prediction

#### 2.2.2.1. Problem Definition for Single Location Cooperative Prediction

The problem of single-location prediction is defined for SUs that are stationary and seek to determine the long-term availability or status of various spectrum channels within a particular frequency band. If a block function $P(.)$ is used to represent the predictor model, then the long-term SP for $l$ time intervals is defined as:

$$\hat{Pr}_{i_m}(t+1:t+l) = P(\bar{Pr}_{i_m}(t-n:t)), \tag{2.7}$$

Where $\bar{Pr}_{i_m}(t-n:t)$ are $n$ past spectrum data as the combined output from fusion center for the SU $m$ location at $i_m$, and $l, n, m \in \mathbb{Z}$. The predicted $\hat{Pr}_{i_m}(t+1:t+l)$ is a multivariate time-series data represented as a Two-Dimensional (2D) (time and frequency) array. Utilizing

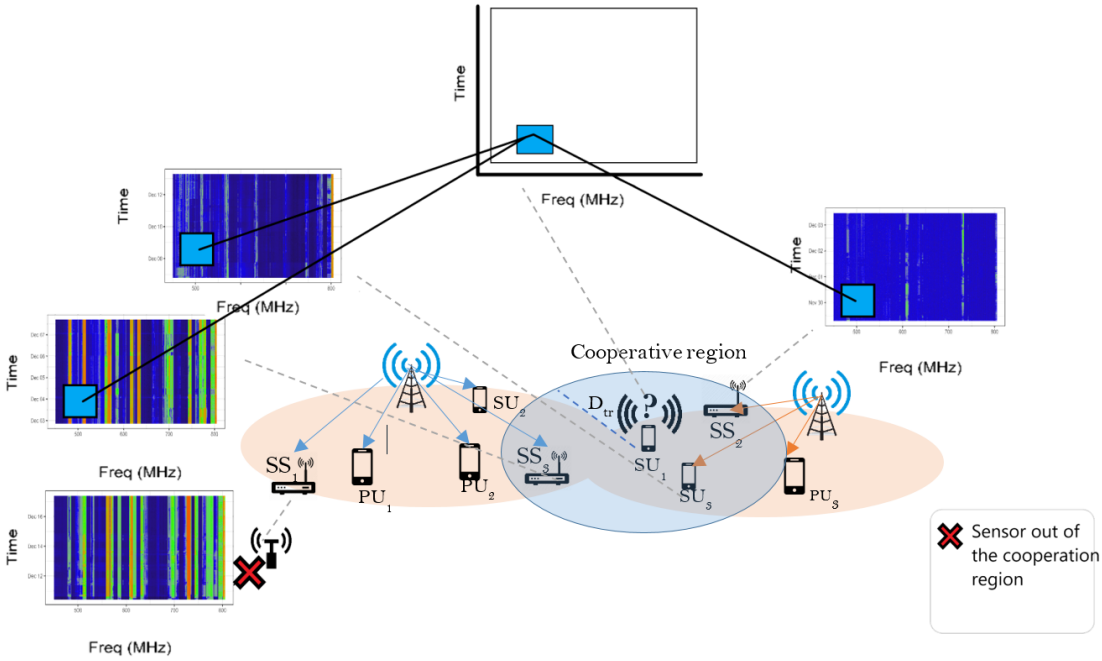


**Figure 2.3:** Cooperative region in a single SU prediction scenario.

the location information of the SU requesting SA from the SME and the locations of neighboring sensing nodes, Pearson's correlation coefficient among the time series datasets is assessed. This evaluation aids in selecting the group of collaborating SUs/ SS and defining the cooperation

region within a maximum threshold distance, $D_{th}$, as depicted in Figure 2.3. Here, the distance between each cooperating SUs/ SS $D_j \leq D_{th}$, and $D_j = ||i_m - i_j||$, where $j, m \in K + M$.

#### 2.2.2.2. Problem Definition for Multi-location Cooperative Prediction

The problem for Multi-location prediction is intended to provide spectrum utilization information not only in future time instances but also across various locations. In this scenario, we consider that a given SU, $m$, located at $i_m$ requests long-term spectrum availability predictions, and the SME provides the information in the form of a spectrum map for a specified spatial region. The spatial region of interest is divided into $X$ grids on one side and $Y$ grids on the

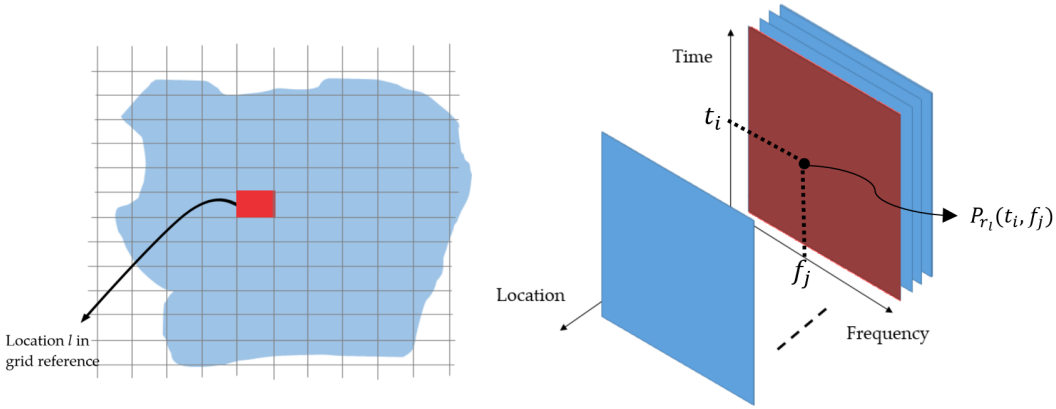


**Figure 2.4:** Grid referencing for a given spatial area where the interpolated value is represented as multidimensional time series data.

other side where randomly distributed sensing nodes, totaling $K + M$, are placed with each providing power level measurements $Pr_{i_j}$, where $j \in K + M$. The fusion center can then generate interpolated power level values $\bar{Pr}_{(x,y)}(f, t - n : t)$ for each grid denoted as $(x, y)$, where $x$ ranges from 1 to $X$ and $y$ ranges from 1 to $Y$. For simplicity, we adopt a grid referencing approach, where a specific location $I$ represents the grid in space $(x, y)$ defined for the square unit area. As depicted in Figure 2.4 the interpolated spectrum data forms a 3D array dataset where three attributes are time, frequency, $f$, and location, $I$.

In this scenario, the predictor model $P(.)$ learns the temporal and spatial dependencies in the multidimensional time series data with $n$ past observations to provide $m$ future predictions as:

$$\hat{Pr}(t + 1 : t + l) = P(\bar{Pr}(t - n : t)), \tag{2.8}$$

## 2.3 Long-term Spectrum Predictor Models

Creating effective prediction algorithms that accurately capture dependencies in space and/or time between spectrum measurements, while maintaining a low false alarm rate, is crucial. Long-term predictors must possess memory for extended temporal dependencies, and when both spatial and temporal availability are required, the model must be spatio-temporal. To address this, we proposed single-location and multiple-location cooperative spectrum predictors that are capable of leveraging the dataset available from spectrum measurements.

### 2.3.1 Single location Predictor Model

We proposed an LSTM-based predictor model with an encoder-decoder architecture to predict power levels for a specific location across a wide frequency and multiple time steps, as depicted in Figure 2.5.

The encoder segment comprises two LSTM layers, comprising 125 and 48 nodes, respectively.

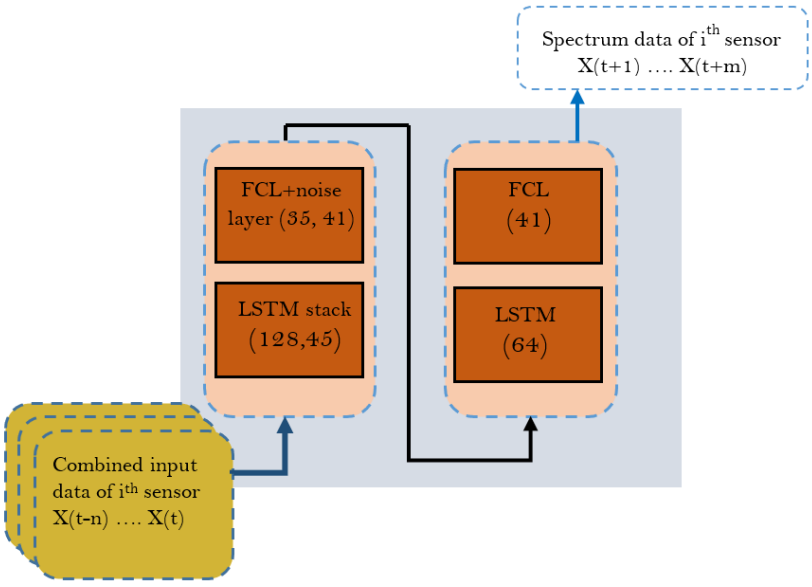


**Figure 2.5:** LSTM-based Long-term spectrum predictor model for a single location.

Additionally, we incorporated a Gaussian noise to introduce controlled noise during training, followed by a fully connected layer to process the hidden state outputs. The noise layer is essential at the encoder of the model as it acts as a regularizer to limit the model from over-fitting to the training dataset. In this case, the variance of the random noise is carefully configured to

ensure that it does not overshadow variations in power levels from the cooperative SUs. The encoder receives $n$ past observations for different channels $f$ as a 2D array, treating the input as multivariate data. The decoder component comprises a single LSTM layer with 64 nodes, followed by a two-dimensional fully connected layer to generate power level outputs $(l \times f)$ for $l$ time step predictions.

### 2.3.2 Multi-location Predictor Model

For multi-location long-term prediction, we proposed a ConvLSTM-based model as depicted in Figure 2.6. The model comprises two 2D-ConvLSTM hidden layers at the encoder and an LSTM hidden layer, which captures memory and hidden states from the encoder output. Additionally, there is a 2D-ConvLSTM hidden layer and a fully connected layer at the decoder. At the encoder's bottom layer, an $n$ sequence of $loc_{num} \times f$ dataset is received, where $n$ denotes the number of historical observations, and $loc_{num}$ and $f$ represent the number of grid locations considered and the multiple spectrum channels in a band, respectively. This dataset is filtered by a kernel with a stride of 1 sample. Similarly, on the decoder side, the dimensionality of the predicted output is given as an $l$ sequence of $loc_{num} \times f$ dataset, where $l$ represents the long-term prediction length. By simplifying the representation of space grids to location mapping, we

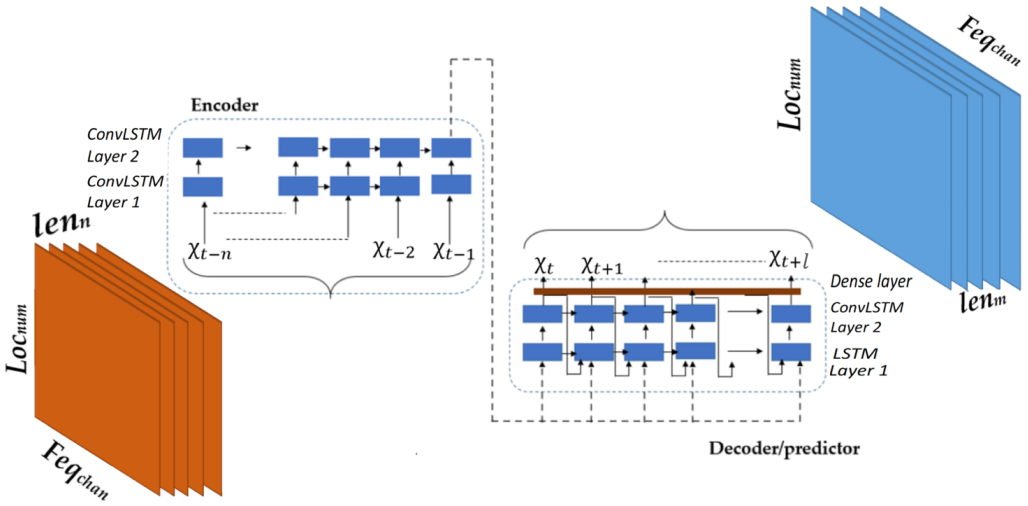


**Figure 2.6:** ConvLSTM based Long term spectrum predictor model for Multiple locations.

could use two-dimensional kernels with a minimal size of $3 \times 3$ at the bottom layer of the encoder and $1 \times 1$ at the top layer of both the encoder and decoder.

## 2.4 Spectrum Measurement and Dataset Description

To evaluate the performance of the proposed models, we used real spectrum measurement data obtained from the ***Electrosense*** open API. Electrosense runs a collaborative spectrum monitoring network, employing a variety of low-cost RF front-ends as SS deployed worldwide. These SS primarily utilize *RTL-SDRs* (version 3 or higher) as their RF front-ends. When paired with specialized frequency extension boards, this setup enables spectrum sensing across a wide frequency range, from lower bands up to 6 GHz [64].

Our initial model implementations, published in [88] and [89], were based on data from five sensors within a six-kilometer radius of Madrid, Spain, collected over five consecutive days across the 450 MHz - 520 MHz spectrum range. We extended our evaluations with longer monitoring data (over 30 days) and encompassed different frequency bands from an additional seventeen SS. Our focus primarily lies on assessing user presence and spectrum usage in sub-1 GHz frequency bands due to their extensive coverage and indoor penetration capabilities. This approach also enables us to utilize measurements from widely distributed SS.

The considered frequency range includes diverse wireless services and PU allocations, such as Digital terrestrial TV (DTT) broadcasting, cellular networks, and public safety networks. These frequency bands were analyzed to investigate spectrum predictability for various use cases. Table 2.1 provides a detailed summary of the spectrum bands, along with the time and frequency resolutions employed during the measurement process.

Regarding the real spectrum measurement data, we took the following baseline assumptions.

***Assumptions***:

- The energy level measured at a particular frequency, is considered to come from any of the sensing nodes (SUs or SS), placed outdoors at roughly the same receiving height.
- All SS are considered to be synchronized and data transmission delay to SME is neglected.
- All SS are noise calibrated to have an equal noise threshold with zero mean Gaussian distribution as $N(0, \sigma^2)$.
- The considered SME does not conduct any form of PU identification or signal classification.

- Any information regarding the operational parameters or the location of the PUs or SUs using the spectrum band is unknown.

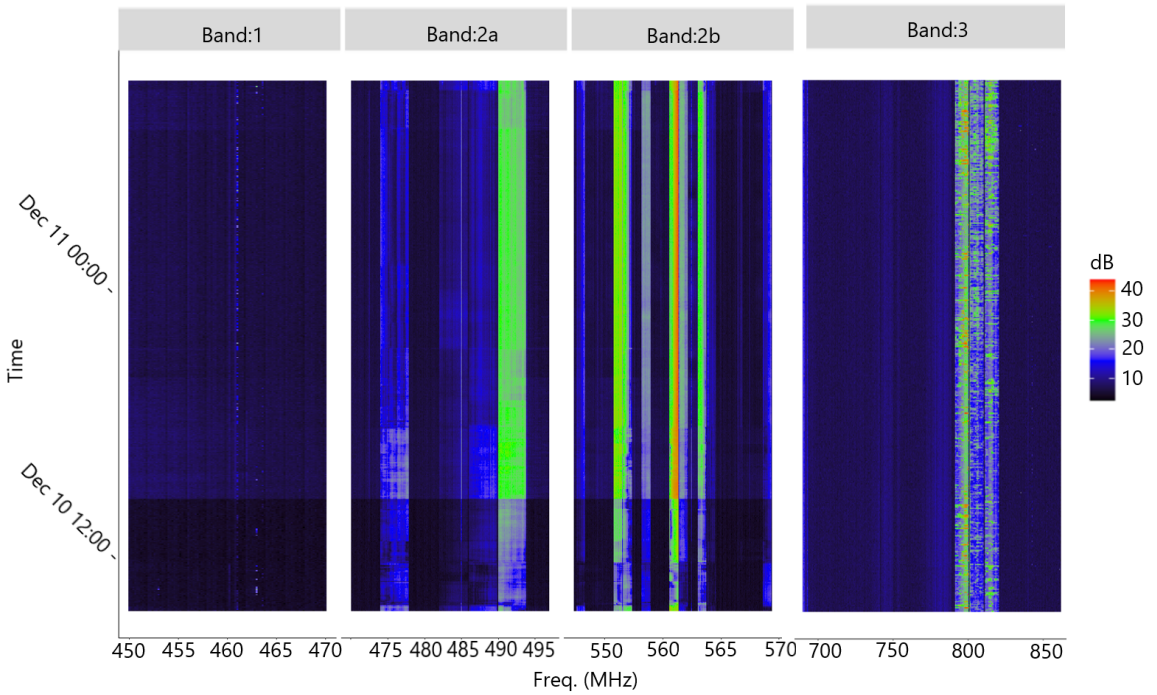


**Figure 2.7:** Two Hrs. real spectrum monitoring data from a single sensing node for a wide range of 450-826 MHz of frequency band.

Figure 2.7 displays the continuous measurement of received signal levels as a ratio with calibrated noise floor (SNR in dB) across a broad spectrum band (450-826 MHz) at a specific SS location. Given limited prior knowledge of PUs and the complexity of multi-PU-SU environments, accurately assessing received power at specific channels is essential for determining spectrum availability. While some lower spectrum bands exhibit consistent availability across multiple locations, availability in other bands varies significantly depending on the location and the type of PU service (broadcasting, cellular, or public networks). This variability is evident in Figure 2.8 for Channel 24 and 26 DTT bands and the LTE band 20 downlink band. In addition to considering real measurement data, we developed an experimental spectrum data set to emulate three spectrum usage scenarios as illustrated in Figure 2.9. These are the *repetitive* data set, which represents continuous usage of a single spectrum band over time; the *sequential* data set, which considers incremental and continuous use of frequency ranges over time; and the *random* data set, which represents a random spectrum user for a given time interval and frequency range. This data set is used to evaluate the LSTM-based predictor model.

**Table 2.1:** Spectrum measurement dataset.

| | **Spectrum Range** | **Exemplary PU Assignments in the region** | **Time granularity** | **Frequency Resolution (channel width)** |
|---|---|---|---|---|
| ***Band 1*** | **450-470 MHz**[a] | • LTE band 31: (UL: 452.5-457.5 MHz \|\| DL: 462.5-467.5 MHz ) *for Public safety networks*<br>• 460 MHz simplex Private Mobile Radio(0.250 KHz bandwidth) | 1 min. ; 3 min. | 200 KHz |
| ***Band 2-a & Band 2-b*** | **450-520 MHz** & **520-694 MHz** | DTT (Ch: 21- 48) or *TVWS Cognitive radio networks* | 3 min. | 200 KHz |
| ***Band 3*** | **790-862 MHz** | LTE band 20 (UL: 832-862 MHz \|\| DL: 791-821 MHz ) *for 4G/5G cellular Networks* | 1 min | 100 KHz |
| ***Band:4*** | **926-934 MHz**[b] | Portion of Band 08 (DL: 925-960 MHz) *for 2G cellular Networks* | 1 min. | 200KHz |

***a*** Part of the frequencies are considered in [88].
***b*** Part of the frequencies are considered in [89].

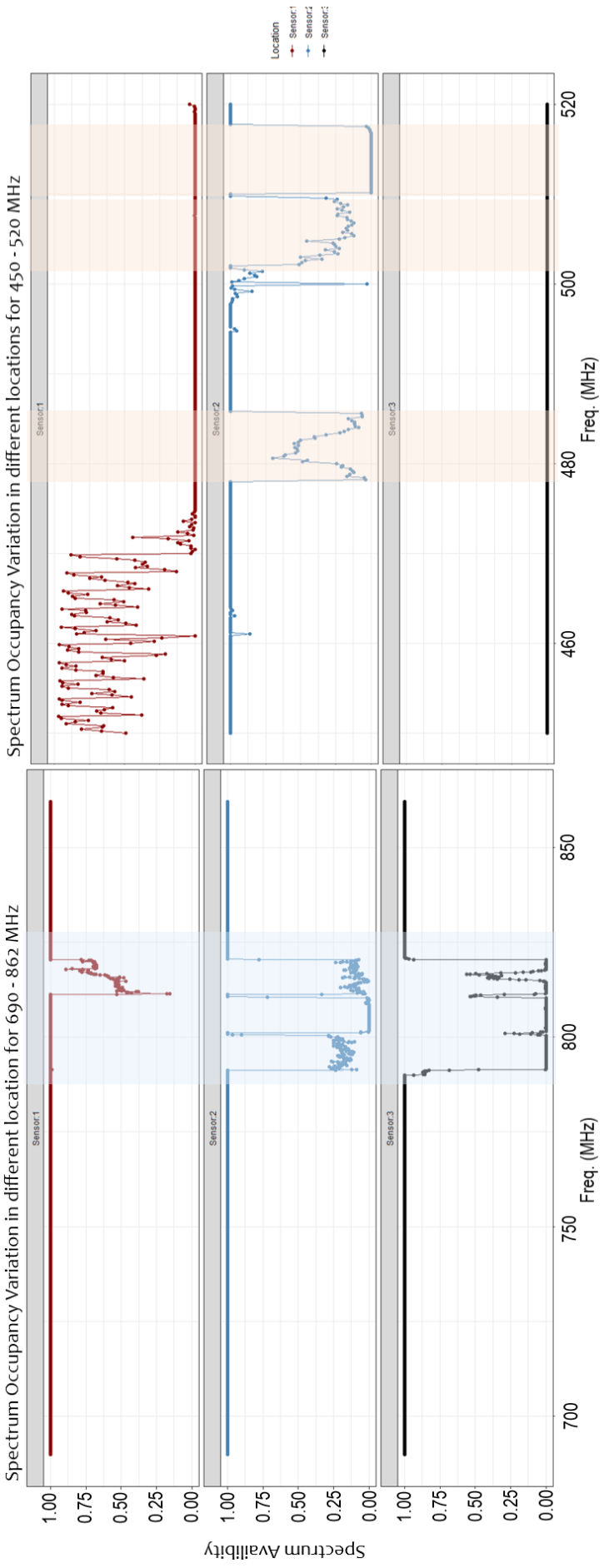


**Figure 2.8:** Spectrum availability rate in different spectrum bands considering three sample locations.

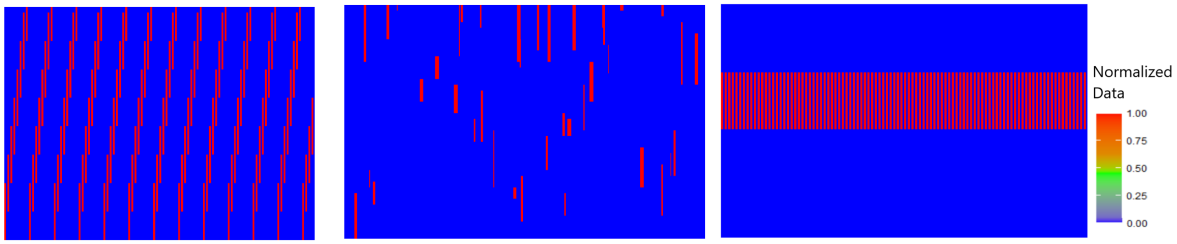


**Figure 2.9:** Sequential, Random, and Repetitive data samples from artificial spectrum measurement datasets.

## 2.5 Results and Discussion

### 2.5.1 Hyper-parameter Tuning

The training of both models is implemented using the TensorFlow framework in R 3.4 and Python 3.7. The model parameters are selected from the list in Table 2.2 with careful tuning using grid search. Layer dropouts are used in the Multi-location predictor model to reduce the effect of overfitting at both the encoder's and decoder's inner layers during the pre-training phase. Additionally, batch normalization is employed as a regularization technique. Selecting a good optimizer relies on its ability to handle non-convex problems and be robust with local minima during model convergence and finding optimal weights [94]. To that end, we selected the Nesterov accelerated adaptive moment estimation algorithm for optimizing the training due to its ability to converge faster with long-term sequential prediction tasks.

The training performance of the LSTM-based model, using MSE loss and a batch size of 8, showed improvement with the updated weights as the number of epochs increased up to 50, after which the performance saturated. For the Conv-LSTM-based model, varying the kernel size and batch size had the most significant impact. We found that a combination of $1 \times 1$ and $3 \times 3$ kernels and a batch size of 4 outperformed other combinations in the grid search and resulted in the minimum Mean Square Error (MSE) training loss.

### 2.5.2 Prediction Performance

The Prediction performance of the proposed models evaluated with the aforementioned datasets is discussed in the following subsections. For both models, the predicted output is based on

**Table 2.2:** Model training parameters for long-term SP.

| Model Parameters | Values | |
|---|---|---|
| | **Single location predictor model** | **Multi-location predictor model** |
| Optimizer | Nesterov accelerated adaptive moment estimation (NADAM) algorithm | |
| Learning rate | 0.0002 | 0.001 |
| Decay rates ($\beta_1$; $\beta_2$ ) | 0 ; 0.999 | |
| Training loss functions | MSE , MAE | |
| Dropout | - | 0.3 |
| Gaussian layer | Mean = 0<br>Variance = 0.2 | - |
| No. of layers | (1,2, 3) both for the encoder and decoder | |
| Kernel size | - | $(1 \times 1, 3 \times 3, 5 \times 5)$ |
| Batch size | (2,4,6,8,16) | |
| Epoch | (30 – 150) | |
| Occupancy threshold, $\lambda$ | 15dB above the noise floor | |
| Calibration noise floor | -130dBm/Hz | |

6 hours of past observations (or 120-time steps with a 3-minute temporal resolution [88]) to predict 2.5 hours (or 50-time steps with a 3-minute temporal resolution [88]) of spectrum usage status in terms of power levels for different blocks of the spectrum band from the dataset listed in Table 2.1. Both models are trained iteratively for randomly selected locations or grids (with a 50-meter by 50-meter grid unit) within the area of interest of the dataset.

To evaluate the accuracy of cooperative long-term prediction models in PU-SU or DSS environment, Root Mean Squared Error (RMSE) is used as a performance metric [66]. RMSE measures the average prediction error of the model over some time and is calculated as the square root of the mean of the squared differences between the predicted values and the actual values as defined in Equation 2.9.

$$\pi_{i_m} = \sqrt{\frac{1}{l \times f} \sum_{i=1}^{l} \sum_{j=1}^{f} (\hat{Pr}_{i_m}(j, t+i) - Pr_{i_m}(j, t+i))^2} \tag{2.9}$$

Where $\pi_{i_m}$ represent the RMSE for predicting Spectrum at particular location $i_m$. $\hat{Pr}_{i_m}(j, t+i)$ and $Pr_{i_m}(j, t+i)$ are defined for the predicted and actual spectrum usage data at location $i_m$ for frequency channel $j$ at time $t+i$.

In some cased, we evaluated scaled version of normalized RMSE as it is crucial to ensure the prediction errors are assessed by preserving the relative difference between error values. Thus, for normalizing the RMSE with in the range of [0,1.5] is defined as:

$$Norm(\pi_{i_m}) = 1.5 \times (\frac{\pi_{i_m} - min}{max - min}) \tag{2.10}$$

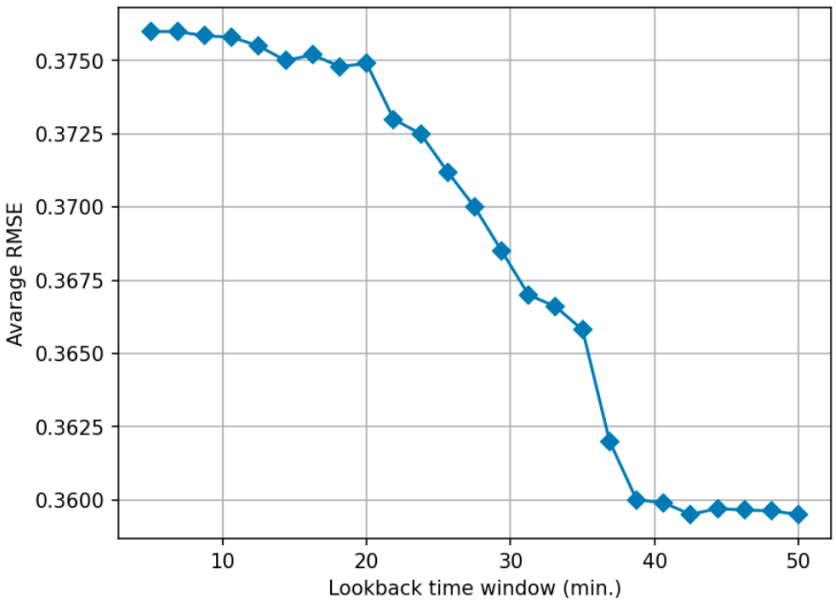


**Figure 2.10:** Prediction accuracy for single location predictor model as a function of the lookback time window at 694 MHz.

First, the analysis of the normalized RMSE for a single location predictor model against increasing past observations (lookback time window with 3-minute temporal resolution) in Figure 2.10 and 2.11. As shown in both figures, a decrease in normalized RMSE is observed with longer lookback windows demonstrating improved prediction accuracy. In Figure 2.10, the prediction performance of the single-location predictor, averaged for different SS, is evaluated for a frequency channel of 694 MHz [88] with a 3-minute temporal resolution. It shows an improvement of 0.015 with a maximum of 120 minutes of past spectrum monitoring data, providing 75 minutes of future predictions. Furthermore, considering the same prediction length (75 minutes of future predictions) and error measure, we expand the analysis for different frequency points in the *Band 2-b* spectrum block, as illustrated in Figure 2.11. This figure demonstrates the influence of PU's spectrum usage pattern on the length of the lookback window. For instance, the channels at 557 MHz, 570 MHz, 599 MHz, and 620 MHz correspond to UHF DTT channels 31, 33, 37, and 39, respectively. These channels are primarily allocated for broadcasting services

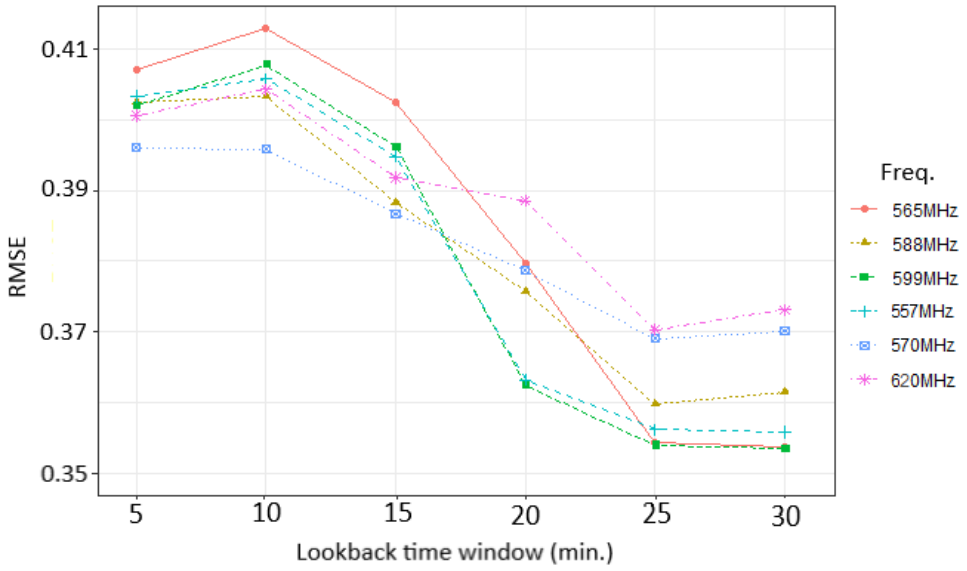


**Figure 2.11:** Prediction accuracy for single location predictor model as a function of the lookback time window.

in the region where the SS are deployed. The deterministic nature of spectrum occupancy in these channels means that increasing the lookback window allows the prediction models to better capture usage patterns, as evidenced by a sharp RMSE reduction up to a lookback of 60–75 minutes. Beyond this point, adding more historical data does not provide additional temporal information, resulting in minimal improvement in prediction accuracy. The location

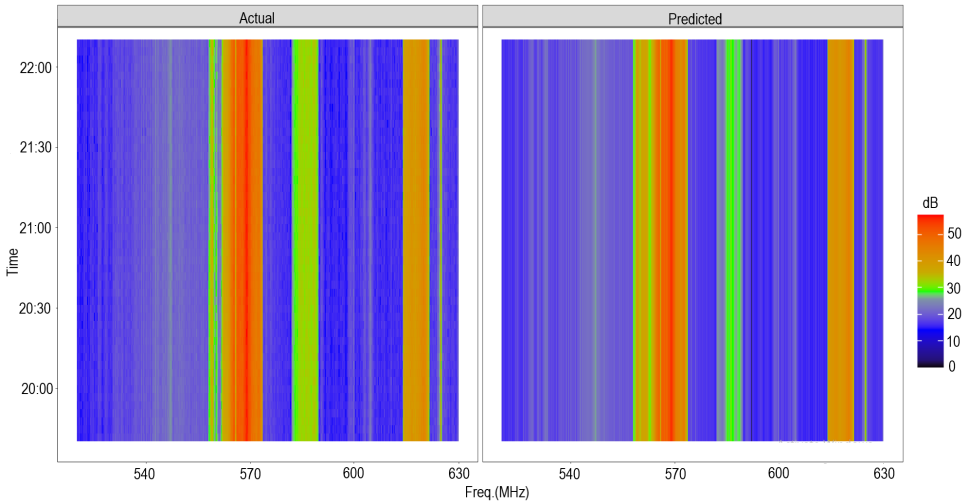


**Figure 2.12:** Single location prediction comparison between the measured spectrum data (left) and the corresponding predicted data (right) for the time slot of 3 Hrs. duration based on 6 Hr. past observation.

of PUs significantly affects how well these patterns are captured by the predictor. For instance,

channels 31 and 37 are assigned to community broadcasters with transmitters located near the SS deployment area, resulting in higher signal strength and quality. This proximity explains the lower RMSE for these frequencies compared to others, such as channels 33 and 39, where broadcasters are situated farther away. Conversely, other channels are only partially allocated, often for short-term use by secondary users (SUs) or for auxiliary broadcasting services during events. This irregularity makes it challenging for the predictor to effectively learn and project usage patterns for these frequencies This spectrum usage variation is observed in Figure 2.12 for frequencies in *Band 2-b*, where the prediction performance of single-location predictor model is presented with actual and the predicted power levels with only 75 minutes of lookback window.

Moreover, the synthetic data in Figure 2.9 was utilized to train and evaluate the performance of the single location predictor model. Since this data simulates error-free monitoring, the outcomes in Figure 2.13 are straightforward and interpretable. The model successfully captured the patterns and accurately provided long-term predictions in the first two pairs of plots (left to right) as their patterns are deterministic. This contrasts with the last pair of plots, which display random patterns representing the dynamic usage or spectrum occupancy by PUs. Table

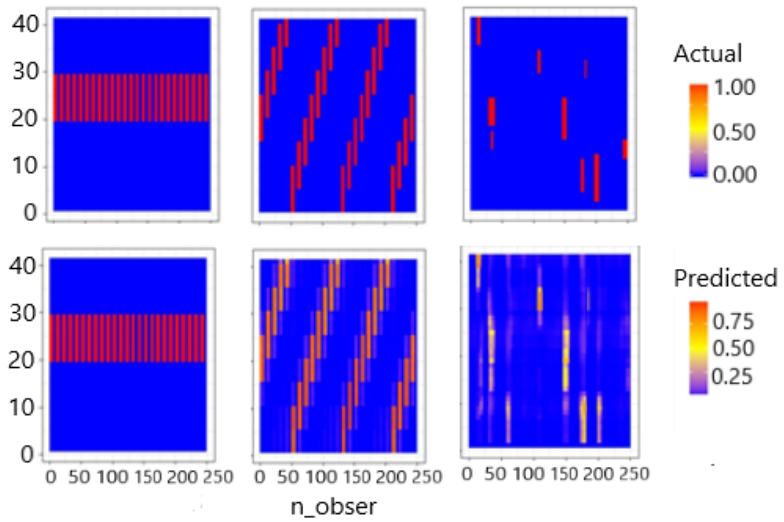


**Figure 2.13:** LSTM model verification for different datasets (the first row represents the actual data and the bottom row represents the predicted data).

2.3 compares the long-term prediction capabilities of the two proposed predictors. As shown, the single-location predictor in Band 1 achieves a slightly lower normalized RMSE, averaged over 100 frequency points (with a 200 kHz frequency resolution). This improved performance is attributed to the strong temporal correlation of the spectrum data in this band due to the

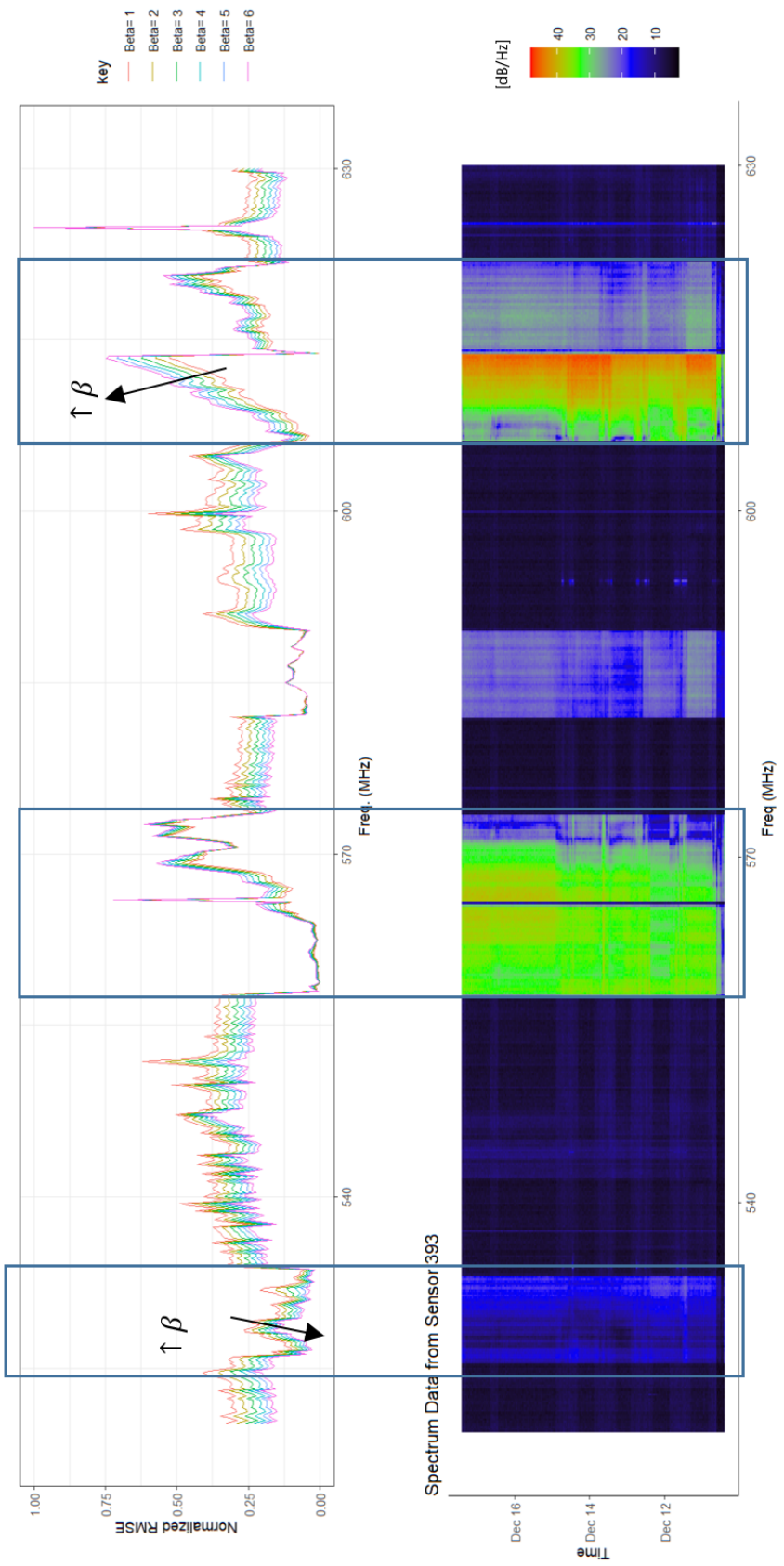


**Figure 2.14:** The impact of varying $\beta$ on the cooperation error at the fusion center for frequency band 520-694 MHz.

**Table 2.3:** Comparison on the prediction accuracy at different future time steps.

| **Models** | **Time steps** | Normalized RMSE | | |
|---|---|---|---|---|
| | | Band 1 | Band 2-b | Band 3 |
| Single-location predictor model | **1** | 0.009 | 0.018 | 0.095 |
| | **10** | 0.0164 | 0.062 | 0.0687 |
| | **20** | 0.0274 | 0.173 | 0.22 |
| | **30** | 0.0097 | 0.508 | 0.449 |
| | **40** | 0.274 | 0.809 | 0.715 |
| | **50** | 0.412 | 0.934 | 0.825 |
| | **60** | 0.702 | 1.349 | 1.191 |
| Multi-location predictor model | **1** | 0.0102 | 0.016 | 0.0177 |
| | **10** | 0.0219 | 0.058 | 0.532 |
| | **20** | 0.0642 | 0.193 | 0.177 |
| | **30** | 0.093 | 0.407 | 0.372 |
| | **40** | 0.316 | 0.716 | 0.691 |
| | **50** | 0.45 | 0.813 | 0.7451 |
| | **60** | 0.764 | 1.238 | 1.153 |

incumbent DTT service assigned to it. Conversely, for Band 2-b (870 frequency points with a 100 kHz frequency resolution) and Band 3 (720 frequency points with a 100 kHz frequency resolution), the multi-location predictor model demonstrates superior accuracy. This advantage is due to ConvLSTM's capability to account for the spatial correlation in spectrum data, despite the random usage patterns and weaker temporal correlation. Considering the same threshold for a maximum tolerable prediction error of 5 dBm (normalized RMSE of 0.85) as used in our original evaluation in [89], the multi-location predictor can achieve a minimum of 50 steps (or 2.5 hours) of future prediction in any spectrum band. However, the single-location predictor model cannot achieve the same. The sparsity of the sensing nodes, coupled with the decreased PU coverage area at high spectrum bands, limits the benefits of cooperative prediction, forcing the model to rely entirely on monitoring data from very few sensing nodes, if any.

To analyze the cooperation impact among the SUs/SS at the fusion center, we use optimal $\beta$ selection and error probability of spectrum availability detection as defined in Equation 2.6. As $\beta$ is the power parameter for the distance weighting factor, finding its optimal value indicates how well the fusion center can capture the distance-attuned correlation between spectrum data at different locations. Figure 2.14 depicts the cooperation error represented by normalized RMSE in different channels in *Band 2-b* for $\beta$ values ranging from $(1-6)$. For PUs spectrum usage with a wider coverage area, the received power level by different sensing nodes

is dominantly impacted by distance showing a direct relationship between increasing $\beta$ and normalized error due to combining as shown in the box at the left in Figure 2.14. However, the same explanation can't hold for the range frequency channels enclosed by the box on the right in Figure 2.14. This gave us an understanding that the spectrum correlation between different sparsely located sensing nodes at different frequencies is not majorly dependent on distance.

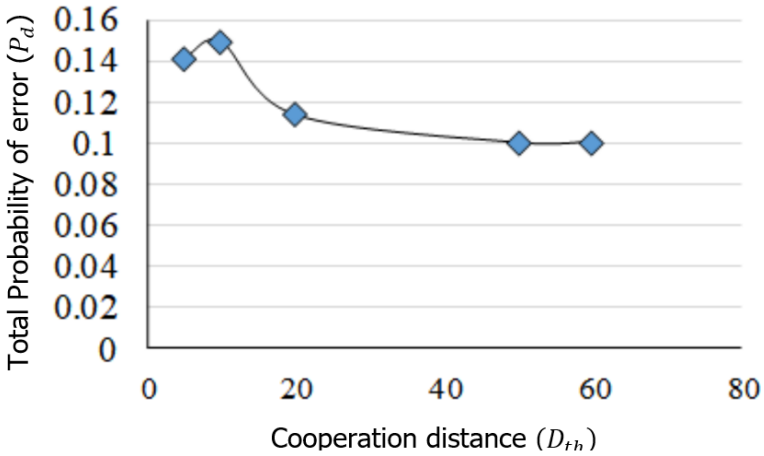


**Figure 2.15:** Total probability of error with a single-location predictor vs cooperative range at different frequency.

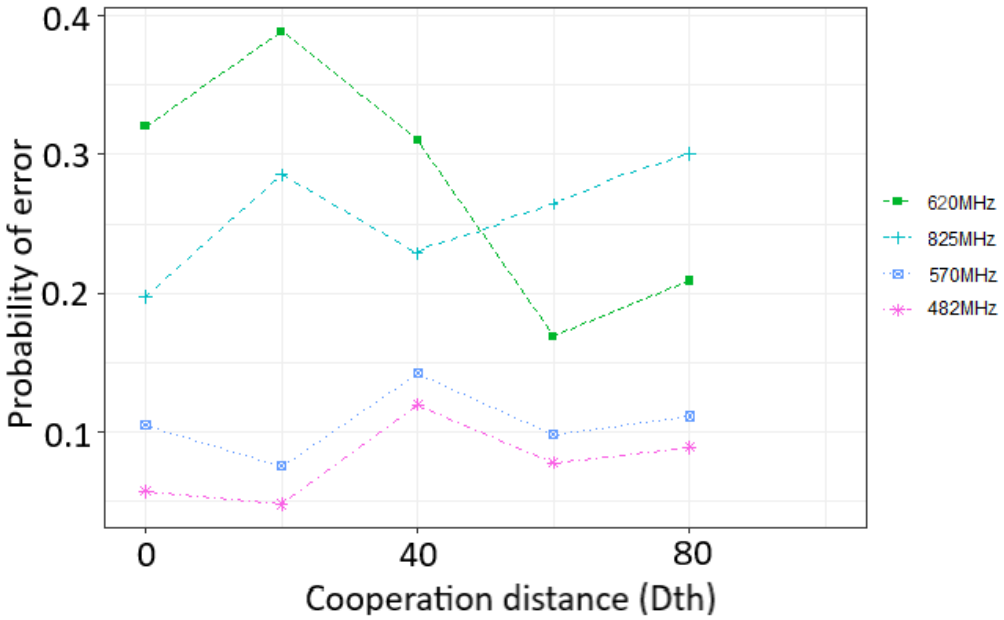


**Figure 2.16:** Average probability of error with a Multi-location predictor vs cooperative range at different frequency.

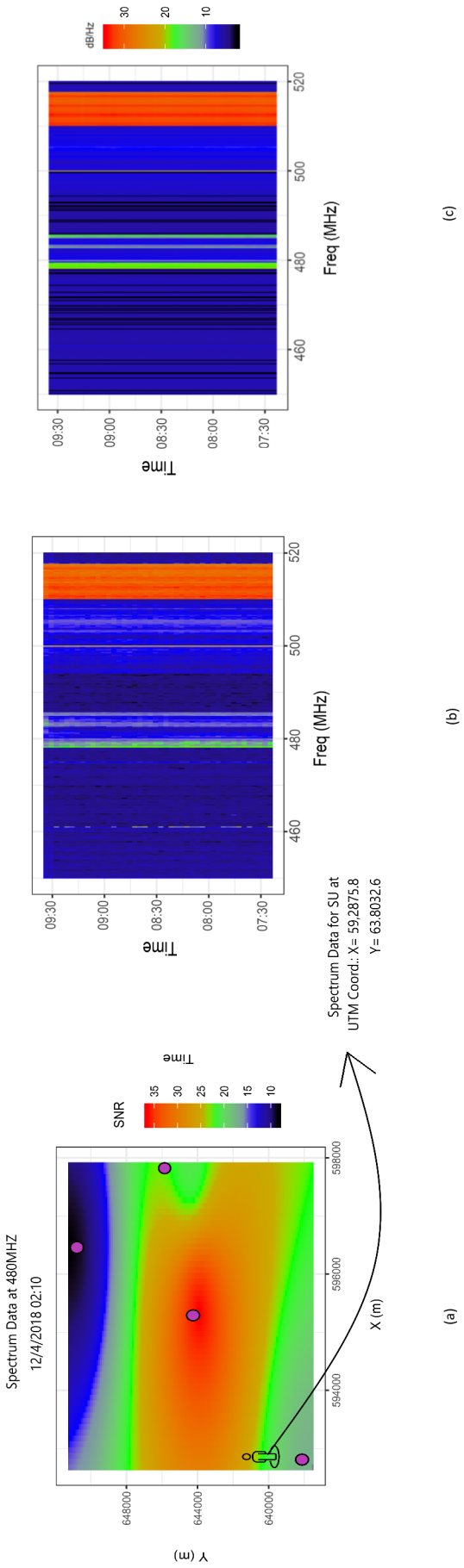


**Figure 2.17:** Comparison between the measured spectrum data (b) and the corresponding predicted data (c) for a time slot of 150 min. duration.

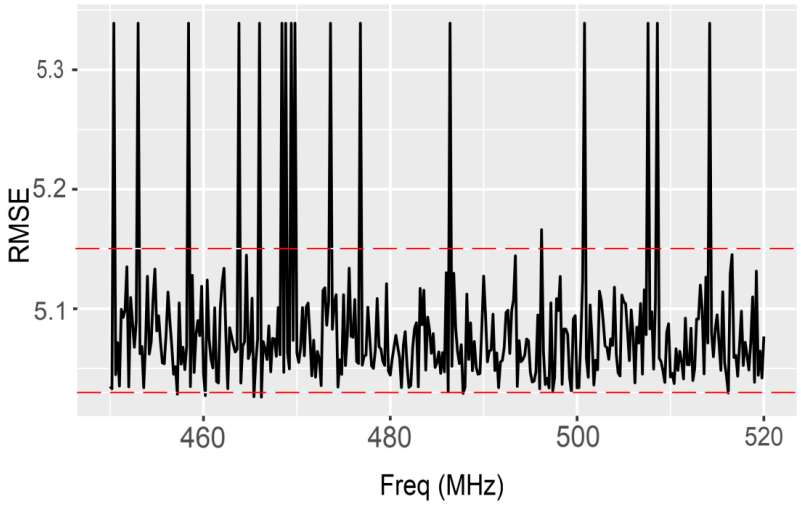


**Figure 2.18:** Average RMSE performance in different spectrum channels averaged for a given 4 square kilometers area.

The performance of the SS cooperation for both predictor models is evaluated by varying the cooperative range for selected SS locations or specific grids, particularly those near existing SS. The chosen location/grid is crucial in determining whether monitoring data from nearby SS will be considered. For a given occupancy threshold, $\lambda$, the cooperative error probability for spectrum availability detection is calculated using Equation 2.6. Without considering user mobility or environmental impacts such as shadowing and multi-path fading for the considered spectrum band (*Band 1*), Figure 2.15 shows that the average error probability for predictions made with a single-location predictor decreases as cooperative distance increases. A slight improvement of error probability 0.04 is observed for cooperative distances up to 30 steps (or 1500 meters), with no further improvement beyond that. This constitutes to the wider coverage area of PUs (terrestrial broadcasters) in the area with a strong received signal energy. For the multi-location predictor model, the error probability averaged over a given area as shown in Figure 2.16 exhibits varying results for different frequencies, primarily reflecting the inherent characteristics of signal propagation in higher frequency bands, wider PU coverage, or dynamic usage patterns. The higher error probability improvement by 0.15 is observed for cooperative distances of 1500 meters at 620 MHz as a result of the prediction conducted for multiple locations at once to create spectrum map. Ideally, increasing the cooperative distance (radius) is expected to improve the prediction error probability or keep it constant. However, due to the possibility of factors such as an more than PUs in the area or unidentified SUs at that frequency acting as an interference the variableness on the result.

Multi-location long-term predictions for signal energy levels are conducted across a bandwidth of 70 MHz within a selected area of 4 square kilometers. The prediction process uses 120 time steps (equivalent to 6 hours of past observations) to forecast output with dimensions of 50 time steps, covering 6,400 location points and 350 spectrum channels. An example of the prediction accuracy is presented in our paper [89] for a specific SU at a particular channel in Band 2-a. As shown in Figure 2.17, the smoothness of the prediction in Figure 2.17(c) compared to the actual monitoring data in Figure 2.17(b) highlights the model's effectiveness in capturing joint dependencies and long-term temporal spectrum usage patterns compared to short-term fluctuations. Furthermore, for a maximum tolerable prediction error of 5 dBm (RMSE of 5.1), the results presented in Figure 2.18 show that 95% of the averaged RMSE values deviate within 0.07 from the mean, indicating the stable prediction performance of the multi-location predictor network in different channels. This suggests the model's strong capability to perform well in high power levels and cases of more steady PU spectrum usage.

## 2.6 Chapter Summary

In this chapter, we proposed two DL-based predictors to enhance the accuracy of long-term SP in CRNs. These predictors were designed to capture extended temporal spectrum usage patterns and perform collaborative SP. Central to our solution is the use of a SME that analyzes historical spectrum monitoring data from SS over an extended period. The models exploit temporal, spatial, and spectral relationships, leveraging LSTM and ConvLSTM-based DL networks with a sequence-to-sequence architecture.

The single-location predictor utilized LSTM networks to predict signal levels for a range of frequencies at a specific location. For lower spectrum bands with deterministic PU usage patterns, such as DTT, the single-location model outperformed the multi-location predictor by 9.7%, providing predictions for up to 2.5 hours with a prediction error below 5 dBm. Furthermore, we observed that prediction accuracy improved with an increase in considered past observations and a greater number of cooperating SS, resulting in a wider cooperation region.

The multi-location predictor made use of a ConvLSTM network and a distance-based interpolation method, incorporating measurements from sparsely located cooperating SS to generate grid like structure spectrum maps. This approach enabled the model to capture the spectral-spatial and temporal dependencies, resulting in approximately a 14% improvement in prediction accu-

racy compared to the single-location model. The superior performance of the multi-location model was particularly evident for higher spectrum bands, with random usage patterns and relatively shorter coverage areas.

These results highlight the effectiveness of incorporating both temporal and spatial correlations in long-term SP, demonstrating that the multi-location approach significantly improves prediction accuracy, especially when network data is sparse or noisy. Additionally, the integration of more historical data and a wider cooperation region from SS further enhanced the model's ability to predict spectrum usage accurately.

# 3 Traffic-driven Spectrum Prediction for Mobile Network Operators

## 3.1 Introduction

Mobile data consumption is rapidly increasing due to widespread connectivity and innovative applications and services. According to a recent Ericsson report, by 2026, there will be 8.8 billion global mobile subscriptions, with mobile broadband accounting for 88 %. This growth translates to a fourfold increase in global traffic demand within the next five years [95].

However, this surge in demand presents significant challenges for MNOs, especially considering the limited available spectrum in the sub-6 GHz bands. With constraints on spectrum availability and dynamic shifts in user behavior driven by innovative applications, MNOs are compelled to optimize their currently allocated spectrum and explore innovative strategies to access additional spectrum when needed [96]. To that end, MNOs are adopting both Intra-operator and Inter-operator DSA approaches, enabling them to dynamically share and allocate spectrum resources among different users or applications based on real-time traffic conditions. Through these strategies, MNOs aim to enhance their spectrum utilization and alleviate network congestion [97, 98].

The successful implementation of DSA strategies depends on MNOs' ability to understand the complex dynamics of user demand and their network capabilities. This understanding necessitates continuous monitoring of network operations, related to coverage and capacity, radio resource allocation, and channel availability within designated frequency bands. MNOs collect various data related to these factors using methods such as field trials, dedicated sensing networks, and network-level monitoring. The data encompasses *radio-layer* information, such as Reference Signal Received Power (RSRP) and SNR, as well as *network and link layer* information, which includes details of network configurations, Call Detail Records (CDRs), cell-level Key Performance Indicators (KPIs), uplink and downlink data throughput, comprehensive traffic load data and much more [99, 100].

In the previous chapter, we explored radio-layer information to gain insights into spectrum usage at the SU level on wider frequency bands. However, acquiring and processing such radio-layer data can be resource-intensive and time-consuming, especially when dealing with large-scale data collection efforts. Conversely, continuous network-level monitoring at various mobile network stages provides access to network and link layer information, which offers different perspectives that indirectly reflect spectral resource utilization [96]. This prompts the question of whether we can leverage the correlation between network and link layer information, such as data and voice traffic volume, to develop a comprehensive understanding of MNO's spectrum utilization across different times and locations.

Predicting spectrum utilization based on traffic information is complex due to the dynamic nature of traffic patterns and the nonlinear relationship between traffic demand and spectrum usage. To address this complexity, we have introduced two approaches for predicting spectrum utilization. These approaches leverage DL models, specifically CNNs and LSTM-based models, along with real-time aggregated voice and data traffic volume information obtained from the operator's network [90, 91]. We argue that by appropriately mapping traffic volume to the spectrum channel utilization and then implementing DL models (or vice versa), as outlined in both of our papers, we can accurately capture the dynamic and nonlinear nature inherent in traffic or utilization data. Moreover, clustering distinct traffic or channel utilization patterns to account for spatial dependencies, along with incorporating additional explanatory parameters such as the number of active users and allocated radio resources, holds significant promise in enhancing the accuracy and reliability of spectrum utilization prediction.

Towards that end, this chapter presents our works from the following publications.

- **Paper 1:** Bethelhem. S. Shawel, Frehiwot Bantigegn, Tsegamlak T. Debella, Sofie Pollin, and Dereje H. Woldegebreal. *"K-Means Clustering Assisted Spectrum Utilization Prediction with Deep Learning Models"*. 2022. Engineering Proceedings 18, no. 1:2.

- **Paper 2:** Bethelhem. S. Shawel, Endale Mare, Tsegamlak T. Debella, Sofie Pollin, and Dereje H. Woldegebreal. *"A Multivariate Approach for Spatio-temporal Mobile Data Traffic Prediction"*. 2022. Engineering Proceedings 18, no. 1: 10.

## 3.2 Overview of Mobile Network Architecture and Monitoring

The allocation of radio resources varies significantly across mobile technologies, influenced by factors such as network architecture, traffic demand, interference conditions, service performance requirements, and spectrum availability. Our research [91] analyzed mobile data traffic from LTE networks, emphasizing the characteristics of data traffic and integrating additional contextual information. Building upon this foundation, this dissertation extends the analysis to evaluate how predicted traffic correlates with spectrum resource utilization. Additionally, in [90], we examined voice traffic loads on GSM communication networks to estimate spectrum utilization. These studies primarily focus on aggregated traffic data at the Radio Access Network (RAN) level across Addis Ababa, Ethiopia. To give a broader overview, an overall

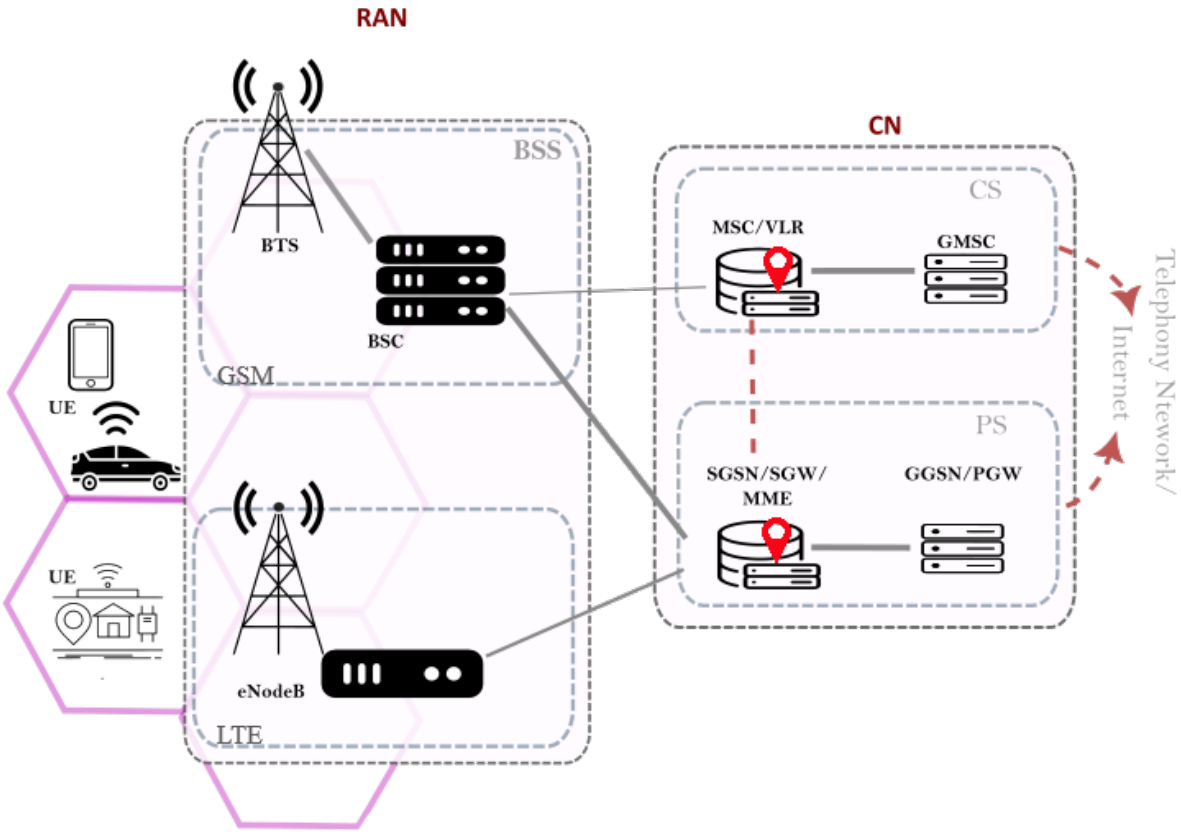


**Figure 3.1:** An Overall mobile communication architecture for GSM and LTE technologies and core-level network.

architecture for GSM and LTE mobile networks is outlined in Figure 3.1. These networks

comprise three primary components: User Equipment (UE), Radio Access Network (RAN), and Core Network (CN). UE devices, encompassing smartphones or machine-to-machine (M2M) communication devices, connect to the mobile network to avail of voice or data services. The RAN, which includes base stations and control units (separately in GSM and jointly as a single unit in LTE), provides wireless access by allocating radio resources to individual UE. Lastly, the CN, serving as the central component, facilitates call and data processing, mobility management, and connectivity services among diverse segments of the RAN and external networks, such as the Public Switched Telephone Network (PSTN) and the Internet.

Voice and text services from UEs in GSM networks are routed to the Circuit Switched-CN for call setup, management, termination, and SMS messaging. Conversely, the Packet Switched (PS)-CN, primarily comprising the Mobility Management Entity (MME), Serving Gateway (SGW), and Packet Data Network Gateway (PGW) in LTE, handles all data (IP-based) services. Although LTE supports voice calls over IP networks, MNOs often activate the 2G/3G circuit-switched fallback option (CSFB) for LTE voice services, ensuring call quality and cost-effective UE connectivity.

MNOs typically have network monitoring systems implemented at various stages of their network infrastructure to quality voice and data service delivery. These enable them to capture KPIs and comprehend detailed voice and data transfer activities. Generally, gathering information from individual UE through crowd-sourcing or at the RAN-level offers a temporally and spatially granular insight into mobile traffic and network performance, aiding in efficient radio/spectral resource utilization. This type of information is also particularly useful for enabling opportunistic spectrum use (as a SU) at the UE level. However, acquiring such data entails additional computational and storage overhead. Conversely, CN-level data collection allows for more efficient monitoring of mobile traffic and provides comprehensive network information with fewer measurement points. Unlike RAN-level data, which focuses on individual UEs and base station activities like intra-handovers, CN-level data encompasses signaling related to voice and data traffic tunneled through the CN from multiple RANs. MNOs often collocate different-generation CNs (e.g., LTE), facilitating comprehensive traffic and information collection [96, 97]. Additionally, since the CN oversees multiple RANs, it can associate location information with collected mobile traffic statistics at the base station level, facilitating Inter-operator DSS.

**Table 3.1:** Voice and data traffic dataset parameters.

| | Voice traffic | Data traffic |
|---|---|---|
| **Temporal resolution (Hr.)** | 1 | 1 |
| **No. of base station/eNodeBs** | 639 | 739 |
| **Total data instances (in days)** | 100 | 120 |
| **Operating freq(MHz)** | 900<br>1800 | 2100 |
| **Max. Allocated Bandwidth(MHz)** | 8 | 20 |

## 3.3 Mobile Traffic Dataset Description and Analysis

### 3.3.1 Dataset Description

In our research, we utilized RAN-level aggregated data collected from the CN of GSM and LTE networks from Ethiopia's telecom operator, Ethio Telecom. This data, summarized in Table 3.1, was collected over various time frames with specific temporal resolutions. For GSM network voice service performance analysis, we examined KPIs such as call setup success rate, aggregated cell traffic, and allocated channel numbers per cell, obtained from the GSM network's Mobile Switching center (MSC). Similarly, for data services, we focused on cell-level KPIs for both downlink and uplink traffic, throughput, and success and failure rates of radio resource access requests. These KPIs were gathered at SGW for LTE networks. In addition to the aforementioned KPIs, our dataset included supplementary information such as base station location data and the number of active and maximum users supported per cell, along with corresponding time stamps.

### 3.3.2 Mobile Traffic Analysis

When analyzing the time series properties of aggregated voice and data traffic, Figures 3.2 and 3.3 reveal notable temporal and spatial variations, unveiling discernible patterns. Despite the relatively brief observation period depicted in Figure 3.2, a consistent upward trend over time in voice and data traffic,respectively, is evident, indicative of the expanding mobile subscriber base and increased utilization of mobile services. The impact of event-driven surges in demand

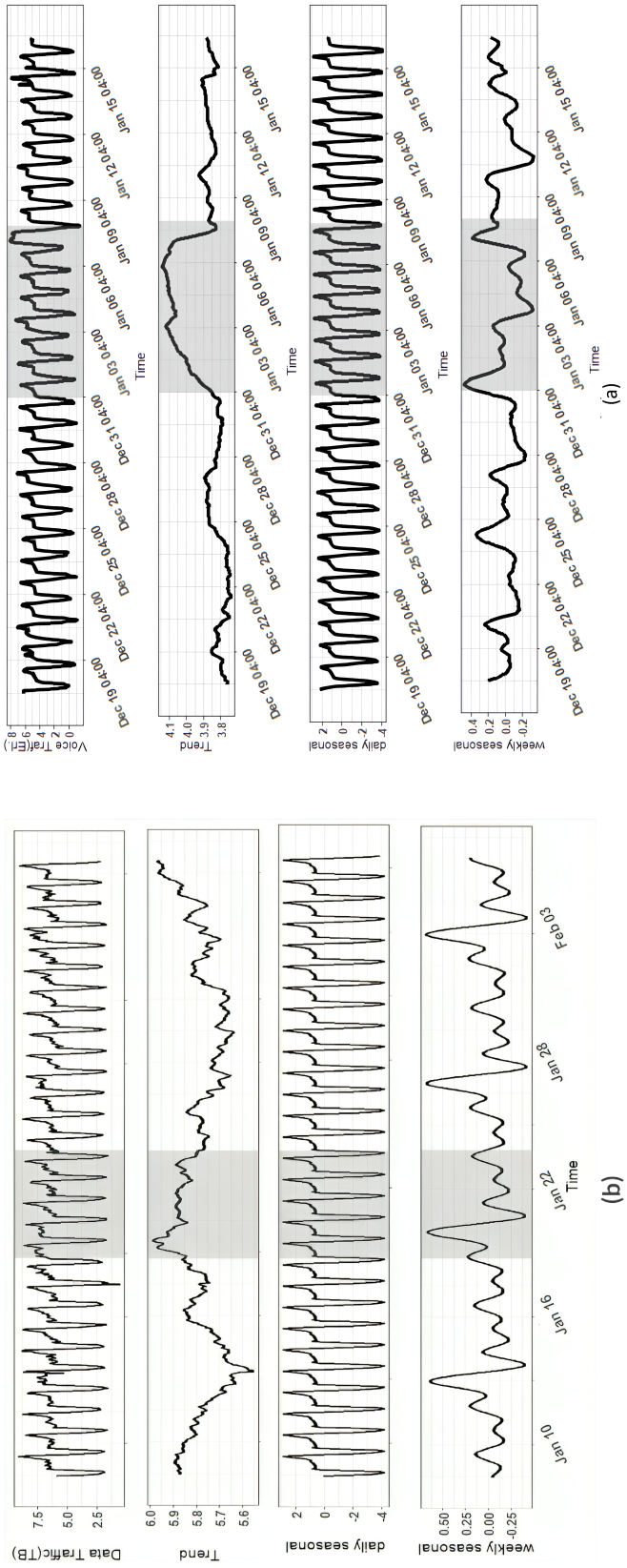


**Figure 3.2:** Temporal dynamics of voice (a) and data (b) traffic decomposed to trend, and seasonal (daily and weekly) components.

on overall trends is conspicuous, as depicted by the gray shaded areas on the Figures. These deviations from typical traffic patterns necessitate proactive measures from MNOs to ensure network quality and meet customer expectations during peak periods.

Both voice and data traffic exhibit daily periodicity, as illustrated in Figures 3.2, with peak demand occurring during specific hours and decreasing in the early morning hours, aligning with typical usage patterns. Additionally, weekly seasonality is apparent, with higher traffic volumes observed on certain days within the week. These temporal correlation, as observed in Figure 3.2, indicates a connection between current and past observations of voice and data traffic, offering potential for predictive modeling. These time series characteristics inform the development of traffic demand prediction models and traffic-utilization mappings, considering their unique impacts on prediction accuracy. Spatial variation and correlation are also crucial

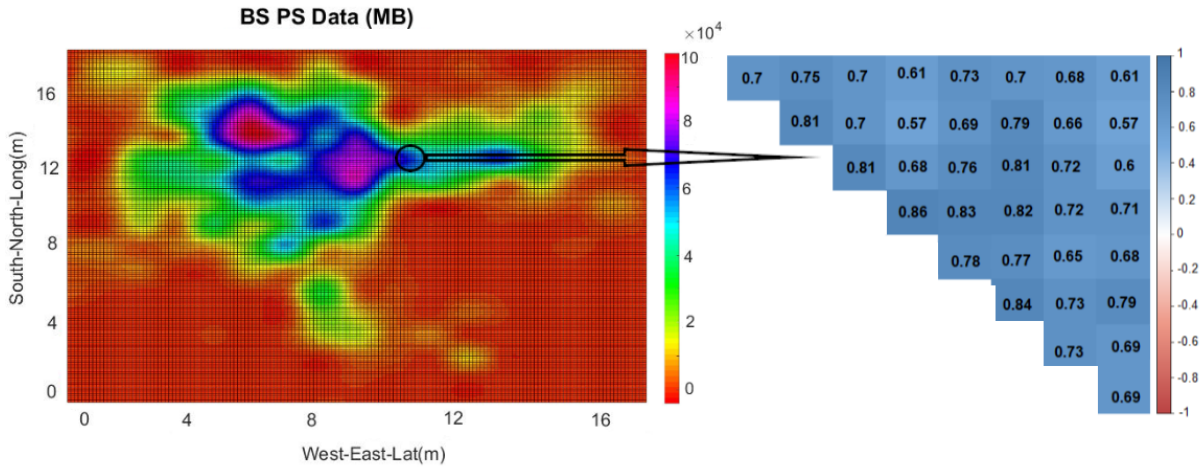


**Figure 3.3:** Spatial distribution of the mobile traffic load and correlation matrix for selected neighboring base stations.

characteristics of mobile traffic, essential for understanding and optimizing cellular networks. Figure 3.3 provides insight into the spatial distribution of data traffic volume among neighboring base stations [101], emphasizing the importance of examining traffic patterns in both spatial and temporal dimensions. As UEs move within the cellular network, traffic patterns across neighboring base stations exhibit correlation and complementarity, as evidenced by high Pearson correlation coefficients exceeding the 0.6 threshold in Figure 3.3. This highlights the necessity of developing predictive models and spectrum utilization mappings that incorporate both spatial and temporal dimensions, offering valuable insights for MNOs.

Spatial analysis can be approached through grid-based or cluster-based methods. The former

involves partitioning a service area into uniform grids, treating base stations within each grid cell as a unit. However, modeling large areas with fine-granularity grids poses challenges due to the non-uniform distribution of base stations. The latter approach, being more flexible, divides the service area into clusters, allowing for the analysis of traffic demand within each cluster and addressing the limitations of grid-based methods. In our papers, we opted for the cluster-based approach due to non-stationarity in traffic volume datasets and its adaptability to real-world network scenarios. Regardless of the method chosen, considerations underscore the intricate interplay between spatial and temporal aspects in mobile traffic analysis, providing insights crucial for enhancing resource allocation and utilization.

## 3.4 Mapping Mobile Traffic to Spectrum Utilization

The allocation of spectrum resources in mobile networks is influenced by the type of traffic being carried, with voice and data traffic having distinct requirements. Based on that, we define general mapping representation of spectrum utilization as a function of traffic load given as:

$$C_k(t) = \mathcal{F}(T_k(t)) \tag{3.1}$$

where $T_k(t)$ is the time-varying aggregated traffic Volume monitored at a particular base station $k$ and $\mathcal{F}(.)$ represents the specific traffic-channel mapping function used to relate the transported voice/data traffic and the assigned channel bandwidth. The focus lies on having information about the allocated spectrum utilization for MNOs, which is determined indirectly by examining voice traffic in GSM networks and data traffic in LTE networks. Thus, we have undertaken the task of associating traffic data with spectrum utilization using established industry methods and approximate approaches.

### 3.4.1 Voice Traffic Mapping

Voice traffic, primarily associated with traditional voice calls, is a narrowband service with relatively low bandwidth requirements compared to data traffic. A key factor contributing to the efficient utilization of spectrum in voice traffic is the fixed and predictable nature of voice call data. Voice calls entail relatively stable bandwidth requirements and are less susceptible to fluctuations in network conditions. This enables MNOs to allocate a fixed amount of channel

resources for voice traffic, ensuring that the necessary resources are available for voice calls without significant variations.

The correlation between the utilized radio spectrum and traffic load is relatively straightforward for voice traffic. For instance, if an MNO obtained a total of $Bw$ MHz GSM band and uses $r$ frequency reuse factor, the maximum number of Traffic Channel (TCH) per sectored-RAN (or GSM cell) can be estimated as:

$$TCH_C = (\lfloor \frac{Bw}{CH_{Bw}.r} \rfloor .TDMA_{ch}) - SDCCH_{no} - BCCH_{no} \tag{3.2}$$

where $CH_{Bw}$ refers to the 200 KHz GSM channel bandwidth and $TDMA_{ch}$ indicates number of time slots. The $SDCCH_{no}$ and $BCCH_{no}$ represent the number of control channels dedicated to carrying signaling information and sending broadcasting information.

Considering calls arriving in a Poisson stream of rate $\lambda$ each with average holding time $H$, the traffic is measured in Erlang as $A = \lambda \times H$. When calls find all channels being busy, they will be blocked and turned away from the system. Thus, for a given blocking probability as a grade of service (GoS) measure for network availability, it is essential to calculate the traffic that can be offered ($A_o$) by the configured traffic channel, $TCH_C$, using Erlang B formula as [102]:

$$B(A_o, TCH_C) = \frac{\frac{A_o^{TCH_C}}{C_{TCH}!}}{\sum_{i=0}^{C_{TCH}} \frac{A_o^i}{i!}} \tag{3.3}$$

However, the traffic load ($A_l$) carried by the trunked channels can vary depending on several factors, including geographical location, time of day, user behavior, and the supported TCH rate (full or half rate). For instance, assuming Erlang B service with a grade of service (GoS) of 98% network availability ($B = 2\%$), the GSM cell-level Spectrum utilization can be computed as:

$$U(\%) = \left( \frac{C_U}{C_{TCH}} \right) x\ 100\% \tag{3.4}$$

$$= \left( \frac{Erl_{Capacity}(A_l, 2\%)}{C_{TCH}} \right) x\ 100\% \tag{3.5}$$

where $Erl_{Capacity}(A_l, 2\%)$ is the utilized channel calculated from Equation 3.3. Given the traffic volume carried on Half rate TCH (TCH/H) and TCH(Erl), $T_{TCH}$ and $T_{TCHH}$ respectively, Equation

3.5 can further be approximated[5] as:

$$U(\%) \approx \left( \frac{C_{TCH}}{C_{TCH}(1 + \frac{T_{TCHH}}{T_{TCH}})} \right) x\ 100\% \tag{3.6}$$

Figure 3.4 shows the calculated 900 MHz GSM band utilization, based on Equation 3.6, for a

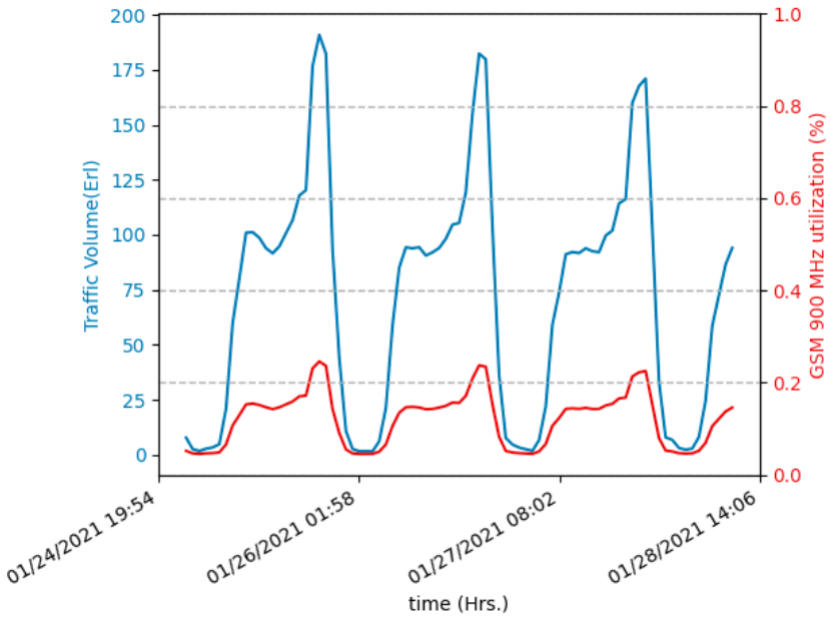


**Figure 3.4:** Spectrum utilization mapping from voice traffic volume at a GSM cell.

particular base station and shows the positive correlation between traffic volume and spectrum utilization with maximum utilization going up to 45%.

### 3.4.2 Data Traffic Mapping

In comparison with voice traffic, data traffic exhibits bursty characteristics primarily due to the diversity of service types, real-time service demands, and variable bit rates. The data rate variability in LTE networks allows bursts of high-speed data transmissions, such as those required for downloading large files or streaming high-definition media through applications like Facebook, YouTube, or TikTok [95]. Additionally, services demanding real-time responsiveness, like video conferencing or online gaming, necessitate intermittent bursts of data to maintain consistent user experiences.

5 industry specific approximation

This irregularity in observed data traffic leads to unpredictable peaks in bandwidth demand, making it challenging to find an appropriate mapping of CN-level aggregated traffic to spectrum resource utilization. To address this, we focus on simplified consideration of the cell traffic Volume and the associated required spectrum resource.

The aggregated traffic Volume ($T_{agg}$) per cell (in uplink or downlink) can be approximated as:

$$T_{agg} \approx Thr.Nu_{avg}.\frac{3600}{8} \tag{3.7}$$

where $T_{agg}$ represents hourly aggregated cell traffic in Bytes and $Thr$ is the physical layer data throughput per user in units of bits/seconds. The $Nu_{avg}$ represents the average number of active users per cell that the network can simultaneously support.

Evaluating the data throughput indicates the physical layer performance of the network, which directly depends on factors such as system bandwidth, the network's ability to allocate a large number of Physical Resource Block (PRBs) for data transmission, the use of advanced modulation schemes (depending on channel or service type), and the use of multiple antenna schemes. In the LTE frame, Resource Element (RE) represents the smallest spectrum resource in the form of a frequency-time grid, and a single PRBs contains 168 REs in 1 ms (12 sub-carriers each with 15 KHz spacing by 14 symbols). The scheduler in the eNodeB is responsible for continuously monitoring the channel conditions and QoS requirements of each UE and allocating one or more PRBs among users for each transmission time interval of 1 ms. This allocated PRBs, $PRB_a$, is used to carry both data traffic and signaling information such as broadcast channels, synchronization signals, reference signals, and control channels. Thus, downlink data throughput can be estimated as [103]:

$$Thr \sim RE_T(PRB_a).(1 - \Gamma_s).B_s.C_r.m \tag{3.8}$$

$RE_T(PRB_a)$ indicates the total REs, which is a function of the $PRB_a$ defined per user in 1 sec as $168.1000msec.PRB_a$. Based on the selected modulation and coding scheme, the code rate ($C_r$) and the bits per symbol $B_s$ for the modulation scheme used (QPSK, 16-QAM, 64-QAM, 256QAM) are defined. $\Gamma_s$ is the ratio of REs allocated for control channels over $RE_T(PRB_a)$. $m$ depends on the input-output multi-antenna technique used (1x1, 2x2 MIMO or 4x4 MIMO). Finally, the spectrum resource utilization in LTE networks, $C_u(\%)$, can be estimated as:

$$C_u(\%) = \frac{PRB_a}{PRB_m} \times 100 \tag{3.9}$$
$$:\sim \frac{T_{agg}}{Nu_{avg}.\frac{3600}{8}.168000.(1-\Gamma_s).B_s.C_r.PRB_m}$$

where $PRB_m$ is the maximum available PRB based on the configured system bandwidth. unfortunately, in practice, it is difficult to find accurate values for $B_s$ and $C_r$. Thus, we opted for setting the lower-limit on spectrum resource utilization with the assumption of providing seamless mobile service of user at cell edge. For that we considered a simpler and basic equation as [77]:

$$Thr \leq PRB_a.\mu_{avg}.Bw_{RB} \tag{3.10}$$

where $\mu_{avg}$ is the average spectral efficiency at cell edges in bits/s/Hz and $Bw_{RB}$ is the bandwidth of an PRB which can be taken as 180 KHz for the evaluation. With that the $C_u(\%)$ in Equation 3.9 is simplified as:

$$C_u(\%) = \frac{PRB_a}{PRB_m} \times 100 \tag{3.11}$$
$$\geq \frac{Thr}{\mu_{avg}.Bw_{RB}.PRB_m}$$
$$\geq \frac{8.Tagg}{3600.Nu_{avg}.\mu_{avg}.Bw_{RB}.PRB_m}$$

Figure 3.5 shows the calculated 20 MHz system bandwidth utilization of LTE's 2100 MHz band for a particular base station assuming proportional fair resource allocation. Despite the visible temporal patterns on the traffic volume, the mapping shows randomness in resource allocation.

## 3.5 Clustering and Prediction

This section presents the methodologies utilized in [90, 91] to elucidate the complex relationship between mobile traffic and spectrum usage. We employ a non-geostatistical model, specifically K-Means clustering, to reveal hidden patterns in both traffic and spectrum data, identifying

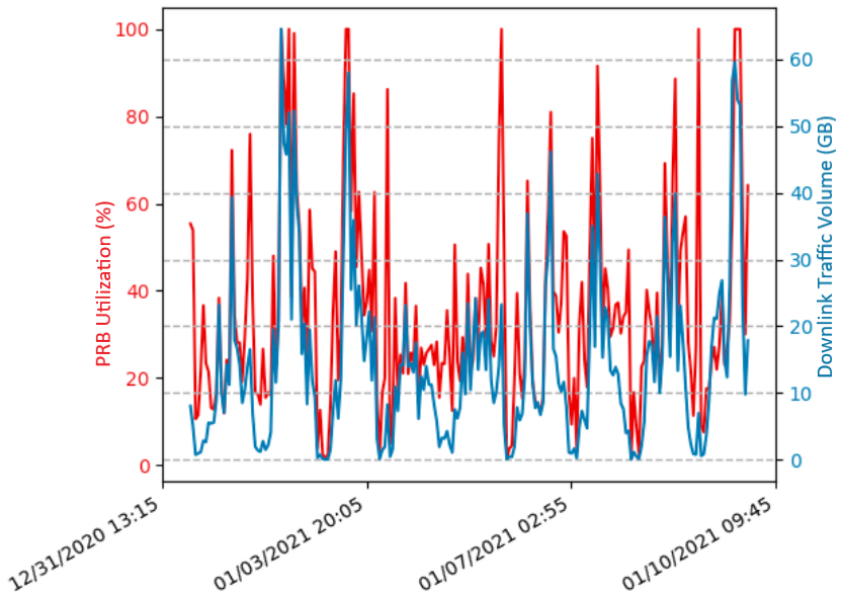


**Figure 3.5:** Spectrum resource utilization mapping from data traffic volume at a LTE cell.

meaningful segments and trends. Following that, we proposed DL-based prediction models for predicting traffic and spectrum usage, highlighting their capability to capture the complex characteristics of spatio-temporal data.

### 3.5.1 Traffic and Spectrum Utilization Clustering with K-Means

To understand the utilization of both traffic and spectrum resources from spatially distributed base stations and identify the unique temporal patterns for different base stations, we used the K-Means clustering Method. K-Means stands as a popular unsupervised clustering algorithm known for its simplicity with its limited hyper-parameters and linear computational complexity [104].

The primary goal with K-Means is to group unlabeled multidimensional data into $K$ disjoint clusters. The grouping involves iterative processes of updating cluster members based on the closeness of a data set to a cluster's mean or centroid. In the context of deploying K-means for time series data, it is essential to discover temporal patterns and group time series data into meaningful clusters based on their similarities. To optimally identify the distinct patterns within such time series data, we utilized intra- and inter-cluster distance with the *Silhouette Index (SI)*. This method enables the clustering of spatially distributed base stations based on

their traffic or spectrum-utilization patterns, assisting in the visualization and categorization of these diverse utilization patterns among different locations [104, 105]. The SI facilitates this clustering by measuring temporal similarity within clusters and dissimilarity from other clusters, thus contributing to the segregation of traffic and spectrum utilization patterns among base stations with varied spatial distributions.

The SI for the time series dataset, $X(t)$ with $N$ observation points, and $K$ the number of clusters, is defined as [106]:

$$SI(K) = \frac{1}{N}\sum_{i=1}^{N}\frac{b(i)-a(i)}{max(b(i)-a(i))}$$

$$= \begin{cases} 1-\frac{a(i)}{b(i)}, & a(i) < b(i) \\ 0, & a(i) = b(i) \\ \frac{b(i)}{a(i)}, & a(i) > b(i) \end{cases} \tag{3.12}$$

Where for observation $i$, $a(i) = \frac{1}{|c_i|}\sum_{\substack{j\neq i \\ j\in c_i}} ||X_i(t) - X_j(t)||$, is the measure of similarity of $X_i(t)$ all other points within the same cluster.This measures how similar $X_i(t)$ is to other points in its cluster. Smaller $a(i)$ implies tighter clustering. $c_i : c_i inK$ is the particular cluster containing $X_i(t)$ and $|c_i|$ is its size measuring the number of observation points in it. Similarly, $b(i) = \min_{c_j\neq c_i}\frac{1}{|c_j|}\sum_{j\in c_j}||X_i(t) - X_i(t)||$, is the measure of dissimilarity of $X_i(t)$ from time series observations in other clusters. The value of SI extends from -1 to 1, with values closer to 1 indicating better clustering quality. The detailed steps for finding the optimal cluster size is presented in Algorithm 1. Figure 3.6, which is presented in our analysis, visually represents the results of the clustering process for GSM Voice services. It shows the spectrum utilization patterns and the spatial distribution of the corresponding base stations within these groups. The four clustered base stations are based on their average spectrum utilization patterns. The top-row plots represent the average utilization pattern of each cluster in five days duration, and the bottom-row plots represent the spatially distributed base stations of each cluster. These plots reveal that there are distinct variations in utilization patterns among these base stations. These variations can be attributed to several factors, including user behavior. For instance, during working hours, we observe a substantial increase in call rates, represented by the prominent peaks in the utilization patterns. This behavior indicates the impact of users' daily routines on spectrum utilization. Additionally, the third cluster from left to right in the figures

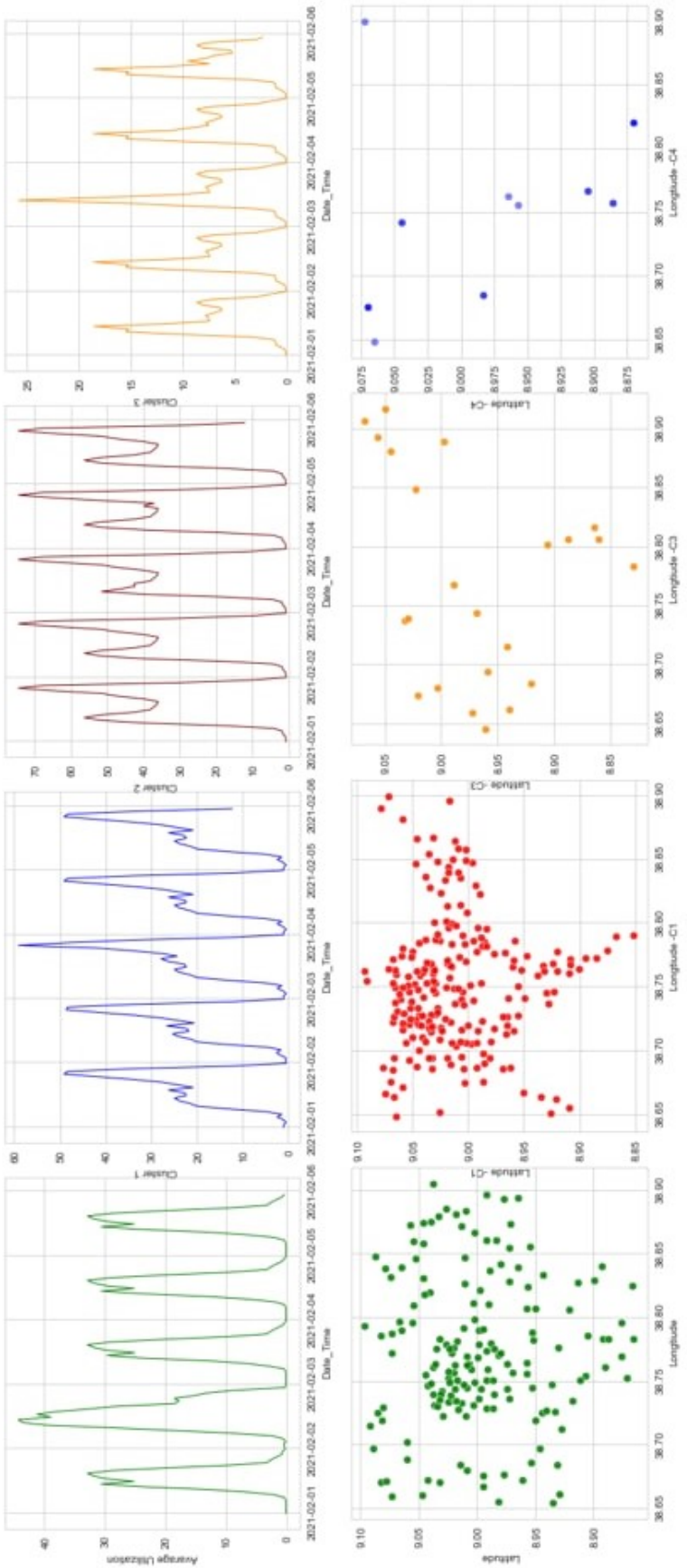

**Figure 3.6:** GSM Voice-Channel utilization clusters analysis.

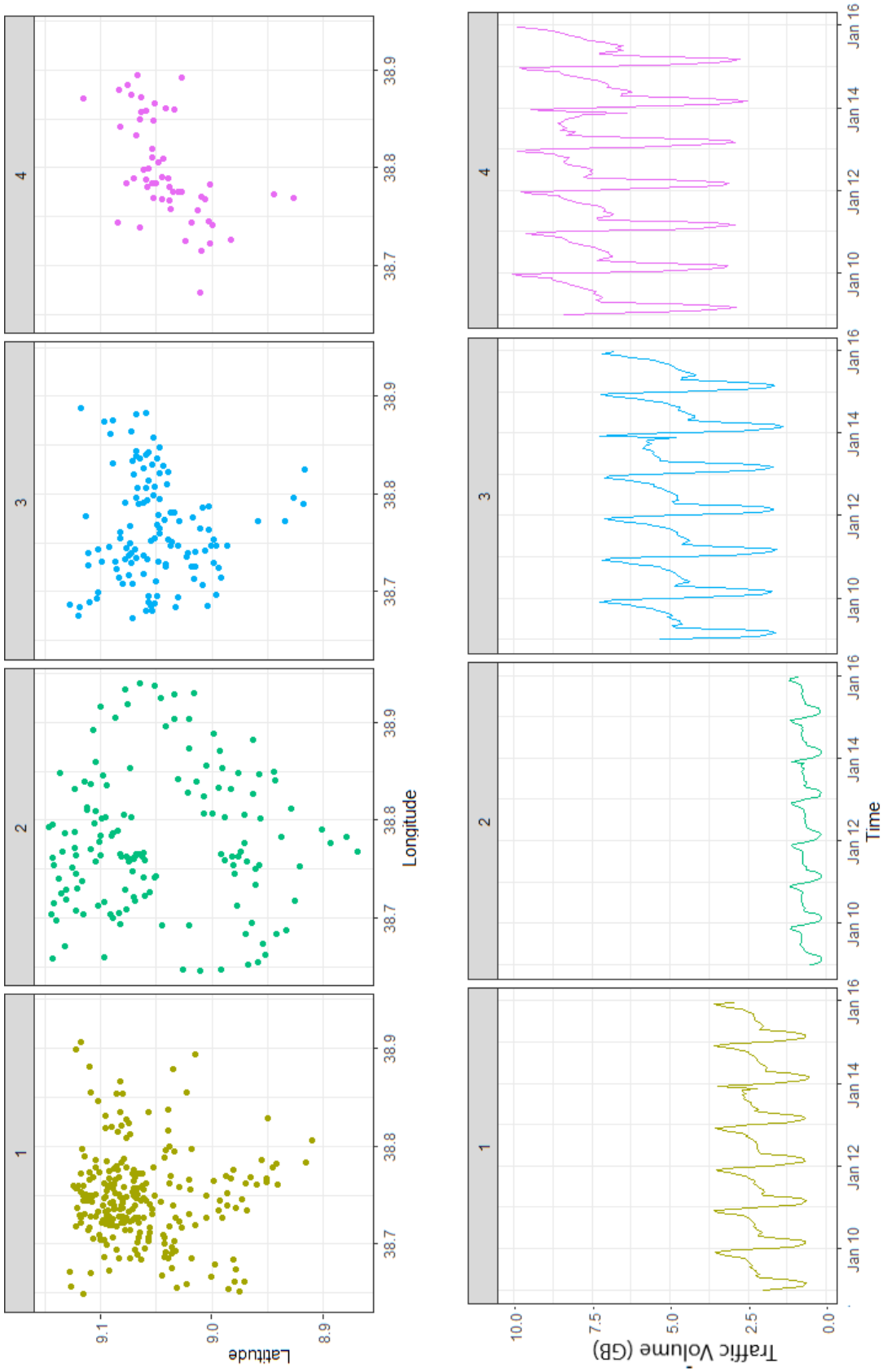


**Figure 3.7:** LTE data traffic load Clusters Analysis.

**Algorithm 1** Traffic and Spectrum utilization Clustering Scheme

**Input**: time series data set **X(t)** $\epsilon$ $\{x(t)_1, ..., x(t)_p$ collected from $p$ base stations$\}$; **m**, max cluster size (temporal patterns)
**Output**: **K**, optimal number of unique temporal patterns (number of clusters); Clustered data sets $X_C(t)_1, ..., X_C(t)_K$
**Variables and Functions:**
  **Kmeans (X,K)**: cluster the x data points into district clusters,
  **SI(k)**: compute the silhouette Index (Eq. 3.12) for k number of clusters
**Clustering:**
Initialize K:= 1; n := -1;
**for** i = 2 : m **do**
  Compute Kmeans (X(t),i)
  Compute SI(i);
  **if** SI(i) > n then
    Set n := SI(i); K:= i;
  **end**
**end**
**if** K != 1 then
  Compute Kmeans (X(t), K);
  Generate $X_C(t)_1, ..., X_C(t)_K$
**else**
  Take X as a single cluster, and set n:= 1;
**end**

reveals a higher number of channel allocations, indicating a specific pattern related to channel usage.

In our study, we extended the application of clustering analysis to the aggregated traffic load data. Specifically, we examined the LTE data service, and the results, as depicted in Figure 3.7. The traffic patterns for the respective five clusters displayed showcased a balance between diversity and similarity in traffic usage among them. Even with the transition to a different service type, a dominant daily pattern rooted in user behavior remained evident. This observation highlights the persistence of certain usage patterns across different service offerings.

In a city where diverse functional areas, such as residential, business, and entertainment districts, coexist, the clustering analysis served to clearly distinguish between these distinct traffic patterns. Notably, the clusters effectively identified areas with very high traffic demand, as seen in the last column of Figure 3.7, from areas with lower data service usage that exhibited

activity primarily during daytime hours, as depicted in the third column of Figure 3.7. The emergence of low correlation among these clusters was not unexpected, given the inherent differences in traffic behavior among these diverse areas.

### 3.5.2 Traffic-based Prediction Problem Formulation

The traffic load information at the CN level offers a consolidated view of the transported user traffic within individual base stations. The data is collected periodically, either on a minute-by-minute or hourly basis, over some time and at different base stations/cells. Thus, by analyzing the changes in spectrum utilization using this traffic information, we can observe how it varies across different time intervals and spatial locations.

Considering this, predicting spectrum utilization or traffic can be approached as a general univariate or multivariate time series prediction problem as [107]:

$$\hat{X}(t+1:t+h) \leftarrow \mathcal{P}(X(t), X(t-1), ..., X(t-n)) \quad \text{(univariate time series)} \tag{3.13}$$

$$\hat{X}(t+1:t+h) \leftarrow \mathcal{P}(X_i(t), X-i(t-1), ..., X_i(t-n)) \quad i \in (1, 2, ..., d) \quad \text{(multivariate time series)} \tag{3.14}$$

Within this equation, for univariate time series $X = \{x_1, x_2, ..., x_t\}$ and for multivariate time series $X = \{X_1, X_2, ..., X_t\}$ signifies the spectrum utilization or aggregated voice or data traffic volume time series vector. $P$ represents the univariate or multivariate predictor model discussed in Section 3.5.3 that uses $n$ past observations to provide $h$ future predictions. $d$ represents the number of variables.

### 3.5.3 Models Description

#### 3.5.3.1. Utilization Predictors

Focusing on efficacy of LSTM and CNN models in tackling the challenge of accurately predicting spectrum utilization, two different DL models as depicted in Figure 3.8 are proposed in [90]. These models were specifically designed to capture the complex temporal dynamics of spectrum utilization without the need to explicitly break down the underlying time series characteristics.

### 1. The Three-Layer LSTM Model

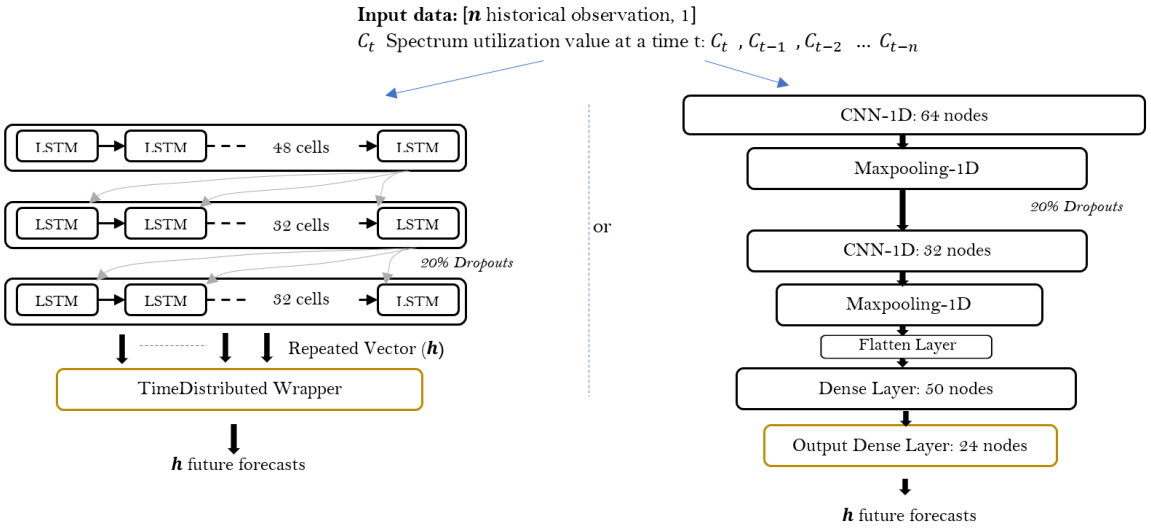


**Figure 3.8:** LSTM and CNN Models for Predicting Spectrum Utilization in GSM Networks for Voice Services.

In Figure 3.8a, we presented a three-layered LSTM model designed for predicting spectrum utilization patterns. Each cell in the architecture received $n$ past mean spectrum utilization values for each cluster, structured into a unified input vector. The first LSTM layer consisted of 48 cells, while the second and third layers each had 32 cells. To address the risk of overfitting, a dropout rate of 20% was applied to the output of the second layer. This specific dropout rate and its placement before the last LSTM network was chosen because it effectively balances model generalization and information retention, forcing the network to avoid over-reliance on specific neurons and improving its ability to generalize from the training data. The output from the final LSTM layer was replicated $h$ times, and a time wrapper was employed to distribute a fully connected layer across these replicated time steps, enabling the model to generate sequential predictions effectively.

### 2. The Two-Layer 1D CNN Model

The second model we introduced in Figure 3.8 is a two-layer, one-dimensional CNN model with 64 and 32 nodes, respectively. This model adhered to the same input data structure as the LSTM model. Given that spectrum utilization values typically fall within the 0 to 1 range, we refrained from applying additional normalization or scaling procedures. Each CNN layer was designed to extract features from a sliding window spanning three consecutive time steps of

the input data. The output of the CNN underwent down-sampling by selecting the maximum value.

In addition to the 1D CNN layer, our model incorporated a series of densely connected layers, featuring 50 and 24 units, respectively. These layers operated on the flattened vector output from the CNN. The choice of 24 units in the latter dense layer aligned with '$h$,' representing the number of multi-step future predictions. To prevent over-fitting, we introduced a 20% dropout rate in the output of the first CNN layer. Across both models, the activation function for each layer was set to *ReLU* (Rectified Linear Unit), enabling the models to provide real-value predictions. To fine-tune these models, we engaged in a meticulous grid search to pinpoint the optimal hyper-parameters, optimizing the models for our specific prediction task.

The decision to employ these models for GSM voice channel utilization prediction is rooted in several compelling intuitions. These models are well-suited to capture the complex temporal dependencies and patterns present in the utilization of spectrum resources for voice services in GSM networks. The key reasons for choosing these models include:

- **Temporal Dependency Handling:** LSTM networks are particularly effective at handling sequences with long-term temporal dependencies. In GSM networks, spectrum utilization for voice services exhibits a strong dependence on previous data, such as daily and weekly patterns. LSTMs excel at capturing these dependencies, making them a natural choice for modeling such time series data.

- **Implicit Feature Extraction:** CNNs are renowned for their ability to automatically extract relevant features from data. In the context of spectrum utilization, there may be complex and non-linear relationships between various factors that influence the channel allocation for voice services. CNNs can uncover these features by processing the data through convolutional layers, which is crucial for accurate prediction.

- **Multi-step Future Prediction:** Evaluating the future channel usage task often involves multi-step future forecasts, where it's necessary to predict utilization for several time steps ahead. Both LSTM and CNN can be structured to provide such predictions.

### 3.5.3.2. Traffic Predictor

To address the complex nature of mobile data traffic, we explored methods to improve predictability. By adding extra attributes like the maximum count of uplink and downlink users per cell, and metrics such as Radio Access Bearer (RAB) requests and success and failure rates, we aimed to enhance the accuracy of downlink data traffic volume predictions in LTE networks. We introduced a CNN-LSTM DL model for predicting LTE data traffic volume as depicted

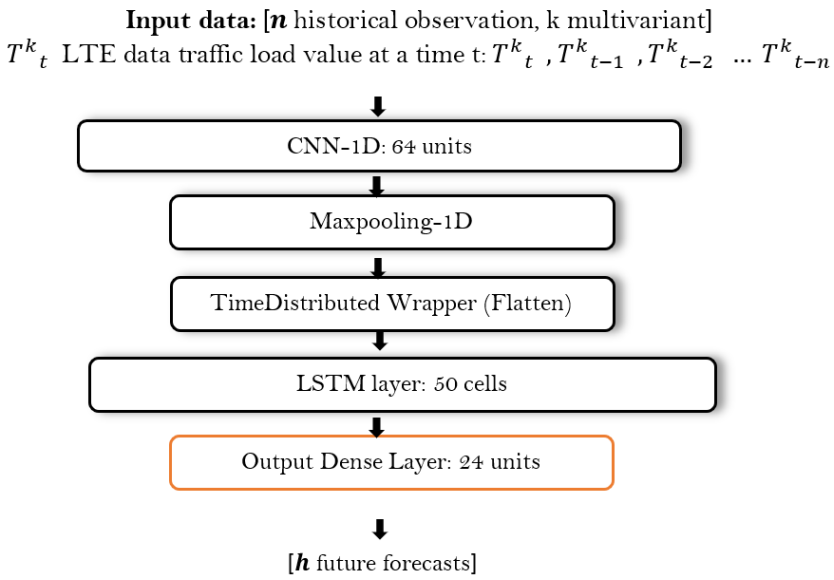


**Figure 3.9:** The CNN-LSTM model for LTE data traffic prediction.

in Figure 3.9. The CNN component of the model integrates a 1D CNN layer consisting of 64 units or nodes, each utilizing a filter size of 3, and is followed by a layer with a down sampling technique that takes the maximum value. Each CNN unit receives input from the past aggregated traffic volume combined with additional explanatory variables. In the LSTM section of the model, 50 LSTM cells take the time-wrapped and flattened output from the preceding layer as input, preserving the temporal structure. The final output layer, a dense or fully connected layer, consists of 24 units (denoted as $h$) linked within the network to deliver $h$ future predictions. To retain the real-valued nature of the output and prevent the occurrence of neurons remaining inactive during training, a leaky-ReLU function is employed as the non-linear activation function for each unit in the network.

### 3.5.4 Model Evaluation Metrics

The Model evaluation aims to estimate the generalization accuracy of a model on future or test data. We jointly used two evaluation metrics to quantify all our models' performance: MAE and RMSE.

$$MAE = \frac{1}{N}\sum_{i=1}^{N}|y_i - \hat{y}_i| \tag{3.15}$$

$$RMSE = \sqrt{\frac{1}{N}\sum_{i=1}^{N}(y_i - \hat{y}_i)^2)} \tag{3.16}$$

where $N$ is the size of the evaluated set and $\hat{y}_i$ is the predicted utilization for $y_i$. The joint evaluation is needed to handle the non-normality of the predicted data (with RMSE) or minimize the impact of outliers (with MAE) that might occur due to sudden network outages or service interruptions.

## 3.6 Results and Discussions

In the subsequent subsections, we will delve into the model parameter tuning and the prediction accuracy achieved by the models on the mentioned datasets. Additionally, we will explore the representations and insights learned from the modeling processes.

### 3.6.1 Hyper-parameter Tuning

Table 3.2 summarizes the key hyperparameters tuned for all proposed models, including the values explored during the optimization process. The model parameters are selected with careful tuning using grid search.

The model architectures were optimized by fine-tuning the number of layers, neurons per layer, and kernel sizes (where applicable). As detailed in Section 3.5.3, the final parameters for each model were determined after empirical evaluations in preliminary experiments. Configurations exceeding three layers or using significantly larger layers showed diminishing returns in accuracy and generalization. This occurred because larger networks tend to overfit the training data, particularly when the dataset is limited or noisy. A batch size of 32 was selected as it

**Table 3.2:** Model training parameters

| Model Parameters | Values | | |
|---|---|---|---|
| | Utilization Predictors | | Traffic Predictor |
| | Three-Layer LSTM Model | Two-Layer 1D CNN Model | Hybrid CNN-LSTM Model |
| Optimizer | Nesterov accelerated adaptive moment estimation (NADAM) algorithm | | |
| Learning rate | 0.0002 | | |
| Decay rates ($\beta_1$; $\beta_2$ ) | 0 ; 0.999 | | |
| Training loss functions | MSE , MAE | | |
| Dropout | (0.1, 0.2,0.3) | (0.1, 0.2,0.3) | - |
| No. of layers | 3 | (1,2 3) | |
| No. of units | (32,48) | (24,32,48,50,64) | (24,32,48,50,64) |
| Kernel size | - | ((1, 3) ) | ((1, 3) ) |
| Output Activation function | Sigmoid | | Relu |
| Batch size | (4,8,16) | | |
| Epoch | (50 - 100) | | |
| Training/validation/Testing | (80%/10%/10%) | | |
| multivariate parameters | - | | Uplink Traffic, RAB success rate Cell Average/ Maximum User |
| Traffic to Spectrum Utilization mapping | Pre-Prediction | | Post-Prediction |

provided an effective balance between training speed and generalization. While increasing the batch size (e.g., to 64) resulted in faster convergence, it led to slightly poorer validation performance. Additionally, training the models for up to 100 epochs with early stopping ensured optimal convergence without overfitting in all three architectures.

## 3.6.2 LTE Data Traffic Prediction Performance

### 3.6.2.1. Multivariate Parameter Selection

In the process of selecting additional explanatory variables for the multivariate prediction of LTE data traffic, eight network parameters, including the target variable downlink traffic vol-

ume, were monitored at the LTE's RAN (eNodeB) level. These parameters encompass downlink throughput, average and maximum user counts within a cell, the count of attempted, successful, and setup failure RABs, uplink data traffic, and the location information of the eNodeBs.

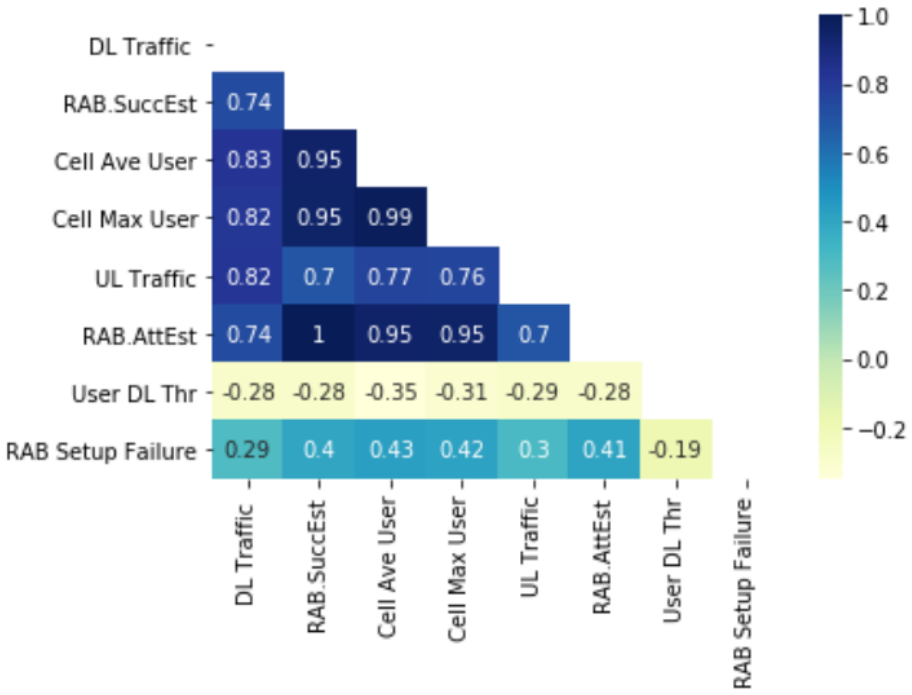


**Figure 3.10:** Correlation Analysis: Exploring the relationship between LTE network parameters and downlink Traffic Volume.

To determine the relevant explanatory variables for the predicting model and identify the linear correlation of the paramenters with the downlink traffic volume, Pearson's based correlation analysis is applied. The outcomes of this analysis are visually presented in Figure 3.10. A correlation threshold of 0.5 or higher served as the basis for parameter selection. Notably, it becomes evident that a higher number of average or maximum users in a cell contributes to increased data service usage in both the uplink and downlink. On the contrary, the setup failure of RABs indicates collective LTE access issues, which can result from factors like weak coverage, coverage overlap, external interference, an excess number of user requests compared to the maximum allowable users in the cell, unavailability of radio resources, or air interface faults in resource admission. Given that setup failure represents an aggregated effect, it is expected to exhibit lower similarity with the traffic volume pattern, hence the lower correlation factor. Moreover, the observed correlation between downlink user throughput and downlink traffic volume was surprisingly close to zero, deviating from the expected direct

proportional relationship. This unexpected outcome can be attributed to two possible factors. First, network congestion may have introduced delays, packet loss, and a degradation in service quality, disrupting the anticipated correlation. Alternatively, it is plausible that the MNO has established predefined minimum throughput levels for specific services, which remain unchanged despite high traffic demands. Consequently, downlink user throughput is not taken into consideration for data traffic prediction.

#### 3.6.2.2. Prediction Model Performance

The CNN-LSTM layer model, shown in Figure 3.9, is trained with clustered-level average LTE traffic volume. The model fitting and 24-hour prediction performance shown in Figure 3.11 and the quantitative metrics provided in Table 3.1 offer valuable insights into the model's performance and its efficacy in predicting LTE data traffic volume. When considering the

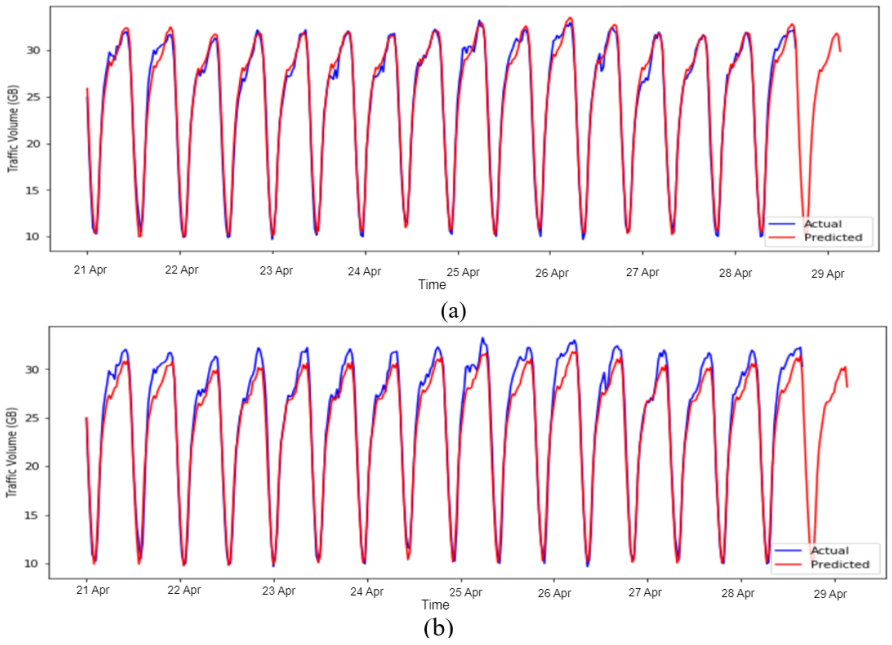


**Figure 3.11:** Predicting Mobile Data Traffic Patterns (Cluseter-level) with CNN-LSTM: (a) Multivariate Feature Use (b) Univariate Focus.

multivariate approach (Figure 3.11a), the predicted data traffic closely aligns with the actual values, particularly in terms of daily seasonality. The model efficiently captures these recurring patterns. Notably, the inclusion of multiple features in a multivariate manner significantly aids in recognizing irregularities and nuances during peak hours. This aspect is paramount

for achieving accurate predictions in dynamic LTE networks. Contrastingly, the univariate approach (Figure 3.11b) showcases a comparable daily seasonal pattern between the predicted and actual traffic data. Nevertheless, the univariate model's capacity to capture variations during peak hours appears relatively limited compared to the multivariate model. This difference in performance becomes even more evident when compared to the baseline CNN model which demonstrated a significant 40% improvement RMSE in prediction accuracy. We extended the

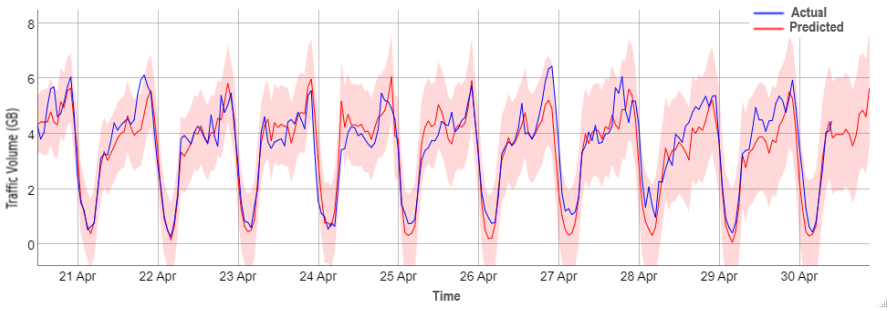


**Figure 3.12:** Predicting Mobile Data Traffic Patterns (Base station-level) with Multivariate Feature Use.

analysis to provide base station level predictions as shown in Figure 3.12 and Table 3.3 using the proposed CNN-LSTM model that was trained on traffic data. Despite the model's limitations in capturing short-term fluctuations due to the burstiness of the clustered data traffic, an improvement by 35% was still observed compared to the baseline. This improvement was primarily attributed to the feature integration achieved in the multivariate approach and the dominant temporal patterns (dual seasonality) effectively captured by the CNN-LSTM model.

**Table 3.3:** Model performance comparison.

| Features | Cluseter-level Average RMSE | Base station-level Average RMSE |
|---|---|---|
| Proposed CNN-LSTM Model, Multivariate | 0.81 | 1.85 |
| Proposed CNN-LSTM Model, Univariate | 1.28 | 2.75 |
| CNN Model Multivariate | 1.34 | 3.04 |
| CNN Model Univariate | 1.53 | 4.97 |

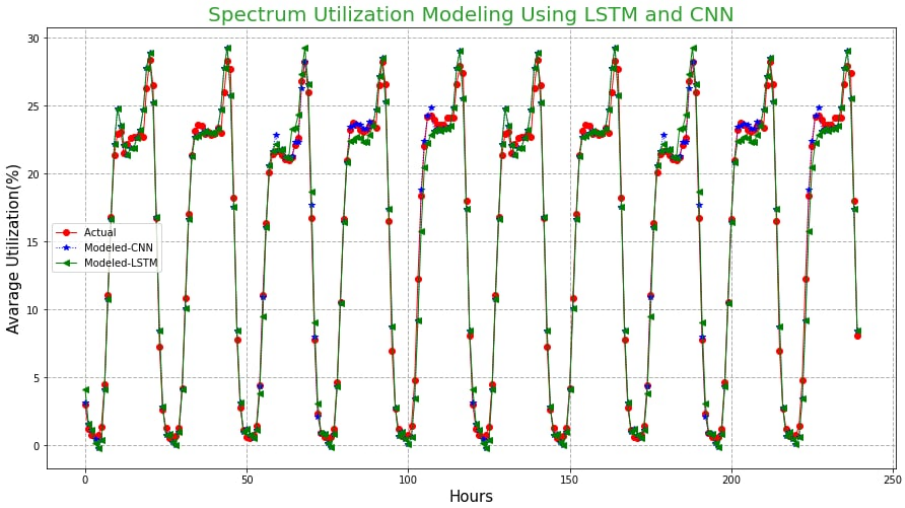


**Figure 3.13:** Comparison of prediction accuracy: Hyperparameter-Optimized LSTM vs. CNN models.

### 3.6.3 Utilization Prediction Performance

Both of the proposed models, as depicted in Figure 3.8, were trained using base station-level and averaged cluster-level utilization data ranging from 0 to 1. During the training process, vectors that contained missing or outlier values were subjected to linear interpolation. This pre-processing step was employed to rectify missing data or anomalies, ensuring the integrity and completeness of the training dataset. The results illustrated in Figure 3.13 and Figure 3.14 are

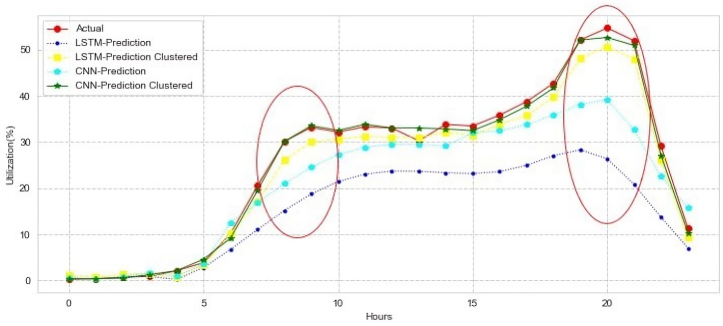


**Figure 3.14:** Base station level prediction with both LSTM and CNN.

summarized in Table 3.4. As shown in the Figures, both the LSTM and CNN models effectively captured the unique characteristics of GSM 900 spectrum usage. Figure 3.13 highlights that while both models performed well in cluster-level data prediction, the CNN model outperformed the LSTM model by 69.2% in MAE and showed a 26.9% improvement in RMSE metrics. This indicates that the CNN model is better at capturing temporal patterns and short-term fluctuations

with higher precision than the LSTM model. The consistent bandwidth requirements and predictable nature of voice calls contribute to the improved predictability of spectrum utilization. Additionally, the CNN model exhibited faster convergence during training, requiring only 100 epochs, compared to the LSTM model, which took approximately 200 epochs to achieve similar convergence. Furthermore, when evaluating the model's generality and applying the cluster-

**Table 3.4:** Cluster level prediction performance.

| | Clustered | | Base station levels | |
|---|---|---|---|---|
| | **Average RMSE** | **Average MAE** | **Average RMSE** | **Average MAE** |
| **LSTM** | 0.8 | 0.845 | 1.197 | 1.057 |
| **CNN** | 0.585 | 0.26 | 0.767 | 0.521 |

level trained model to individual base station predictions, Figure 3.14 clearly demonstrates the performance differences. The prediction error is particularly pronounced during high utilization or peak hour congestion periods, which can lead to network conditions and QoS degradation if prediction-based network resource allocation and optimization are employed.

## 3.7 Chapter Summary

In this chapter, we explored the indirect approach to provide SA for MNOs by leveraging aggregated voice and data traffic volume information, along with other network-level data. By mapping traffic data to spectrum utilization and using DL models based on LSTM and CNN, we successfully predicted spectrum channel utilization with improved accuracy.

For voice channel prediction, traffic-to-spectrum utilization mapping was performed prior to the prediction task, as generated voice traffic is typically direct and application-independent. The performance of both the proposed LSTM and CNN-based DL models was evaluated, with the CNN model demonstrating superior performance. It showed improvements of 26.9% and 36% at the cluster and base station levels, respectively, by better capturing temporal patterns and short-term fluctuations.

For LTE data traffic, directly mapping traffic to spectrum resource utilization proved to be challenging. Therefore, we proposed performing the data traffic prediction first, then using the predicted aggregated traffic for lower-bound spectrum resource utilization mapping. This

post-prediction mapping approach helped avoid the propagation of errors that could arise from mapping approximations. For prediction task, the CNN-LSTM hybrid model showed significant improvements compared to the baseline CNN model showcasing the benefit of combining CNN's feature extraction capabilities with LSTM's ability to handle temporal dependencies. The 24-hour prediction performance revealed that the model effectively captured daily seasonality and peak-hour variations. With cluster-level prediction performance showing a significant 40% improvement in RMSE, it was evident that the model's capability to handle the multivariate greatly improved the model's ability to recognize aggregated irregularities during peak hours. Even for base station-level predictions, the CNN-LSTM model demonstrated a 35% improvement compared to the baseline model, despite the limitations in capturing short-term fluctuations due to bursty traffic patterns.

# 4 Spectrum Situational Awareness with Volumetric Radio Environment Maps

## 4.1 Introduction

### 4.1.1 Situational Insight in Three-Dimensional Spectrum Use

The relentless growth of wireless connectivity demands a paradigm shift from the conventional 2D network architecture to a 3D approach. This shift is driven not merely by the growing demand for ubiquitous wireless access but also by the emergence and integration of Non-Terrestrial Networks (NTNs), encompassing Low Earth Orbit (LEO) satellites, High Altitude Platforms (HAPs), and UAVs with the Terrestrial Networks (TNs). These NTNs, with their Line of Sight (LoS) communication capabilities and extensive coverage reach, offer a promising solution to overcome the limitations of terrestrial networks in catering to remote or underserved areas [5, 108, 109].

While 3D network architectures offer numerous advantages for integrating NTNs into next-generation wireless networks, they also introduce unique challenges related to spectrum utilization and access. One challenge arises from the increased complexity of spectrum access management in a 3D network. The presence of NTNs introduces new dynamics to spectrum access, as both terrestrial and non-terrestrial nodes need to coordinate their spectrum usage to avoid interference. This coordination becomes more challenging in a 3D environment due to the increased number of nodes and the constant variability of their locations and communication paths. But the more critical challenge lies in understanding the complex spectrum occupancy patterns in a 3D environment, where the distribution of radio frequencies is influenced by factors such as non-terrestrial node placement, varying radio propagation characteristics, and potential interference patterns [110, 111]. Efficient use of spectrum in this context requires a comprehensive situational awareness throughout the coverage area, which is significantly more intricate in a 3D architecture compared to its 2D counterpart [112, 113].

Building SSA[6] requires more than just understanding the current state of the network; it involves comprehending factors such as network conditions and radio environmental changes to gain a complete understanding of spectrum usage. This involves monitoring and/or modeling parameters such as radio propagation characteristics and the location and operation of the radio devices [85]. To this aspect, this chapter provides a new insight into providing SSA in a 3D environment, emphasizing the importance of understanding and constructing the 3D propagation environment for building preliminary spectrum knowledge.

Towards that end, this chapter presents the following peer-reviewed published article.

- **Paper:** Bethelhem. S. Shawel, Dereje H. Woldegebreal and Sofie Pollin *"A Deep Learning Approach to a Volumetric Radio Environment Map Construction for UAVs-Assisted Networks"*, In: International Journal of Antennas and Propagation. 2024:9062023 (2024), 16. doi: 10.1155/2024/9062023.

### 4.1.2 Radio Environment Maps for 3D Wireless Networks

In the context of integrated TNs and NTNs, 3D radio propagation models are indispensable for accurately characterizing the signal propagation environment. These models serve as predictive tools, employing mathematical simulations to depict how radio waves traverse diverse and complex 3D environments. By estimating parameters like path loss and signal strength, these models facilitate a more precise assessment of spectrum occupancy throughout the coverage area.

The propagation models hold particular relevance in addressing the unique challenges posed by NTNs elements, such as UAVs. Existing propagation models encompass a wide range of methodologies, spanning from empirical models based on measurements to more sophisticated analytical models like ray-tracing models that account for complex environmental details. Ray-tracing models excel at accurately simulating signal propagation in 3D environments by tracing individual ray paths, especially when utilizing real terrain data and detailed geometry. However, this enhanced accuracy comes at the cost of computational complexity due to intricate propagation mechanisms, environmental variability, and the need for extensive data collection and analysis. Additionally, ray-tracing models are inherently site-specific, requiring

6 This is a term defined by the US Defense Advanced Research Projects Agency (DARPA) under its Advanced RF Mapping (RadioMap) project.

re-generation for each new environment and deployment scenario [114, 115]. This can limit their applicability in dynamic and rapidly changing environments.

In addressing the limitations of these models, REMs have emerged as fine-grained digital radio maps that provide a spatially distributed representation of the radio environment, enabling more accurate and efficient propagation prediction [33]. This approach leverages data from various points in the environment to create a comprehensive map of signal quality, network capabilities, or environmental factors that affect radio wave propagation. By integrating spatially distributed measurements, REMs capture the variability and complexity of the propagation environment, allowing for more precise modeling and prediction of signal propagation. In recent years, the use of such maps has been explored to optimize the placement, operation, and performance of NTNs elements in cellular networks [34, 116–119].

To that aspect, our work in [92] explores and proposes two novel VREMs approaches to capture complex RF characteristics influenced by altitude, showcasing the additional degree of freedom introduced by varying heights in REM construction. Despite substantial research on REM construction, much has been confined to 2D contexts, disregarding altitude-related characteristics of electromagnetic wave propagation or confining REMs to 2D formats. This limitation restricts the comprehensive and continuum visualization of propagation environment variation in spatial dimensions, diminishing the applicability of REMs across scenarios, including UAV-assisted cellular networks. Extending the concept of 2D REMs, VREMs capture the additional dimension of altitude, providing a more comprehensive and realistic understanding of radio propagation within a given area in 3D space.

We formulated the VREM problem as an image translation challenge, exploring the two approaches using CNNs and GAN based architecture. For the first Volume-to-Volume (Vol2Vol) method, a DL model is trained to generate the VREM representation by utilizing the complex details of the 3D environmental map and transmitter coordinates. With the Sliced-map construction (Sliced-VREM), the complexity associated with learning from volumetric data is addressed by capturing the altitude dependency of propagation characteristics from stacked 2D environmental maps and transmitter location information.

## 4.2 System Model

### 4.2.1 Scenario Definition and Propagation Loss Model

To address the challenge of limited measurement data for training the DL models, we opted to generate a synthetic propagation loss dataset. This was achieved by utilizing a realistic 3D environment map alongside a propagation loss model, specifically the dominant-path model.

Assume a simplified depiction of an air-ground integrated network, featuring a terrestrial cellular network that leverages UAVs. The UAV can function as an Aerial User Equipment (AUE) or an Aerial Base station (ABS), both located at an altitude of tens to hundreds of meters. AUEs and ABSs are used to offload traffic in cellular hotspots [120], [121], for remote sensing, remote monitoring and control, surveillance and security, emergency communications, and entertainment, to name a few. The cellular network, on the other hand, is represented by a Ground Base Station (GBS) that serves both Ground User Equipment (GUEs), located at different elevations depending on the user's location, and AUE [108]. Our approach involved setting up two distinct scenarios within a 3D environment, as illustrated in Figure 4.1. Scenario one consists of a GBS, situated within a designated spatial region $\chi \subset R^3$, serving GUEs and AUEs at varying altitudes. Similarly, in scenario two, a low-altitude ABS is serving GUEs while hovering at a specific geographic region. In both of these scenarios, a 3D Cartesian coordinate system is employed, defining $l_b = (x_b, y_b, h_b)$ and $l_u = (x_u, y_u, h_u)$ as the coordinates of GBS/ABS and GUE/AUE locations within the environment. Here, $h_b$ indicates the height of the GBS antenna above the ground in the first scenario or the hovering altitude of the ABS in the second scenario.

The 3D environment depicted in Figure 4.1, denoted as $\psi$, is characterized by environment-dependent coefficients, as outlined in the ITU recommendation report [114]. These coefficients include parameters such as the mean building width, $W$, the number of obstacles (mainly building), $N_o$, and the maximum height of obstacles along the LoS link between the transmitter and receiver, $h_o$. In both scenarios, we focus on the downlink propagation channel, where a signal with power $P_t$ is transmitted (by GBS or ABS) and received by a receiver (AUE or GUE) at a ground distance, $d_{tr} = \sqrt{(x_b - x_u)^2 + (y_b - y_u)^2}$ and height of $h_b$, with signal strength $P_r$.

The propagation channel modeling in integrated terrestrial and NTNs involves both Air-to-ground and terrestrial channel considerations. Due to the similarity in channel statistics for both

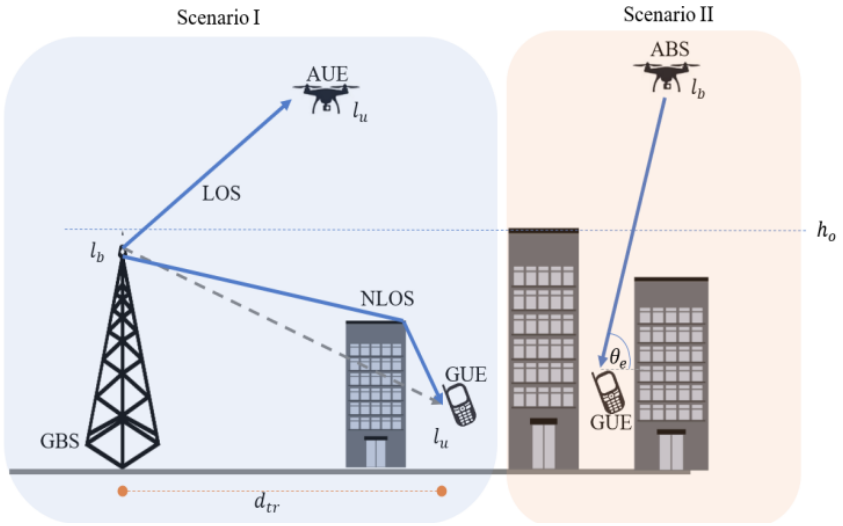


**Figure 4.1:** System model illustrating the 3D propagation environment, encompassing two distinct scenarios denoted by varying color shades. The blue shade indicates GBS-based communication, encompassing the GBS-GUE link and GBS-AUE link, while the red shade illustrates the ABS-GUE link.

cases, the propagation loss is generally defined between any transmitter and receiver, factoring in distance, environment-dependent path loss, and shadowing effects [122]. Depending on whether the propagation path is in LoS or Non-LoS conditions, the loss between the transmitter at $l_b$ and the receiver at $l_u$ is quantified in decibels (dB) as follows [102]:

$$\gamma(l_b, l_u)_{dB} = P_{t_{dB}} - P_{r_{dB}} \tag{4.1}$$

$$\gamma(l_b, l_u)_{dB} = \beta_{(l_b,l_u)} + \alpha.10.\log_{10}(||l_b - l_u||) + \xi_{(l_b,l_u)} \tag{4.2}$$

In which $\beta_{(.)}$ and $\alpha$ and $\xi(.)$ are the propagation channel coefficients that denote the mean free space loss, the path loss exponent, and the shadowing factor of the propagation, respectively. The Frobenius norm is

$$||l_b - l_u|| = \sqrt{(x_b - x_u)^2 + (y_b - y_u)^2 + (h_b - h_u)^2} \tag{4.3}$$

the distance between the transmitter and receiver, measured in meters.

For the given operating frequency $(f)$, and elevation angle $(\theta_e = \tan^{-1}(\frac{|h_b - h_u|}{d_{tr}}))$, between the

transmitter and receiver, the parameter $\beta(.)$ is evaluated as

$$\beta = -27.56dB + 20.\log_{10}(f_{MHz}) + 20.\log_{10}(\frac{|h_b - h_u|}{\sin\theta_e}) \tag{4.4}$$

which emphasizes its significant influence, especially with increased height difference and at higher frequencies [122, 123]. The specific values of $\alpha$ and $\xi$, on the other hand, are dependent on environmental factors, such as the distribution of 3D obstacles (e.g., buildings, terrain) that categorize the environment as suburban, urban, dense urban, or highrise urban. This determination is influenced by factors such as the transmitter–receiver location, geographical area ($A$), the ratio of the total region covered in buildings ($\zeta = f(N_o/A)$), the mean number of buildings per unit area ($\rho = f(1/\zeta)$), and the variation of the building heights that can be modeled as Rayleigh probability density function ($\gamma = f(h_o/A)$) [123]. For instance, when considering larger values of $\gamma$ and $\zeta$, the scenario typically involves an environment with a substantial number of buildings, many of which are tall structures. This points towards an urban setting dominated by high-rise buildings, suggesting a higher likelihood of Non-LOS conditions. This holds true for both GBS or ABS to GUE, as well as GBS to low-altitude AUE communication links. In contrast, lower values of $\gamma$ and $\zeta$ tend to correspond to suburban areas, where there's a greater chance of near LoS conditions for GBS-GUE/AUE links. Following that, the parameter $\alpha$ typically falls within the range of 2 to 6, which is fitted based on whether the link between the transmitter and receiver is in a LoS or NLoS condition. Similarly, the standard deviation of $\xi$ exhibits higher values in high-rise urban regions when compared to suburban areas.


(a) (b)

**Figure 4.2:** Different propagation methods: (a) Ray-tracing model and (b) Dominant path model [39].

To address the complexities of ray tracing, the *Urban Dominant Path (UDP)* model [124], a simpler yet equally accurate alternative is employed. As shown in Figure 4.2, this model concentrates solely on the most prominent propagation path, referred to as the dominant path, connecting the transmitter (GBS or ABS) with the receiver (AUE or UE). It's notable that in a majority of propagation scenarios, approximately 90% of the received power emanates from this single path [124, 125]. The UDP model is designed to collectively represent propagated waves guided by reflections and diffractions at walls and corners, forming the dominant path. It intentionally limits interactions between transmitters and receivers, reducing computational complexity while maintaining accuracy [123, 125]. With this, it's possible to refine the propagation loss expression in Equation 4.2, where the deterministic approximation of $\gamma$ is realized through the equation as [124]:

$$\gamma_{dB} = -27.56dB + 20.\log_{10}(f_{MHz}) + 20.\log_{10}(\frac{|h_b - h_u|}{\sin\theta_e}) + \alpha.10.\log_{10}(\frac{|h_b - h_u|}{\sin\theta_e}) + \sum_{i=1}^{N_I} r(\phi, i) - \Omega \tag{4.5}$$

Here, $N_I$ represents the number of interactions involving the actual propagation path interacting with reflecting obstacles. It is dependent on The function $r(\phi, i)$ captures the interaction loss in decibels, accounting for changes in propagation direction represented by angle $\phi$ due to the wave's interaction with $i^{th}$ obstacle. The loss follows a regression function with a positive intercept, gradually increasing as $\phi$ rises until stabilizing for larger $\phi$ values. The *waveguiding factor*, $\Omega$, represents collective wave propagation (explained in [126]) and varies based on reflection loss, angle, and obstacle-path distance. In densely urban areas with higher $h_o$ and $N_o$ values, the reflection loss for GUE diminishes in turn increasing $\Omega$.

In both scenarios shown in Figure 4.1, the transmitter (GBS or ABS) maintains a constant altitude above ground level, while the receiver's height changes discretely. With increasing altitude above ground, $\alpha_{(\cdot)}$ tends to approximate 2, indicating free space propagation. Consequently, the loss becomes more dependent on the separation distance between transmitter and receiver, $d_{th}$. Furthermore, $\xi(\cdot)$ decreases for higher altitudes compared to ground-level users, as the number of reflections and diffractions within the area decreases. This means that the propagation loss for the GBS-AUE link is primarily determined by $\beta$, while the GBS-GUE and ABS-GUE links are more sensitive to environmental effects, depending on $\alpha(\cdot)$ and $\xi(\cdot)$. Notably, a comprehensive examination of gradual altitude changes from 0 to 50 m and their implications on propagation loss across different frequency ranges (sub-6G and at 60 GHz) is expounded upon in [127, 128].

### 4.2.2 Volumetric Radio Environment Maps

Given a 3D propagation environment, we defined a mathematical expression of the VREM as follows:

$$\Gamma(l_b, l_u)_{dB} = \iiint_V \gamma(l_b, l_u)\, dx\, dy\, dh \tag{4.6}$$

Here, the 3D space is discretized along the X, Y, and Z (or h) axes, each with a unit resolution of $d_x, d_y$, and $d_h$, respectively. This discretization results in a cubic grid or pixel encompassing N, M, and S dimensions. Thus, a distinct receiver position represented as $l_u = [x_{ui}, y_{uj}, h_{uk}]^T \mid i \in [0, N), j \in [0, M)$ and $k \in [0, S)$. As depicted in Figure 4.3, the VREM slices obtained at

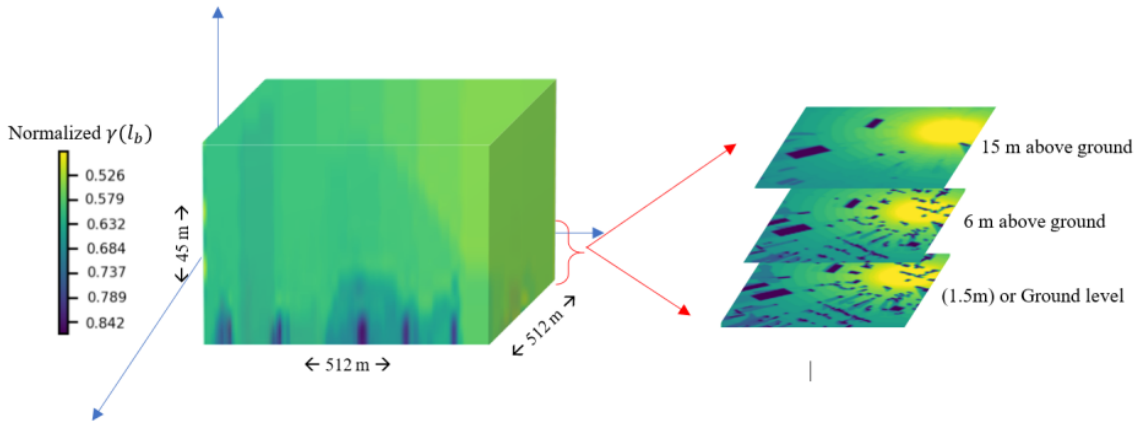


**Figure 4.3:** Illustration of the VREM concept depicting the spatial distribution of propagation loss within a 3D environment.

varying altitudes (e.g., ground level at 1.5 m receiver height, 6 m, and 15 m above ground) offer insights into altitude-specific changes in propagation loss and environmental effects. Each slice represents a 2D REM snapshot stacked sequentially to form the 3D VREM, with each altitude slice separated by $d_h$. As the altitude changes, the composition of obstacles, reflective surfaces, and potential signal obstructions can significantly influence the propagation characteristics.

## 4.3 Problem Formulation

The construction of VREMs is framed as a supervised Image-to-Image (I2I) translation problem. To elaborate, a mapping model, denoted as $M_{S \to T}$, is trained with a substantial dataset of training image pairs to convert input images from a source domain ($S$) into corresponding

images in a target domain ($T$). This model aims to generate a synthesized target domain image, represented as $\tilde{Y}_{\tilde{t}} \in T$, which closely resembles the true image $Y_t \in T$ corresponding to the input source image $X_s \in S$. This relationship can be expressed as:

$$\tilde{Y}_{\tilde{t}} \in T : Y_t \in T = M_{S \to T}(X_s) \tag{4.7}$$

Each input image within the dataset, $\{X_1, X_2, \ldots X_N\} : X_i \in S$ encapsulates the environmental map and transmitter location information, while the corresponding REM $Y_i \in T$ captures the signal propagation characteristics. This pairing serves as the basis for training our VREM construction models, enabling them to learn the transformation from one image domain to another. Various I2I translation methods are available, which attempt to learn the mapping between different image domains [129–132].

Notable architectures like Radio UNets (UNets specifically designed for REM construction in [133]), and Spider-UNets ((a fusion of UNets and LSTM networks designed for segmented image construction in [132])) utilize generative models such as UNets and GANs networks for image translation. The two modelsof GAN, The generator ($G$) and a discriminator ($D$) work in tandem to generate target images and distinguish them from real ones. UNets, a deep convolutional autoencoder network, is originally designed for image segmentation to facilitate direct feature mapping between input and output images.

To address the VREM construction task in our approaches, GANs, and UNets are employed independently or in combination. They serve as foundational frameworks for the proposed approaches, providing a basis for generating VREMs that effectively capture the complex interplay between the radio environment and propagation phenomena. The subsequent section delves into further detail on these frameworks, elucidating their utilization in the context of this research.

## 4.4 Proposed Deep-Learning Approaches for Volumetric Radio Map Construction

### 4.4.1 Vol2Vol VREM Construction with 3D-Generative Adversarial Networks

To estimate the characteristics of the volumetric channel directly by learning the 3D inputs or as a form of vol2vol translation, we proposed a 3D-GAN-based network that has a similar concept to the Pix2Pix architecture in [131]. However, in contrast to Pix2Pix architecture that uses a conditional GAN network to translate a semantic label to a realistic-looking image, the proposed Vol2Vol VREM Construction approach, in Figure 4.4 implements UNet-based 3D-GAN to learn the one-to-one mapping between 3D environment and transmitter location maps with corresponding REM. ***Architecture***. The main structure of the 3D-GAN network is illustrated

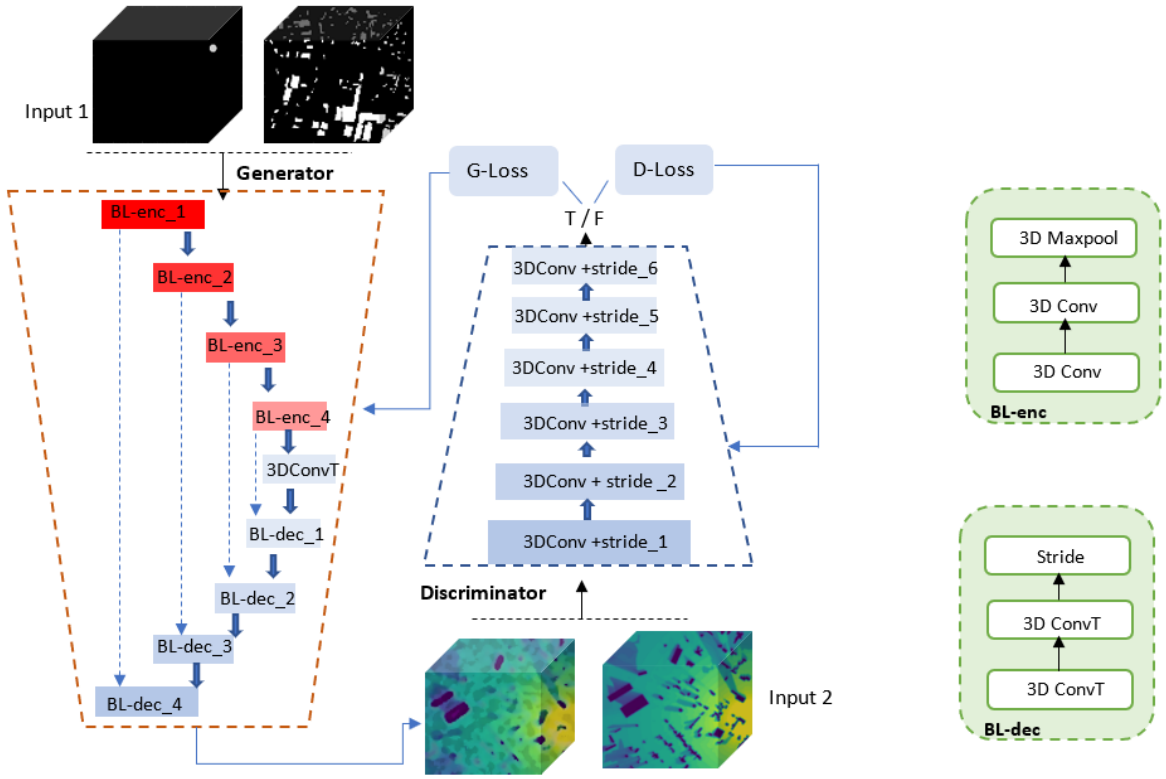


**Figure 4.4:** 3D-GAN architecture (high-level) for the Vol2Vol2 VREM construction.

in Figure 4.4 and the detailed architecture is tabularized in Table 4.1. The generator, G, part

of the network "translates" the environment and transmitter location map input image to the corresponding propagation loss map image and uses a "3D-UNet"-based architecture that relies on Skip connections (represented by the broken arrows) between each layer of the encoder (red blocks) and decoder (dark blue blocks). With 3D convolution and Max-pooling layers, the encoder part can extract features that correspond to the 3D effect of distance, buildings, and other environmental factors between the transmitter-receiver propagation link. A max-pooling follows each paired convolution layer to shirk the input resolution and assist each layer of the UNets to extract the spatial correlated features under the various input resolutions. Two convolution units and a Max-pooling layer are referred to as Encoder basic layers (BL-enc) of UNets and are used as a building block for G to construct the four-layered encoder UNet architecture. For the decoder, the key aspect is the use of a transposed 3D convolution layer and double-stride instead of the 3D convolution and Max-pooling, respectively, to construct the Decoder basic layers (BL-dec). The double-stride is used as an *upsampling unit* to upscale with the same settings as that of the encoder layers. Also, those Skip connections that are weaved between every encoder and decoder layer are anticipated to give the decoder's performance a boost. They allow extra environmental features from each encoder level to flow through, compensating for any potential loss due to compression. In contrast, the discriminator, $D$, part

**Table 4.1:** 3D-GAN model parameters for volumetric REM construction.

| **Model Parameters** | **Values** | | |
|---|---|---|---|
| | **Generator** | | **Discriminator** |
| | **Encoder** | **Decoder** | |
| **Basic Building Layers (BL)** | 3D-Conv. → 3D-Conv. → 3D Max pooling (2) | transposed 3D-Conv. → transposed 3D-Conv. → 3D-stride(2) | **CNN** |
| Layers | **4 BL-enc** | transposed 3D-Conv. + 4 BL-dec | **6** |
| Input resolution (pixel size of the image) | **(128,128,128,1) +(128,128,128,1)** | | (128,128,128,1) + (128,128,128,1) |
| **Filters** | (10,10) → (64,64) → (128,128) → (256,256)→ (512,512) | (512) → (512,512) → (512,512) → (256,256) → (128,128) → (64,64) → (32,32) → 1 | 64 → 128 → 256 → 512 → 512 → 1 |
| **Kernel size** | 4 | 4 | 4 |
| **Output activation** | LeakyReLU (alpha=0.2) | LeakyReLU (alpha=0.2) | LeakyReLU (alpha=0.2), Sigmoid (output later) |

estimates the probability that the generated VREM from the source data $x$ is real, $z_{real}$, or not. To achieve this, $D$ is formulated as a typical image classifier comprising six layers of progressively shrinking 3D convolution layers. This classifier takes both the generated VREM and the original VREM as inputs. The LeakyReLU activation function is employed after each convolutional layer, except for the final layer, which uses the Sigmoid activation function, ensuring real-value generation and model stability. The sigmoid layer produces a scalar output, indicating whether the input VREM image is an accurate reconstruction or not. Batch normalization with random normal input is applied across all layers of $G$ and $D$, excluding the output layer of $G$ and the input or output layer of $D$. Consequently, the optimization objective forms a Min-Max strategy, working to enhance the capability of the model to correctly classify estimated VREM and learn from input data. This approach is formally defined as [134]:

$$\min_{G} \max_{D} L(D, G) = \mathbb{E}_{Z \sim Z_{real}}[\log(D(z))] + \mathbb{E}_{Z \sim X}[\log(1 - D(G(x)))] \tag{4.8}$$

To help create a less blurry (average) construction of VREM images, reconstruction loss is defined by the least absolute deviation function, and binary cross-entropy is used at the generator and discriminator, respectively.

### 4.4.2 Sliced-VREM Construction with Altitude-Aware Spider-UNets

To create a VREM, it is essential to have a model that accounts for how the channel's characteristics vary with altitude. However, using 3D models for this purpose poses challenges due to high memory usage and difficulties in handling the varying numbers of altitude slices caused by the diverse propagation environment and scattering object randomness. To overcome this, we adopted an alternative approach called Sliced-VREM (S-VREM). This involves using altitude-aware 2D U-Nets networks, similar to the Spider-UNets architecture proposed for medical image segmentation in [132]. This architecture captures altitude dependency by processing a sequence of 2D images in parallel, where each modified 2D U-Net focuses on a single-plane image while sharing information to learn altitude-related patterns. This approach, akin to "2.5D" REM construction, maintains altitude awareness but does not generate a full VREM without a simple interpolation along the altitude axis. As it is possible to represent volumetric images as a sequential stack of 2D images, the propagation loss at a given altitude can be learned with modified 2D UNets parallelly processing a single-plane image and sharing information among themselves to capture the altitude dependence. Although the Spider-UNet-like architec-

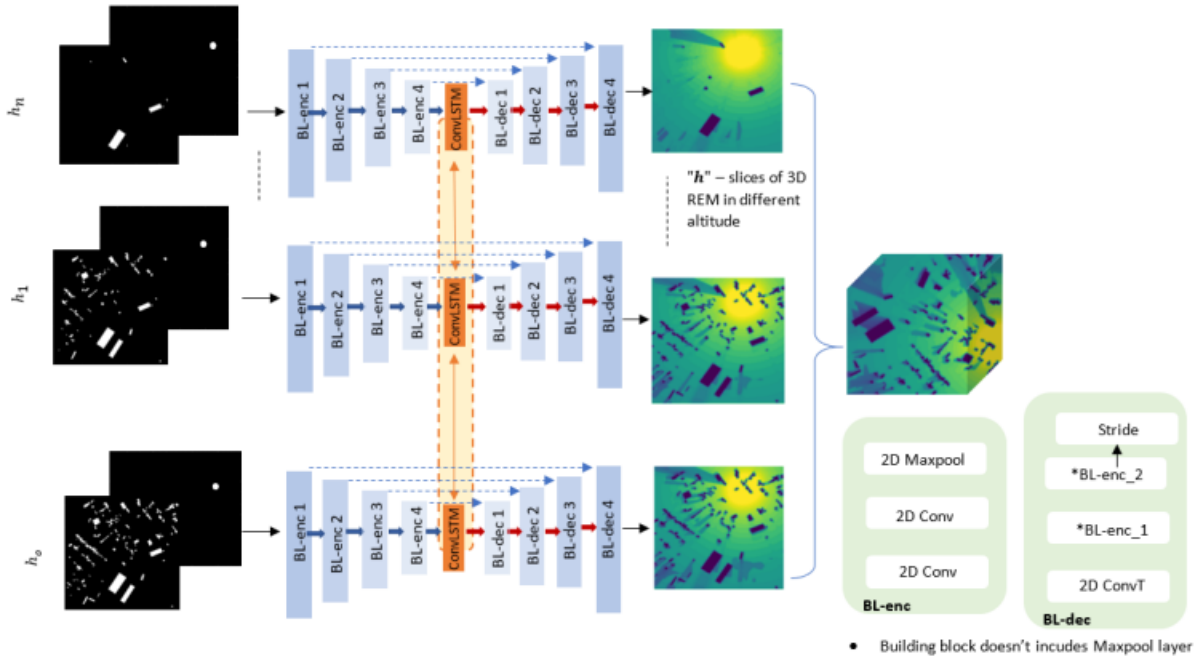


**Figure 4.5:** Sliced VREM with altitude–aware Spider-Unet.

ture processes slices of VREMs and retains altitude awareness, it does not directly generate a complete VREM in three dimensions. Instead, it relies on a simple interpolation along the height or altitude axis to reconstruct the volumetric data. For this reason, the model is often referred to as partial 3D or 2.5D REM construction, highlighting its intermediate capability between fully 2D and full 3D modeling.

***Architecture***. The high-level architecture of our Sliced-VREM methodology is outlined in Figure 4.5, with detailed components described in Table 4.2. The network consists of two main pathways, similar to the setup described in reference [132]. The first path entails the parallel stacking of $n$ 2D convolutional layer-based autoencoders, U-Nets. Each U-Net is designed to comprehend environmental impacts and transmitter locations within a specified geographical region, constructing a 2D-REM to represent propagation loss at a particular altitude level. This simultaneous processing of image slices improves efficiency. The encoder part of the U-Net includes 4 sets of custom layers each consisting of a pair of 2D convolution and 2D max-pooling layers forming basic building blocks, (BL-enc). while the decoder integrates four custom layers, each comprising transposed 2D convolutions, skip connectors, and single building blocks. Similarly, the decoder part of UNet is built with four custom layers, each including a transposed 2D convolution, a skip connector from the encoder, and a single BL-enc layer. The second path,

**Table 4.2:** Altitude-aware Spider UNet model parameters for Sliced VREM construction.

| Model Parameters | Values | | |
|---|---|---|---|
| | Encoder | Decoder | Interconnector |
| Parallel Unet stack | 3 | | |
| Basic 2D-Building blocks | 2D Conv. → 2D Conv. → 2D Maxpool(2) | Transposed 2D Conv. → Concatenate → 2D Conv. → 2D Conv. → stride(2) | ConvLSTM (bi-directional) |
| Layers | 4 | 4 | 1 |
| Filters | (64,64) → (128,128) → (196,196) → (256,256) | (256,256,256) → (196,196,196) → (128,128,128) → (64,64,64) → 1* | **512** |
| Input resolution for single stack | (128,128,1) + (128,128,1) | - | - |
| Output resolution for single stack | (128,128,1) + (128,128,1) | - | - |
| Kernel size | 4 | | |
| Output activation | LeakyReLU (alpha=0.2) | | |

depicted by the orange shaded section in Figure 4.5, captures inter-slice correlations within sequential REM image slices. This is facilitated by a memory-based recurrent neural network, specifically the LSTM in conjunction with the convolutional layer forming ConvLSTM layers. ConvLSTM layer is used at the center of each UNet stack with a bidirectional connection to share spatial features learned at various heights. In both the encoder and decoder parts, the LeakyReLU activation function is used after each convolutional layer. By accommodating variations across both positive and negative input ranges, this activation function substantially enriches the model's adeptness in fully representing complex patterns and subtle intricacies intrinsic to the radio propagation environment.

The quantity of U-Nets stacked in parallel, denoted as $n$, plays a crucial role in shaping the depth of the VREM and determining the maximum sequence size the model can manage. As the number of stacked U-Nets increases, so does the intricacy of model training. To ensure efficient and effective training, a stack length of 3 or 5 has been chosen. This implies that three or five consecutive REMs are simultaneously constructed and consolidated to form the VREM. This approach strikes a balance between complexity and training performance, facilitating the creation of a comprehensive and accurate VREM representation.

The network's training performance is optimized by minimizing the Least Absolute Deviation (LAD) loss function. The LAD function is a non-parametric loss function that measures the absolute difference between the predicted and actual values and is selected in this case due to its tolerance to outliers on the training data and relative ease of optimization.

## 4.5 Experiment and Results

### 4.5.1 Addis Dataset Description

The VREM construction is based on 3D radio environmental data derived from the Addis Dataset, which contains 54,000 samples, each representing a volumetric area of 512 m x 512 m x 45 m. Each sample includes the 3D terrain model of the area, a 3D representation of the transmitter's location and height, and a 3D propagation loss map (REM) generated using *WinProp from the Feko 2021.1 suite*. Each REM with a grid resolution of 1 m x 1 m is simulated with UDP model for a particular geographical area, transmitter location at every 3 meters per iteration. As the simulation is repeated for 15 different altitude levels, it is possible to stack them and create a VREM. The dataset covers an urban area of 59 square kilometers in the southeastern part of the city, and it incorporates two distinct UAV-assisted network scenarios, as detailed in Section 4.2.1 of this document. A set of simulation parameters used to calculate propagation loss and generate REM in Winprop is provided in Table 4.3. The altitude range for GBS or hovering ABS to GUE links is from ground level to 45 m. This height is determined by adding 5 m to the maximum building height in the geographical area, ensuring comprehensive coverage. For GBS to low-altitude AUE communication, the altitude range is from 75 to 90 m, which accommodates the practical flight heights of AUE.

***DL training setup:*** To train the two proposed models more efficiently with memory-constrained GPUs, the original 512 x 512 resolution of the input images, the environment map, and transmitter location information, are reshaped to $128 \times 128$ resolution. In addition, the end-to-end training is performed with an early stopping strategy to stop the training when no improvement is observed in the validation loss after 50 epochs.

The choice of loss functions in both the 3D-GAN and altitude-aware Spider-UNet architectures was driven by the need to maintain computational efficiency while ensuring effective model performance. For the altitude-aware Spider-UNet and generator of the 3D-GAN, the MAE loss

**Table 4.3:** Winprop Simulation and DL Model Training Parameters.

| Parameters | Values |
|---|---|
| **WinProp-related Parameters** | |
| Areal resolution, $d_x$,$d_y$ | 1m |
| Height resolution, $d_h$, | 3m |
| Network | LTE - Advanced |
| Bandwidth | 10MHz |
| Center Frequency, $f$ | 2600 MHz |
| GBS/ABS transmission power | 43 dBm/33 dBm |
| GBS/ABS height | 35 m / 150m |
| GUE height | 1.5 m – 45m |
| AUE height | 75 m - 90 m |
| **DL related parameters** | |
| Learning rate | 0.002 |
| Training/test/validation data split (for the 80 transmitters in each scenario) | 80/10/10 % |
| epochs | 30 - 80 |
| Batch size | 2, 4 |

function was selected, as it provides an accurate representation of the generated REM slices or volumetric data without introducing the added complexity of perceptual loss functions. MAE helps in minimizing the average magnitude of the errors in the predicted output, making it especially useful when the focus is on generating precise numerical values (such as pixel intensities or voxel data in VREM construction).

For the discriminator of the 3D-GAN, the binary cross-entropy loss was employed to evaluate the *"realness"* of the generated VREM. This choice is common in generative adversarial networks, as it helps the discriminator distinguish between real and fake data, driving the generator to improve its output quality over time.

Training 3D GANs presents unique challenges due to their sharp gradient space, which can lead to instability during training. To address this issue, we experimented with two primary solutions: *gradient penalties* and *weight clipping*. Gradient penalties, with a regularization value of 10, helped stabilize the model by penalizing large gradients that could lead to unstable updates. However, the computational cost of using gradient penalties was high, significantly extending training time by more than four hours. Therefore, we opted for a more efficient

approach: **weight clipping**. By restricting the discriminator's weight values to a maximum of 30, we maintained model stability while reducing training time. Additionally, we used a zero-mean normal initializer with a standard deviation of 0.02 for the model's weights, which is a common strategy to help in achieving convergence and avoiding vanishing or exploding gradients.

### 4.5.2 VREM Construction Performance

In this section, we present the performance results of the two proposed approaches considering MAE and Structural Similarity Index (SSIM) as a comparison metric. For assessing the VREM construction error, MAE is defined as:

$$l_1(z, \hat{z})) = \frac{1}{n} \sum_{i=0}^{n-1} ||z - \hat{z}||_1 \tag{4.9}$$

In this context, $z_i$and $\hat{z}_i$ denote the actual and predicted propagation losses for each pixel in the VREM image, where $n$ represents the total number of pixels. The SSIM metric on the other hand, evaluates the structural similarity between the reconstructed and actual VREM images by analyzing luminance $(l)$, contrast $(c)$, and structure $(s)$. The combined similarity index is mathematically expressed as [135]:

$$SSIM(x, y) = [l(x, y)]^a \times [c(x, y)]^b \times [s(x, y)]^g \tag{4.10}$$

$$SSIM(x, y) = [\frac{2\mu_x\mu_y + C_1}{\mu_x^2 + \mu_y^2 + C_1}]^a \times [\frac{2\sigma_x\sigma_y + C_2}{\sigma_x^2 + \sigma_y^2 + C_2}]^b \times [\frac{\sigma_{xy} + C_3}{\sigma_x\sigma_y + C_3}]^g \tag{4.11}$$

where $\mu_x, \mu_y, \sigma_x, \sigma_f, and \sigma_{xy}$ are the local means, standard deviations, and cross-covariance for the constructed and real REM images. $a, b$, and $g$ are parameters that control the relative importance of luminance, contrast, and structural components, respectively. The constants $C_1, C_2, and C_3$ are there to stabilize the quotation at low luminance and contrast regions of the images. If the following common assumptions are taken as $a = b = g = 1$ and $C_3 = \frac{C_2}{2}$, the Equ. 4.11 can then be simplified to:

$$SSIM(x, y) = (\frac{(2\mu_x\mu_y + C_1)(2\sigma_{xy} + C_2)}{(\mu_x^2 + \mu_y^2 + C_1)(\sigma_x^2 + \sigma_y^2 + C_2)} \tag{4.12}$$

The results of the Vol2Vol approach for VREM construction, as shown in Figure 4.6, highlight

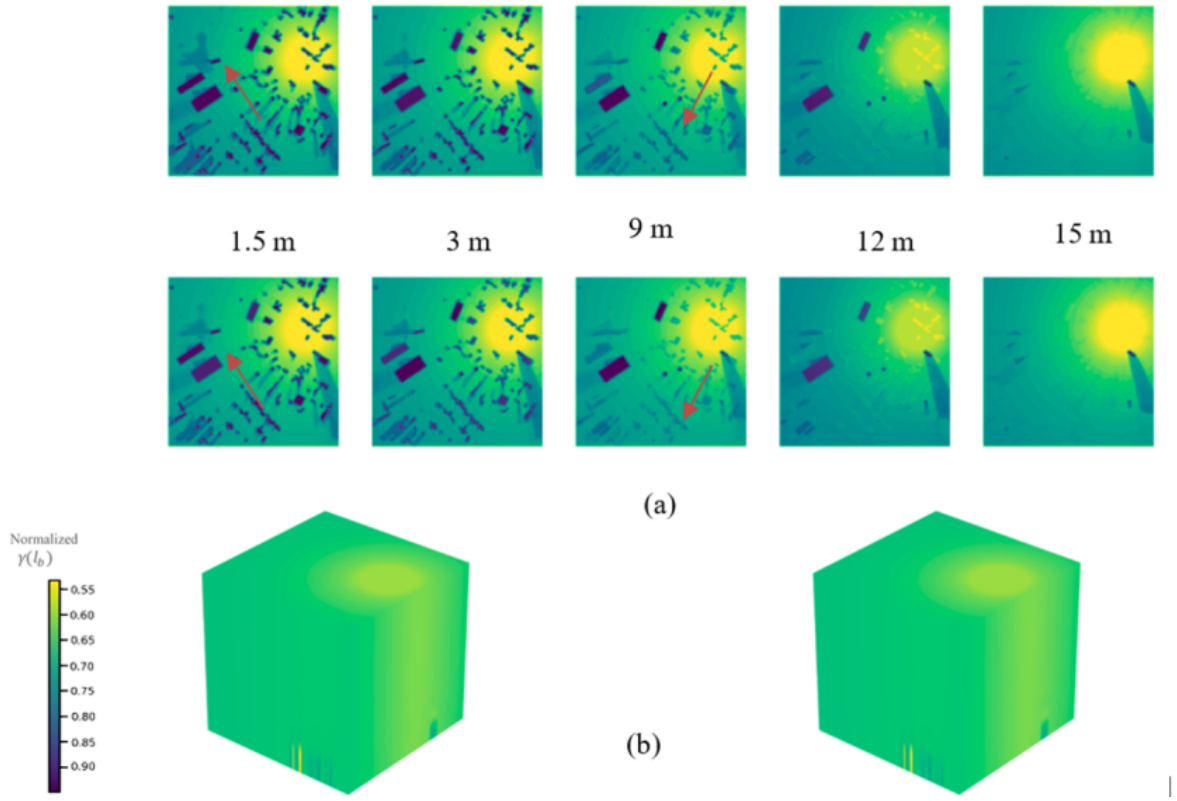


**Figure 4.6:** Comparison of the constructed VREM with the Vol2Vol approach with the ground truth. In (a) the ground truth (top row) is compared with the constructed map at a different height above the ground; and in (b) the constructed VREM (to the left) is compared to the ground truth (to the right).

the model's performance in capturing the environmental effects on signal propagation for a randomly selected communication link, specifically the GBS-GUE link. Comparisons with ground truth data are presented both at various heights and across the overall VREM. The model demonstrates a strong ability to learn and represent environmental impacts, such as attenuation and scattering, caused by surrounding structures. However, as illustrated in Figure 4.6(a), the model struggles to accurately capture the extended propagation effects of narrow streets and closely spaced buildings positioned farther away from the transmitter, particularly at lower altitudes. This limitation, marked by red arrows, arises from the model's reduced capability to account for long-range propagation effects caused by these structures, particularly at lower heights. At lower altitudes, signal propagation is more heavily affected by obstructions and multipath effects, which the model finds challenging to account for. In contrast, at higher altitudes, where obstructions are fewer, the propagation patterns become simpler, and the model achieves better accuracy.

This disparity in performance is quantitatively supported by the SSIM values listed in Table 4.4, which evaluate the image quality of VREM constructions at different altitudes. The SSIM metric, ranging from 0 (no similarity) to 1 (perfect similarity), reflects the similarity between the predicted VREM and the ground truth. Higher SSIM values at greater altitudes indicate the model's improved capability to accurately reconstruct the VREM in these regions. This suggests that the model's architectural design is better suited for urban areas or a propagation environments, while additional adjustments or enhancements may be required to better handle complex, obstructed propagation scenarios at highly densified cities. Figure 4.7 illustrates the

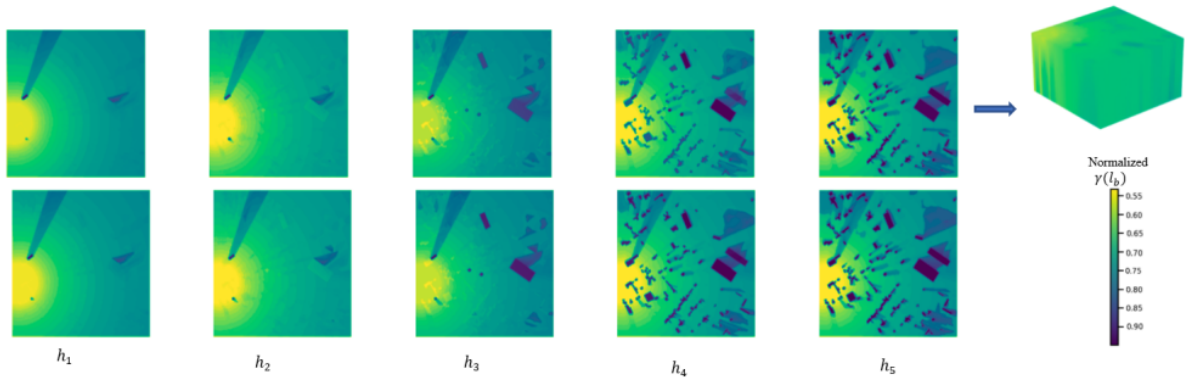


**Figure 4.7:** Comparison of the constructed REM with Sliced-VREM (5-stack) (top row) with the ground truth (bottom row).

construction of the VREM with the Sliced-VREM (n=5-stack) approach, where the estimated map is pictorially compared to the ground truth. The 5-stack model refers to five UNets simultaneously learning the propagation channel characteristics from five consecutive REMs. In this case, the VREM that is generated at once will have 15 m (5 × 3 m resolution) of height.

As mentioned in Section 4.4.2, it is straightforward to infer that the number of parallelly stacked UNets in the Sliced-VREM approach governs the trade-off between the complexity and depth of the constructed VREM. If the number of stacks increases to the maximum, , $n = S$, where $S$ represents the maximum discretized altitude, one can construct the VREM by accounting for the broad altitude dependency.

As altitude increases, the channel characteristics become more deterministic due to the reduced number of scatterers between the transmitter and receiver. This allows the model to effectively capture parameters like $\alpha$ and $\beta$, with the channel primarily influenced by the GBS-GUE/AUE or ABS-GUE distance. Beyond a certain altitude, shadowing effects diminish, and propagation loss can be largely attributed to frequency loss and space loss. This understanding suggests that

it may be feasible to extrapolate channel characteristics for altitudes above a specific threshold, as illustrated in Table 4.4. Additionally, reducing the number of stacks in the Sliced-VREM approach decreases both the complexity and memory requirements for map construction, resulting in a shorter volumetric height (stack) for the reconstructed map. When the Sliced-VREM utilizes only a single layer, it closely resembles 2D REM construction models, as discussed in [133, 136]. The performance of the two proposed approaches is summarized in Table 4.4

**Table 4.4:** Comparing the image quality of the contracted VREM at different altitudes.

| | **Mean SSIM** | | | | |
|---|---|---|---|---|---|
| | **1.5m** | **3 m** | **9 m** | **12 m** | **15 m** |
| Vol2Vol - VREM | 0.748 | 0.802 | 0.842 | 0.927 | 0.9447 |
| Sliced-VREM | 0.799 | 0.833 | 0.868 | 0.905 | 0.922 |

**Table 4.5:** Comparing the map construction with the maximum probability of LoS.

| | **MAE** | | | |
|---|---|---|---|---|
| | **Mean Sliced-VREM** | **Mean Vol2Vol-VREM** | **Sliced-VREM** (at PLoS = .95) | **Vol2Vol – VREM** (at PLoS = .95) |
| Addis Dataset | 0.02 | 0. 018611 | 0.01 | 0.0084 |

and 4.5. At lower altitudes, Vol2Vol-VREM shows slight degradation in constructed image quality compared to sliced-VREM, as evidenced by Table 4.4. This can be attributed to the inherent limitations of the 3D GAN in capturing finer details and sharper edges. However, as altitude increases, the deterministic nature of propagation loss benefits Vol2Vol-VREM. Its direct modeling of signal propagation enables it to outperform the sliced approach, resulting in superior performance at higher altitudes. This superiority is further confirmed by Table 4.5, where Vol2Vol-VREM achieves consistently lower MAE than Sliced-VREM, demonstrating its accuracy despite the increased complexity of training and constructing large-volume VREMs.

Although a direct approach for one-to-one benchmark comparison in VREM construction was not available, we evaluated the richness of the Addis dataset for DL approaches used in [133, 136]. As illustrated in Table 4.6, while the 2D REM models exhibit performance levels comparable to the proposed VREM methods, they face significant limitations. Specifically, the 2D REM models struggle to exploit altitude dependencies, which are crucial for accurate

propagation loss modeling and spectrum map construction. This shortcoming arises because the 2D models rely on almost identical flat maps, which fail to account for variations in elevation. Consequently, their ability to accurately predict signal behavior in three-dimensional space is hindered, underscoring the advantage of using VREM approaches that incorporate altitude information for improved performance.

**Table 4.6:** Evaluating the richness of the Addis dataset.

| MAE | RadioNet (2D) [136] | Radio UNets [133] | Sliced-VREM | Vol2Vol-VREM |
|---|---|---|---|---|
| Addis Dataset | 0.054 | 0. 0439 | 0.02 | 0. 018611 |

### 4.5.3 Preliminary Spectrum Situational awareness

With the constructed VREM at a particular location, the quality of the signal level can be further evaluated to estimate and build preliminary spectrum availability and occupancy awareness. Specifically, for a given occupancy threshold, which is assumed to be a received signal level of -90 dBm, the spectrum occupancy map at different altitudes can be generated, as illustrated in Figure 4.8. In this context, the occupancy state is determined as follows: if the received signal level $Pr$ is greater than or equal to the threshold level $Prth$, it is considered occupied and represented by a value of 1. Conversely, if the received signal level $Pr$ is less than the threshold $Prth$, it is considered available and represented by a value of 0. This generated occupancy

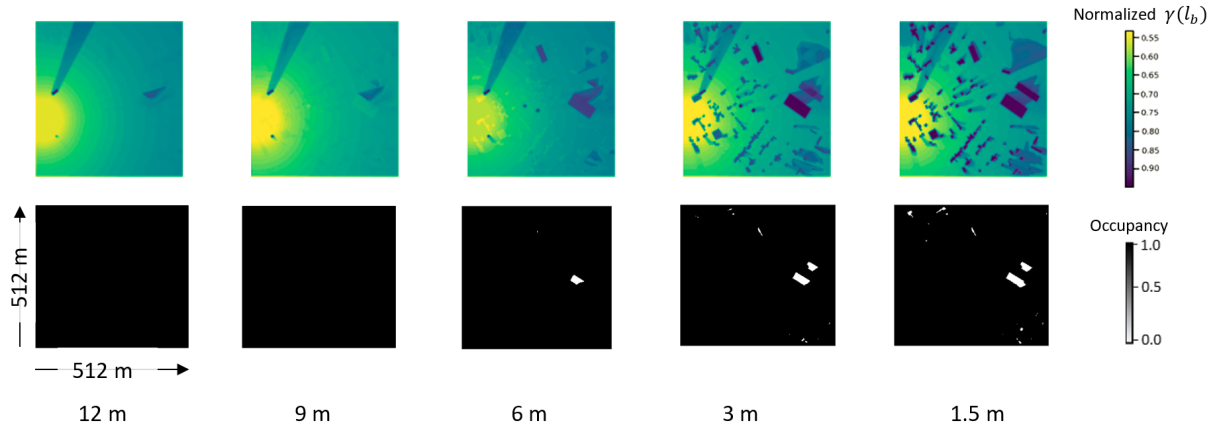


**Figure 4.8:** Constructed spectrum map for a VREM.

map at different altitudes showed the potential of spectrum avaliblity at a of can provide

valuable insights into the spatial and altitudinal variations of the spectrum use. Such maps are particularly useful in DSS scenarios where directional and narrower beams are employed.

## 4.6 Chapter Summary

This chapter investigates the construction of VREMs using DL, a critical step toward developing SSA for networks with 3D architectures, such as UAV-assisted communication systems with limited or no real spectrum monitoring data. Two novel approaches are proposed, offering insights into their trade-offs and advancements over existing methods.

The first approach, Vol2Vol VREM construction using 3D-GAN, directly learns 3D inputs, translating environmental and transmitter location maps into propagation loss maps. This method achieves high accuracy, particularly at higher altitudes, with a mean SSIM of 0.9447 at 15m and an MAE of 0.0186. However, its fully 3D nature presents challenges in memory usage and managing altitude slices. The second approach, Sliced-VREM construction using Altitude-Aware Spider-UNets, adopts a memory-efficient strategy by processing sequences of 2D images in parallel while capturing altitude dependencies through stacked U-Nets. Though less accurate than the 3D-GAN, with a mean SSIM of 0.799 at 1.5m, Sliced-VREM effectively handles altitude variations and is computationally more efficient.

A comparative analysis using MAE and SSIM underscores the importance of altitude-aware modeling in achieving accurate VREM construction. The Vol2Vol approach outperforms Sliced-VREM by 7%, excelling in capturing complex volumetric details and achieving superior accuracy at higher altitudes. In contrast, Sliced-VREM performs better at lower altitudes, where finer propagation details and obstructions have a more significant impact. Both models significantly outperform 2D REM baselines, with MAE reductions of 62.9% (Vol2Vol-VREM) and 54.5% (Sliced-VREM), highlighting the necessity of altitude-aware modeling for 3D environments.

Preliminary SSA maps, generated using the constructed VREM, demonstrate spatial and altitudinal variations of spectrum occupancy for specific areas, even at low heights of 9 m or less, based on a signal threshold of -90 dBm. These maps showcase the potential of REMs in providing actionable insights for Dynamic Spectrum Sharing (DSS) scenarios, significantly reducing reliance on extensive monitoring infrastructure. Altitude-aware modeling proves es-

pecially critical for capturing deterministic propagation loss at higher altitudes and addressing shadowing and multipath effects in urban environments.

This chapter advances the state of VREM construction while offering valuable insights for future research in building efficient SSA frameworks for 3D networks.

# 5 Conclusions and Recommendations

In conclusion, we revisit the challenges addressed in this research, summarizing its contributions to attaining accurate and comprehensive SA. Additionally, we outline directions for future investigation, setting the stage for continued advancements in this field.

## 5.1 Research Conclusions

### 5.1.1 Addressing Challenge 1: Accurate long-term predictability of Spectrum data

Achieving accurate long-term spectrum predictions is crucial for effective spectrum management. The cooperative prediction framework implemented in Chapter 2 combined data from distributed sensing nodes using a central fusion center and DL based models for single location and grid like multi location Spectrum predictions. This scheme combined measurements from various sensing nodes in a centralized soft fusion entity, prioritizing nodes based on their proximity to ensure data relevance. Additionally, integrating monitoring data from nearby SS when continuous monitoring isn't feasible or in cases of missed detections enhances the availability of historical spectrum data crucial for temporal prediction tasks. That gave our proposed models the ability to capture spectrum data's temporal patterns effectively, providing accurate predictions up to 2.5 hours into the future with a maximum acceptable prediction error of less than 5 dBm, as validated using real-world datasets. The prediction performance of our models vary due to factor such as different PU usage patterns, network configurations and the radio propagation characteristics at various frequency. A sight dominance in prediction is observed for the single location predictor model for lower spectrum bands with deterministic PU usage patterns. At higher frequency range, due to model's ability to understand the joint spatial-spectral-temporal dependencies, the multi-location predictor shows approximately a 14% improvement in prediction accuracy compared to the single-location model. Furthermore,

a maximum of 13% improvement in the long-term prediction accuracy has been seen with an 75 minute increase in lookback window of the past measurement data, enabling them to better understand the temporal dynamics of spectrum usage. Dispute the sparsity of SS, increasing cooperative region have also shown a positive impact on improving the long term prediction accuracy by enriching the quality of spectrum monitored data. Our framework's flexibility in integrating monitoring data from nearby SS ensures that historical data gaps minimally affect predictive performance. However, synchronization and coordination delays between nodes and the fusion center, not considered in this study, remain avenues for future exploration.

To address the limitations of spectrum sensing data availability, we proposed an approach in Chapter 3 that utilizes network monitoring data related to voice and data service traffic for MNOs, offering valuable insights for indirectly building SA. By employing DL-based predictors to capture temporal correlations in the data and using appropriate traffic-to-utilization mapping techniques, we attained a 24 hrs. of spectrum utilization awareness without directly conducting any spectrum sensing. However, future research should focus on how MNOs can integrate additional network data while accounting for the dynamic nature of user distribution, behavior, and the Qos requirements of various applications generating data traffic. This represents a promising path for further exploration.

### 5.1.2 Addressing Challenge 2: Building Multi-dimensional SA

In this research, the challenge of limited multi-dimensional SA was addressed through spatial correlation modeling. To enhance the accuracy of long-term spectrum prediction and achieve comprehensive knowledge of spectrum availability over a given geographical area in CRNs, we implemented distance-based interpolation with IDW in Chapter 2 for the proposed multi-location predictor model. By accounting for the distance dependency in the correlation of received signals from different SS and interpolating spectrum usage across unmonitored areas, the model demonstrated an overall improved prediction performance by 14% compared to a single-location predictor model. This was particularly evident for higher spectrum bands with PUs that have shorter coverage areas and more dynamic usage patterns. Overall, this approach successfully captured spatial dependencies in spectrum data, making it highly effective for predicting spectrum availability over large regions.

Another approach presented in Chapter 3 involves using K-means clustering over both spatial

and temporal dimensions to partition the spectrum monitoring or user-generated traffic volume data from MNOs into $k$ temporally correlated clusters. This method identifies unique spectrum usage patterns at different times and locations and develops a more generalized predictor model capable of learning each unique feature more clearly. This enables for defining more generalized model that can be trained to predict for more that a single base station.

In the context of wireless networks with 3D architectures, such as UAV-assisted networks, chapter 4 introduced the VREM construction concept and two novel approaches to capture the dependency of the propagation environment in both areal and altitude dimensions. Using innovative 3D-GAN and Spider-UNet models, we constructed volumentric propagation loss maps that integrate altitude and spatial variability, even achieving up to a 7% improvement in accuracy over traditional 2D approaches. With this situational knowledge about signal propagation characteristics in a given area, we computed a preliminary spectrum occupancy map, unlocking sharing opportunities at different altitudes/heights.

### 5.1.3 Addressing Challenge 3: Improving prediction Accuracy with Deep Learning models

The integration of DL models has emerged as a powerful approach to enhancing the accuracy of spectrum knowledge. In this research, we demonstrated the application of CNN and LSTM networks to effectively capture temporal and spatial dependencies in dynamic spectrum data. These models also enabled us to understand the intricate correlations among multivariate features, thereby significantly improving prediction accuracy.

Additionally, advanced generative DL architectures, such as GAN and Volumetric Unets, were employed to reconstruct knowledge about the spectrum environment, even when the input data was limited or indirect. These architectures proved capable of generating high-resolution and detailed representations of the radio environment by learning underlying patterns and relationships from datasets. This capability underscores the potential of DL models to provide more accurate and comprehensive insights into the radio spectrum, facilitating better decision-making for spectrum management and dynamic resource allocation in wireless communication networks.

## 5.2 Recommendations

Technological trends in advanced DL models and learning approaches, as well as intelligence at wireless devices and networks, are becoming the pillars for addressing different challenges in spectrum awareness. These advancements are crucial for bringing DSS to fruition in B5G networks.

Decentralizing the conventional ML approach, federated learning has shown significant potential in enhancing the performance of spectrum monitoring and prediction activities. Unlike the conventional cloud-centric approach, federated learning enables collaborative learning between sensing nodes without continuously transferring monitoring data to a central server. Instead, each sensing node can independently process local spectrum data and only share model updates with a centralized cloud, reducing the need for real-time communication and minimizing the impact of network latency on overall system performance [137, 138]. This approach could be particularly beneficial for mobile sensing nodes, as it allows devices to localize the process of attaining SA information while collaboratively conducting global model training, thus potentially mitigating communication overhead and coordination delays enhanced by their mobility. However, further investigation is needed to consider the heterogeneity of mobile sensing nodes and variability in the propagation environment to ensure the global model updates are robust to sensor capabilities and variations in data quality [139].

Edge computing and distributed wireless networks are another promising solution that complements federated learning by offering a distributed and decentralized architecture. This architecture facilitates real-time data processing and decision-making closer to the edge of the network, i.e., the SUs or SS [140]. When these devices are designed to directly communicate and share their localized SA with each other, the constant need to coordinate and synchronize with centralized cloud servers is reduced. This improves the end-to-end latency and minimize synchronization issue that have significant effect in cooperative prediction. Moreover, the distributed nature of such spectrum monitoring is expected to further enhance the robustness of spectrum prediction systems by reducing dependency on a single point of failure and allowing for more dynamic and resilient data collection.

An important solution for enhancing spectrum prediction accuracy is the adoption of advanced algorithms and DL techniques. These approaches leverage the computational power of DL to develop adaptive models capable of accurately predicting spectrum usage patterns while

dynamically adjusting to changing environmental conditions over a wide spectrum range. For instance, deep reinforcement learning offers a novel way to improve spectrum allocation strategies by continuously learning the best rules for selecting the most reliable sensing data, considering not only the location but also the quality and relevance of the sensing information or by incorporating a reward-based mechanism for SS providing accurate sensing data [141]. Moreover, replacing traditional LSTM networks with transformer architectures or hybrid LSTM variants offers significant potential for improving long-term spectrum predictability. Transformer networks, with their attention mechanisms, excel in capturing complex relationships and dependencies within data, allowing for a more nuanced understanding of spectrum usage patterns. These models are particularly adept at handling diverse patterns, short-term fluctuations, and long-term dependencies, making them ideal for dynamic and heterogeneous wireless environments [142].

# Bibliography


[1] Jennifer Manner. **Spectrum Wars: The Rise of 5G and Beyond**. Artech House Publisher, 2021, 240. ISBN: 9781630819163.

[2] Silvia Ruiz, Hamed Ahmadi, Gordana Gardašević, Yoram Haddad, Konstantinos Katzis, Paolo Grazioso, and et al. In: *Inclusive Radio Communications for 5G and Beyond*. 2021.

[3] Maziar Nekovee and Richard Rudd. *5G Spectrum Sharing*. 2017. DOI: 10.48550/arXiv.1708.03772. arXiv: 1708.03772 [cs.NI]. URL: https://arxiv.org/abs/1708.03772.

[4] Walid Saad, Mehdi Bennis, and Mingzhe Chen. **A Vision of 6G Wireless Systems: Applications, Trends, Technologies, and Open Research Problems**. *IEEE Network*: 3 (2020), 134–142. DOI: 10.1109/MNET.001.1900287.

[5] M. Mozaffari, A. Taleb Zadeh Kasgari, W. Saad, M. Bennis, and M. Debbah. **Beyond 5G With UAVs: Foundations of a 3D Wireless Cellular Network**. *IEEE Transactions on Wireless Communications* 18:1 (2019), 357–372. DOI: 10.1007/s11432-020-2955-6.

[6] Zixiao Zhao, Qinghe Du, Dawei Wang, Xiao Tang, and Houbing Song. **Overview of Prospects for Service Aware Radio Access towards 6G Networks**. *Electronics* 11:8 (2022), 5711–5722. ISSN: 2079-9292. DOI: 10.3390/electronics11081262.

[7] Ahmet Yazar, Seda Dougan-Tusha, and Hüseyin Arslan. **6G Vision: An Ultra-Flexible Radio Access Technology Perspective**. *ITU Journal on Future and Evolving Technologies* 9:1(1) (2020), 1–20. DOI: 10.48550/arXiv.2009.07597. URL: http://handle.itu.int/11.1002/pub/8173e1cc-en.

[8] Qian Mao, Fei Hu, and Qi Hao. **Deep Learning for Intelligent Wireless Networks: A Comprehensive Survey**. *IEEE Communications Surveys & Tutorials* 20:4 (2018), 2595–2621. DOI: 10.1109/COMST.2018.2846401.

[9] Adrian Kliks, Lukasz Kulacz, Pawel Kryszkiewicz, Hanna Bogucka, Marcin Dryjanski, Magnus Isaksson, George P. Koudouridis, and Per Tengkvist. **Beyond 5G: Big Data Processing for Better Spectrum Utilization**. *IEEE Vehicular Technology Magazine* 15:3 (2020), 40–50. DOI: 10.1109/MVT.2020.2988415.

[10] Raza Umar and Asrar U.H. Sheikh. **A comparative study of spectrum awareness techniques for cognitive radio oriented wireless networks**. *Physical Communication* 9 (2013), 148–170. ISSN: 1874-4907. DOI: https://doi.org/10.1016/j.phycom.2012.07.005. URL: https://www.sciencedirect.com/science/article/pii/S1874490712000687.

[11] Marko Höyhtyä, Atso Hekkala, Marcos D. Katz, and Aarne Mämmelä, 353–372. In: *Cognitive Wireless Networks: Concepts, Methodologies and Visions Inspiring the Age of Enlightenment of Wireless Communications*. Ed. by Frank H. P. Fitzek and Marcos D. Katz. Springer Netherlands, 2007. DOI: 10.1007/978-1-4020-5979-7_18. URL: https://doi.org/10.1007/978-1-4020-5979-7_18.

[12] Muhammad Muzamil Aslam, Liping Du, Xiaoyan Zhang, Yueyun Chen, Zahoor Ahmed, and Bushra Qureshi. **Sixth Generation (6G) Cognitive Radio Network (CRN) Application, Requirements, Security Issues, and Key Challenges**. *Wireless Communications and Mobile Computing* 2021:1331428 (2021), 18. DOI: 10.1155/2021/1331428.

[13] Oladiran G. Olaleye, Alaa Ali, Kasem Khalil, Bappaditya Dey, Dmitri Perkins, and Magdy Bayoumi. **Spectrum-Awareness-Based Performance and Scalability of Cognitive Radio Networks**. In: *2018 IEEE International Conference on Communications Workshops (ICC Workshops)*. 2018, 1–6. DOI: 10.1109/ICCW.2018.8403542.

[14] Oliver Holland, Vasilis Friderikos, and A. Hamid Aghvami. **Green spectrum management for mobile operators**. In: *2010 IEEE Globecom Workshops*. 2010, 1458–1463. DOI: 10.1109/GLOCOMW.2010.5700180.

[15] Roya H. Tehrani, Seiamak Vahid, Dionysia Triantafyllopoulou, Haeyoung Lee, and Klaus Moessner. **Licensed Spectrum Sharing Schemes for Mobile Operators: A Survey and Outlook**. *IEEE Communications Surveys and Tutorials* 18:4 (2016), 2591–2623. DOI: 10.1109/COMST.2016.2583499.

[16] Rony K. Saha and John M. Cioffi. **Dynamic Spectrum Sharing for 5G NR and 4G LTE Coexistence - A Comprehensive Review**. *IEEE Open Journal of the Communications Society* 5 (2024), 795–835. DOI: 10.1109/OJCOMS.2024.3351528.

[17] Petri Luoto, Pekka Pirinen, Mehdi Bennis, Sumudu Samarakoon, Simon Scott, and Matti Latva-aho. **Co-Primary Multi-Operator Resource Sharing for Small Cell Networks**. *IEEE Transactions on Wireless Communications* 14:6 (2015), 3120–3130. DOI: 10.1109/TWC.2015.2402671.

[18] Mostafizur Rahman, Murat Yuksel, and Thomas Quint. **A Game-Theoretic Framework to Regulate Freeriding in Inter-Provider Spectrum Sharing**. *IEEE Transactions on Wireless Communications* 20:6 (2021), 3941–3957. DOI: 10.1109/TWC.2021.3054558.

[19] Ling Zhang, Zhiqing Wei, Lin Wang, Xin Yuan, Huici Wu, and Wenyan Xu. **Spectrum Sharing in the Sky and Space: A Survey**. *Sensors* 23:1 (2023). ISSN: 1424-8220. DOI: 10.3390/s23010342. URL: https://www.mdpi.com/1424-8220/23/1/342.

[20] Pawel Kaniewski, Janusz Romanik, Edward Golan, and Krzysztof Zubel. **Spectrum Awareness for Cognitive Radios Supported by Radio Environment Maps: Zonal Approach**. *Applied Sciences* 11:7 (2021). ISSN: 2076-3417. DOI: 10.3390/app11072910. URL: https://www.mdpi.com/2076-3417/11/7/2910.

[21] Bin Qi, Wensheng Zhang, and Lei Zhang. **Spectrum Situation Awareness for Space–Air–Ground Integrated Networks Based on Tensor Computing**. *Sensors* 24:2 (2024). ISSN: 1424-8220. DOI: 10.3390/s24020334. URL: https://www.mdpi.com/1424-8220/24/2/334.

[22] Yonghong Zeng, Ying-Chang Liang, Anh Tuan Hoang, and Rui Zhang. **A Review on Spectrum Sensing for Cognitive Radio: Challenges and Solutions**. *EURASIP J. Adv. Signal Process* 2010 (2010). ISSN: 1110-8657. DOI: 10.1155/2010/381465. URL: https://doi.org/10.1155/2010/381465.

[23] Tevfik Yucek and Huseyin Arslan. **A survey of spectrum sensing algorithms for cognitive radio applications**. *IEEE Communications Surveys and Tutorials* 11:1 (2009), 116–130. DOI: 10.1109/SURV.2009.090109.

[24] Takeo Fujii, Kei Inage, and Koya Sato, 1797–1820. In: *Handbook of Cognitive Radio*. Vol. 3-3. Springer Singapore, 2019. DOI: 10.1007/978-981-10-1394-2_56.

[25] Marko Hoyhtya, Aarne Mammela, Alessandro Chiumento, Sofie Pollin, Martti Forsell, and Danijela Cabric. **Database-Assisted Spectrum Prediction in 5G Networks and Beyond: A Review and Future Challenges**. *IEEE Circuits and Systems Magazine* 19:3 (2019), 34–45. DOI: 10.1109/MCAS.2019.2925293.

[26] Xiaoshuang Xing, Tao Jing, Wei Cheng, Yan Huo, and Xiuzhen Cheng. **Spectrum prediction in cognitive radio networks**. *IEEE Wireless Communications* 20 (2013), 90–96.

[27] Hamid Eltom. **Spectrum Prediction in Dynamic Spectrum Access Systems**. PhD thesis. 2018, 127. URL: https://link.springer.com/Article/10.1186/s13638-017-1019-8.

[28] Salim Eryigit, Suzan Bayhan, and Tuna Tugcu. **Channel switching cost aware and energy-efficient cooperative sensing scheduling for cognitive radio networks**. In: *2013 IEEE International Conference on Communications (ICC)*. 2013, 2633–2638. DOI: 10.1109/ICC.2013.6654933.

[29] Munawwar Sohul, Miao Yao, Taeyoung Yang, and Jeffrey Reed. **Spectrum Access System for the Citizen Broadband Radio Service**. *IEEE Communications Magazine* 53 (July 2015), 18–25. DOI: 10.1109/MCOM.2015.7158261.

[30] Anirudha Sahoo, Naceur El Ouni, and Vineet Shenoy. **A Study of Timing Constraints and SAS Overload of SAS-CBSD Protocol in the CBRS Band**. In: *2019 IEEE Globecom Workshops*. 2019, 1–6. DOI: 10.1109/GCWkshps45667.2019.9024407.

[31] Topias Kokkinen, Heikki Kokkinen, and Seppo Yrjölä. **Spectrum Broker Service for Micro-operator and CBRS Priority Access Licenses**. In: *Cognitive Radio Oriented Wireless Networks*. Springer International Publishing, 2018, 237–246. ISBN: 978-3-319-76207-4. DOI: 10.1007/978-3-319-76207-4_20.

[32] Youping Zhao, Bin Le, and Jeffrey H. Reed. "Chapter 11 - Network Support: The Radio Environment Map." In: *Cognitive Radio Technology*. Ed. by Bruce A. Fette. Burlington: Newnes, 2006, 337–363. ISBN: 978-0-7506-7952-7. DOI: https://doi.org/10.1016/B978-075067952-7/50012-X. URL: https://www.sciencedirect.com/science/Article/pii/B978075067952750012X.

[33] H. Birkan Yilmaz, Tuna Tugcu, Fatih Alagöz, and Suzan Bayhan. **Radio environment map as enabler for practical cognitive radio networks**. *IEEE Communications Magazine* 51:12 (2013), 162–169. DOI: 10.1109/MCOM.2013.6685772.

[34] S. Bi, J. Lyu, Z. Ding, and R. Zhang. **Engineering Radio Maps for Wireless Resource Management**. *IEEE Wireless Communications* 26:2 (2019), 133–141. DOI: 10.1109/MWC.2019.1800146.

[35] Miguel Lopez Benitez. **Smart spectrum awareness in future wireless communications: State-of-the-art, open challenges and the way forward**. In: *2017 2nd International Conference on Telecommunication and Networks (TEL-NET)*. 2017, 1–1. DOI: 10.1109/TEL-NET.2017.8343281.

[36] Sepp Hochreiter and Jürgen Schmidhuber. **Long Short-Term Memory**. *Neural Computation* 9:8 (1997), 1735–1780. ISSN: 0899-7667. DOI: 10.1162/neco.1997.9.8.1735. URL: https://doi.org/10.1162/neco.1997.9.8.1735.

[37] Benjamin Lindemann, Timo Müller, Hannes Vietz, Nasser Jazdi, and Michael Weyrich. **A survey on long short-term memory networks for time series prediction**. *Procedia CIRP* 99 (2021), 650–655. ISSN: 2212-8271. DOI: https://doi.org/10.1016/j.procir.2021.03.088. URL: https://www.sciencedirect.com/science/article/pii/S2212827121003796.

[38] Alex Graves and Jürgen Schmidhuber. **Framewise phoneme classification with bidirectional LSTM and other neural network architectures.** *Neural Network* 18:5-6 (2005), 602–610. DOI: 10.1016/j.neunet.2005.06.042.

[39] Sepp Hochreiter and Jürgen Schmidhuber. **Long short-term memory**. *Neural computation* 9:8 (1997), 1735–1780.

[40] Rikiya Yamashita, Mizuho Nishio, Richard Kinh Gian Do, and Kaori Togashi. **Convolutional neural networks: an overview and application in radiology**. *nature* 9 (2018), 611–629. DOI: 10.1007/s13244-018-0639-9.

[41] Xingjian Shi, Zhourong Chen, Hao Wang, Dit-Yan Yeung, Wai-kin Wong, and Wang-chun Woo. **Convolutional LSTM Network: A Machine Learning Approach for Precipitation Nowcasting**. In: *Proceedings of the 28th International Conference on Neural Information Processing Systems*. Vol. 1. NIPS'15. Montreal, Canada: MIT Press, 2015, 802–810.

[42] Emad Ul Haq Qazi, Abdulrazaq Almorjan, and Tanveer Zia. **A One-Dimensional Convolutional Neural Network (1D-CNN) Based Deep Learning System for Network Intrusion Detection**. *Applied Sciences* 12:16 (2022). ISSN: 2076-3417. DOI: 10.3390/app12167986. URL: https://www.mdpi.com/2076-3417/12/16/7986.

[43] Arohan Ajit, Koustav Acharya, and Abhishek Samanta. **A Review of Convolutional Neural Networks**. In: *2020 International Conference on Emerging Trends in Information Technology and Engineering (ic-ETITE)*. 2020, 1–5. DOI: 10.1109/ic-ETITE47903.2020.049.

[44] Rahul Dev Singh, Ajay Mittal, and Rajesh K. Bhatia. **3D convolutional neural network for object recognition: a review.** *Multimedia Tools and Applications* 78 (2019), 15951–15995. DOI: 10.1007/s11042-018-6912-6.

[45] Kyunghyun Cho, Bart van Merrienboer, Caglar Gulcehre, Dzmitry Bahdanau, Fethi Bougares, Holger Schwenk, and Yoshua Bengio. *Learning Phrase Representations using RNN Encoder-Decoder for Statistical Machine Translation*. 2014. DOI: 10.48550/ARXIV.1406.1078. URL: https://arxiv.org/abs/1406.1078.

[46] Cong Zou, Fang Yang, Jian Song, and Zhu Han. **Generative Adversarial Network for Wireless Communication: Principle, Application, and Trends**. *IEEE Communications Magazine* (2023), 1–7. DOI: 10.1109/MCOM.011.2200731.

[47] Xuedong Wu, Yaonan Wang, Jianxu Mao, Zhaoping Du, and Chunhua Li. **Multi-step prediction of time series with random missing data**. *Applied Mathematical Modelling* 38:14 (2014), 3512–3522. DOI: 10.1016/j.apm.2013.11.029.

[48] Jing Zhang, Guoru Ding, Yitao Xu, and Fei Song. **On the usefulness of spectrum prediction for dynamic spectrum access**. In: *2016 8th International Conference on Wireless Communications & Signal Processing (WCSP)*. 2016, 1–4. DOI: 10.1109/WCSP.2016.7752555.

[49] Yuh-Ren Tsai. **Sensing Coverage for Randomly Distributed Wireless Sensor Networks in Shadowed Environments**. *IEEE Transactions on Vehicular Technology* 57:1 (2008), 556–564. DOI: 10.1109/TVT.2007.905624.

[50] M. Wellens, J. Riihijarvi, M. Gordziel, and P. Mahonen. **Spatial Statistics of Spectrum Usage: From Measurements to Spectrum Models**. In: *2009 IEEE International Conference on Communications*. 2009, 1–6. DOI: 10.1109/ICC.2009.5199473.

[51] Lixing Yu, Qianlong Wang, Yifan Guo, and Pan Li. **Spectrum availability prediction in cognitive aerospace communications: A deep learning perspective**. In: *2017 Cognitive Communications for Aerospace Applications Workshop (CCAA)*. 2017, 1–4. DOI: 10.1109/CCAAW.2017.8001877.

[52] Mohammad Parvini, Amir Hossein Zarif, Ali Nouruzi, Nader Mokari, Mohammad Reza Javan, Bijan Abbasi, Amir Ghasemi, and Halim Yanikomeroglu. *A Comprehensive Survey of Spectrum Sharing Schemes from a Standardization and Implementation Perspective*. 2022. arXiv: 2203.11125 [eess.SP].

[53] Dong Liu, Yang Huang, and Zhen Gao. **Spectrum Situation Completion Based on Model-Enhanced Generative Learning**. In: *2021 13th International Conference on Wireless Communications and Signal Processing (WCSP)*. 2021, 1–5. DOI: 10.1109/WCSP52459.2021.9613512.

[54] Feng Shen, Guoru Ding, Zheng Wang, and Qihui Wu. **UAV-Based 3D Spectrum Sensing in Spectrum-Heterogeneous Networks**. *IEEE Transactions on Vehicular Technology* 68:6 (2019), 5711–5722. DOI: 10.1109/TVT.2019.2909167.

[55] Hamid Eltom, Sithamparanathan Kandeepan, Robin J. Evans, Ying-Chang Liang, and Branko Ristic. **Statistical spectrum occupancy prediction for dynamic spectrum access: a classification**. *EURASIP Journal on Wireless Communications and Networking* 2018 (2018), 1–17.

[56] Ali Gorcin, Hasari Celebi, Khalid A. Qaraqe, and Huseyin Arslan. **An autoregressive approach for spectrum occupancy modeling and prediction based on synchronous measurements**. In: *2011 IEEE 22nd International Symposium on Personal, Indoor and Mobile Radio Communications*. 2011, 705–709. DOI: 10.1109/PIMRC.2011.6140056.

[57] Simon D. Barnes, Bodhaswar T. Maharaj, and Attahiru S. Alfa. **Cooperative Prediction for Cognitive Radio Networks**. *Wireless Personal Communications* 89:4 (2016), 1177–1202. ISSN: 1572834X. DOI: 10.1007/s11277-016-3311-z. URL: https://doi.org/10.1007/s11277-016-3311-z.

[58] Pavel Baltiiski, Ilia Iliev, Boian Kehaiov, Vladimir K. Poulkov, and Todor Cooklev. **Long-Term Spectrum Monitoring with Big Data Analysis and Machine Learning for Cloud-Based Radio Access Networks**. *Wireless Personal Communications* 87 (2015), 815–835. URL: https://api.semanticscholar.org/CorpusID:35542525.

[59] Bertold Van den Bergh, Domenico Giustiniano, Héctor Cordobés, Markus Fuchs, Roberto Calvo-Palomino, Sofie Pollin, Sreeraj Rajendran, and Vincent Lenders. **Electrosense: Crowdsourcing spectrum monitoring**. In: *2017 IEEE International Symposium on Dynamic Spectrum Access Networks (DySPAN)*. 2017, 1–2. DOI: 10.1109/DySPAN.2017.7920766.

[60] Roberto Calvo-Palomino, Domenico Giustiniano, Vincent Lenders, and Aymen Fakhreddine. **Crowdsourcing spectrum data decoding**. In: *IEEE INFOCOM 2017 - IEEE Conference on Computer Communications*. 2017, 1–9. DOI: 10.1109/INFOCOM.2017.8057078.

[61] Yousi Lin, Yuxian Ye, and Yaling Yang. **Crowdsourcing-based Spectrum Monitoring at A Large Geographical Scale**. In: *2019 IEEE International Symposium on Dynamic Spectrum Access Networks (DySPAN)*. 2019, 1–10. DOI: 10.1109/DySPAN.2019.8935832.

[62] Mariya Zheleva, Ranveer Chandra, Aakanksha Chowdhery, Paul Garnett, Anoop Gupta, Ashish Kapoor, and Matt Valerio. **Enabling a Nationwide Radio Frequency Inventory Using the Spectrum Observatory**. *Transactions of Mobile Computing* 17 (2018). URL: https://www.microsoft.com/en-us/research/publication/enabling-nationwide-radio-frequency-inventory-using-spectrum-observatory/.

[63] Ana Nika, Zengbin Zhang, Xia Zhou, Ben Y. Zhao, and Haitao Zheng. **Towards commoditized real-time spectrum monitoring**. In: *Proceedings of the 1st ACM Workshop on Hot Topics in Wireless*. 2014, 25–30. ISBN: 9781450330763. DOI: 10.1145/2643614.2643615.

[64] Sreeraj Rajendran, Roberto Calvo-Palomino, Markus Fuchs, Bertold Van den Bergh, Hector Cordobes, Domenico Giustiniano, Sofie Pollin, and Vincent Lenders. **Electrosense: Open and Big Spectrum Data**. *IEEE Communications Magazine* 56:1 (2018), 210–217. DOI: 10.1109/MCOM.2017.1700200.

[65] Nikolaus Kleber, Abbas Termos, Gonzalo Martinez, John Merritt, Bertrand Hochwald, Jonathan Chisum, Aaron Striegel, and J. Nicholas Laneman. **RadioHound: A pervasive sensing platform for sub-6 GHz dynamic spectrum monitoring**. In: *2017 IEEE International Symposium on Dynamic Spectrum Access Networks (DySPAN)*. 2017, 1–2. DOI: 10.1109/DySPAN.2017.7920764.

[66] Hamid Eltom, Sithamparanathan Kandeepan, Ying Chang Liang, Bill Moran, and Robin J. Evans. **HMM-based cooperative spectrum occupancy prediction using hard fusion**. In: *2016 IEEE International Conference on Communications Workshops (ICC)*. 2016, 669–675. DOI: 10.1109/ICCW.2016.7503864.

[67] Ling Yu, Jin Chen, and Guoru Ding. **Spectrum prediction via long short-term memory**. In: *2017 3rd IEEE International Conference on Computer and Communications (ICCC)*. 2017, 643–647. DOI: 10.1109/CompComm.2017.8322623.

[68] Jiachen Sun, Jinlong Wang, Guoru Ding, Liang Shen, Jian Yang, Qihui Wu, and Ling Yu. **Long-Term Spectrum State Prediction: An Image Inference Perspective**. *IEEE Access* 6 (2018), 43489–43498. DOI: 10.1109/ACCESS.2018.2861798.

[69] Zhenghao Zhang, Husheng Li, Hannan Ma, Kun Zheng, Depeng Yang, and Changxing Pei. **Spectrum Prediction via Temporal Conditional Gaussian Random Field Model in Wideband Cognitive Radio Networks**. In: *Quality, Reliability, Security and Robustness in Heterogeneous Networks*. Ed. by Xi Zhang and Daji Qiao. Berlin, Heidelberg: Springer Berlin Heidelberg, 2012, 16–27. ISBN: 978-3-642-29222-4.

[70] Babita R. Jose Jaison Jacob and Jimson Mathew. **Bayesian analysis of spectrum occupancy prediction in cognitive radio**. *Smart Science* 4:2 (2016), 52–61. DOI: 10.1080/23080477.2016.1182360.

[71] Chao Ge, Zheng Wang, and Xiaofei Zhang. **Robust Long-Term Spectrum Prediction With Missing Values and Sparse Anomalies**. *IEEE Access* 7 (2019), 16655–16664. DOI: 10.1109/ACCESS.2018.2889161.

[72] Xiaoshuang Xing, Tao Jing, Wei Cheng, Yan Huo, Xiuzhen Cheng, and Taieb Znati. **Cooperative spectrum prediction in multi-PU multi-SU cognitive radio network**. *Mobile Networks and Applications* 19:4 (Aug. 2014), 502–511. ISSN: 1383-469X. DOI: 10.1007/s11036-014-0507-x.

[73] Hamid Eltom, Sithamparanathan Kandeepan, Ying-Chang Liang, and Robin J. Evans. **Cooperative Soft Fusion for HMM-Based Spectrum Occupancy Prediction**. *IEEE Communications Letters* 22:10 (2018), 2144–2147. DOI: 10.1109/LCOMM.2018.2861008.

[74] Nagwa Shaghluf and T. Aaron Gulliver. **Spectrum and energy efficiency of cooperative spectrum prediction in cognitive radio networks**. *Wireless Networks* 25 (2018). ISSN: 3265–3274. DOI: 10.1007/s11276-018-1720-5.

[75] K.C. Sriharipriya and K. Baskaran. **Optimal Number of Cooperators in the Cooperative Spectrum Sensing Schemes**. *Circuits Syst Signal Process* 37 (2018), 1988–2000. DOI: 10.1007/s00034-017-0649-8.

[76] Sixing Yin, Dawei Chen, Qian Zhang, Mingyan Liu, and Shufang Li. **Mining Spectrum Usage Data: A Large-Scale Spectrum Measurement Study**. *IEEE Transactions on Mobile Computing* 11:6 (2012), 1033–1046. DOI: 10.1109/TMC.2011.128.

[77] Seungkeun Park, Mamta Agiwal, Hyeyeon Kwon, and Hu Jin. **An Evaluation Methodology for Spectrum Usage in LTE-A Networks: Traffic Volume and Resource Utilization Perspective**. *IEEE Access* 7 (2019), 67863–67873. DOI: 10.1109/ACCESS.2019.2918646.

[78] Marko Angjelicinoski, Vladimir Atanasovski, and Liljana Gavrilovska. **Comparative analysis of spatial interpolation methods for creating radio environment maps**. In: *2011 19thTelecommunications Forum (TELFOR) Proceedings of Papers*. 2011, 334–337. DOI: 10.1109/TELFOR.2011.6143557.

[79] Jingming Li, Guoru Ding, Xiaofei Zhang, and Qihui Wu. **Recent Advances in Radio Environment Map: A Survey**. In: *Machine Learning and Intelligent Communications*. Ed. by Xuemai Gu, Gongliang Liu, and Bo Li. Cham: Springer International Publishing, 2018, 247–257. ISBN: 978-3-319-73564-1.

[80] Anirudh Agarwal and Ranjan Gangopadhyay. **Predictive spectrum occupancy probability-based spatio-temporal dynamic channel allocation map for future cognitive wireless networks**. *Transactions on Emerging Telecommunications Technologies* 29:8 (2018). e3442 ett.3442, e3442. DOI: https://doi.org/10.1002/ett.3442. eprint: https://onlinelibrary.wiley.com/doi/pdf/10.1002/ett.3442. URL: https://onlinelibrary.wiley.com/doi/abs/10.1002/ett.3442.

[81] Yves Teganya and Daniel Romero. *Deep Completion Autoencoders for Radio Map Estimation*. 2021. arXiv: 2005.05964 [eess.SP].

[82] Md. Shaifur Rahman, Himanshu Gupta, Ayon Chakraborty, and Samir Das. **Creating Spatio-temporal Spectrum Maps from Sparse Crowdsensed Data**. In: *2019 IEEE Wireless Communications and Networking Conference (WCNC)*. 2019, 1–7. DOI: 10.1109/WCNC.2019.8885811.

[83] Mengyun Tang, Guoru Ding, Qihui Wu, Zhen Xue, and Theodoros A. Tsiftsis. **A Joint Tensor Completion and Prediction Scheme for Multi-Dimensional Spectrum Map Construction**. *IEEE Access* 4 (2016), 8044–8052. DOI: 10.1109/ACCESS.2016.2627243.

[84] H. Birkan Yilmaz, Chan-Byoung Chae, and Tuna Tugcu. **Sensor placement algorithm for radio environment map construction in cognitive radio networks**. In: *2014 IEEE Wireless Communications and Networking Conference (WCNC)*. 2014, 2096–2101. DOI: 10.1109/WCNC.2014.6952633.

[85] Sudharman K. Jayaweera and Mohamed A. Aref. **Cognitive Engine Design for Spectrum Situational Awareness and Signals Intelligence**. In: *2018 21st International Symposium on Wireless Personal Multimedia Communications (WPMC)*. 2018, 478–483. DOI: 10.1109/WPMC.2018.8712936.

[86] Yang Huang, Haoyu Cui, Yuqi Hou, Caiyong Hao, Wei Wang, Qiuming Zhu, Jie Li, Qihui Wu, and Jiabo Wang. **Space-Based Electromagnetic Spectrum Sensing and Situation Awareness**. *Space: Science & Technology* 4 (2024), 0109. DOI: 10.34133/space.0109. eprint: https://spj.science.org/doi/pdf/10.34133/space.0109. URL: https://spj.science.org/doi/abs/10.34133/space.0109.

[87] Todd Martin and K C Chang. **Development and analysis of a probabilistic reasoning methodology for spectrum situational awareness and parameter estimation in uncertain environments**. In: *2015 18th International Conference on Information Fusion (Fusion)*. 2015, 1475–1482.

[88] Bethelhem S. Shawel, Dereje H. Woldegebreal, and Sofie Pollin. **Deep-learning based Cooperative Spectrum Prediction for Cognitive Networks**. In: *9th International Conference on Information and Communication Technology Convergence: ICT Convergence Powered by Smart Intelligence, (ICTC 2018)*. 2018. DOI: 10.1109/ICTC.2018.8539570.

[89] Bethelhem S. Shawel, Dereje H. Woldegebreal, and Sofie Pollin. **Convolutional LSTM-based Long-Term Spectrum Prediction for Dynamic Spectrum Access**. In: *27th European Signal Processing Conference (EUSIPCO 2019)*. 2019. DOI: 10.23919/EUSIPCO.2019.8902956.

[90] Bethelhem S. Shawel, Frehiwot Bantigegn, Tsegamlak T. Debella, Sofie Pollin, and Dereje H. Woldegebreal. **K-Means Clustering Assisted Spectrum Utilization Prediction with Deep Learning Models**. *Engineering Proceedings* 18:1 (2022). ISSN: 2673-4591. DOI: 10.3390/engproc2022018002. URL: https://www.mdpi.com/2673-4591/18/1/2.

[91] Bethelhem S. Shawel, Endale Mare, Tsegamlak T. Debella, Sofie Pollin, and Dereje H. Woldegebreal. **A Multivariate Approach for Spatiotemporal Mobile Data Traffic Prediction**. *Engineering Proceedings* 18:1 (2022). ISSN: 2673-4591. DOI: 10.3390/engproc2022018010. URL: https://www.mdpi.com/2673-4591/18/1/10.

[92] Bethelhem S. Shawel, Dereje H. Woldegebreal, and Sofie Pollin. **A Deep Learning Approach to a Volumetric Radio Environment Map Construction for UAV-Assisted Networks**. *International Journal of Antennas and Propagation* 2024:9062023 (2024), 16. DOI: 10.1155/2024/9062023.

[93] George Y. Lu and David W. Wong. **An adaptive inverse-distance weighting spatial interpolation technique**. *Computers and Geosciences* 34:9 (2008), 1044–1055. ISSN: 0098-3004. DOI: https://doi.org/10.1016/j.cageo.2007.07.010. URL: https://www.sciencedirect.com/science/article/pii/S0098300408000721.

[94] Dami Choi, Christopher J. Shallue, Zachary Nado, Jaehoon Lee, Chris J. Maddison, and George E. Dahl. **On Empirical Comparisons of Optimizers for Deep Learning**. *ArXiv* abs/1910.05446 (2019). URL: https://api.semanticscholar.org/CorpusID:204509533.

[95] Ericsson. *Ericsson Mobility Report (June. 2023)*. URL: https://www.ericsson.com/49dd9d/assets/local/reports-papers/mobility-report/documents/2023/ericsson-mobility-report-june-2023.pdf. (Accessed: Aug. 10, 2023).

[96] Diala Naboulsi, Marco Fiore, Stephane Ribot, and Razvan Stanica. **Large-Scale Mobile Traffic Analysis: A Survey**. *IEEE Communications Surveys and Tutorials* 18:1 (2016), 124–161. DOI: 10.1109/COMST.2015.2491361.

[97] S. K. Joshi, K. B. S. Manosha, M. Codreanu, and M. Latva-aho. **Inter-operator dynamic spectrum sharing: A stochastic optimization approach**. In: *2017 13th Annual Conference on Wireless On-demand Network Systems and Services (WONS)*. Jackson, WY, USA, 2017, 124–127. DOI: 10.1109/WONS.2017.7888759.

[98] Eduard A. Jorswieck, Leonardo Badia, Torsten Fahldieck, Eleftherios Karipidis, and Jian Luo. **Spectrum sharing improves the network efficiency for cellular operators**. *IEEE Communications Magazine* 52:3 (2014), 129–136. DOI: 10.1109/MCOM.2014.6766097.

[99] Chuanting Zhang, Haixia Zhang, Jingping Qiao, Dongfeng Yuan, and Minggao Zhang. **Deep Transfer Learning for Intelligent Cellular Traffic Prediction Based on Cross-Domain Big Data**. *IEEE Journal on Selected Areas in Communications* 37:6 (2019), 1389–1401. DOI: 10.1109/JSAC.2019.2904363.

[100] Ufuk Uyan, M. Tugberk Isyapar, and Mahiye Uluyagmur Ozturk. *5G Long-Term and Large-Scale Mobile Traffic Forecasting*. 2022. arXiv: 2212.10869 [cs.LG].

[101] Bethelhem S. Shawel, Tsegamlak T. Debella, Getinet Tesfaye, Yonas Y. Tefera, and Dereje H. Woldegebreal. **Hybrid Prediction Model for Mobile Data Traffic: A Cluster-level Approach**. In: *2020 International Joint Conference on Neural Networks (IJCNN)*. 2020, 1–8. DOI: 10.1109/IJCNN48605.2020.9207655.

[102] Theodore S. Rappaport. **Wireless communications: Principles and practice**. Prentice Hall, 1996. ISBN: 0133755363.

[103] Stefania Sesia, Issam Toufik, and Matthew Baker. **LTE - The UMTS Long Term Evolution: From Theory to Practice, Second Edition**. John Wiley & Sons, Ltd, 2011. ISBN: 0470978503.

[104] Saeed Aghabozorgi, Ali Seyed Shirkhorshidi, and Teh Ying Wah. **Time-series clustering – A decade review**. *Information Systems* 53 (2015), 16–38. ISSN: 0306-4379. DOI: https://doi.org/10.1016/j.is.2015.04.007.

[105] Chunhui Yuan and Haitao Yang. **Research on K-Value Selection Method of K-Means Clustering Algorithm**. *J* 2:2 (2019), 226–235. ISSN: 2571-8800. DOI: 10.3390/j2020016.

[106] Peter J. Rousseeuw. **Silhouettes: A graphical aid to the interpretation and validation of cluster analysis**. *Journal of Computational and Applied Mathematics* 20 (1987), 53–65. ISSN: 0377-0427. DOI: 10.1016/0377-0427(87)90125-7. URL: https://www.sciencedirect.com/science/article/pii/0377042787901257.

[107] George Edward Pelham Box and Gwilym Jenkins. **Time Series Analysis, Forecasting and Control**. USA: Holden-Day, Inc., 1990. ISBN: 0816211043.

[108] X. You, CX. Wang, J. Huang, and et. al. **Towards 6G wireless communication networks: vision, enabling technologies, and new paradigm shifts**. *Science China Information Sciences* 64:110301 (2021), 1–22. DOI: 10.1007/s11432-020-2955-6.

[109] Dali Zhu Shunliang Zhang and Yongming Wang. **A survey on space-aerial-terrestrial integrated 5G networks**. *Computer Networks* 174 (2020), 107212. ISSN: 1389-1286. DOI: https://doi.org/10.1016/j.comnet.2020.107212.

[110] Xiaohui Li, Qi Zhu, Tianqi Yu, and Xianbin Wang. **Coordinated 3D spectrum utilization for B5G indoor HetNets: A collaborated crowdsensing approach**. *IET Communications* 16:2 (2022), 111–119. DOI: https://doi.org/10.1049/cmu2.12322.

[111] Zhiqing Wei, Rubing Yao, Jie Kang, Xu Chen, and Huici Wu. **Three-Dimensional Spectrum Occupancy Measurement Using UAV: Performance Analysis and Algorithm Design**. *IEEE Sensors Journal* 22:9 (2022), 9146–9157. DOI: 10.1109/JSEN.2022.3161311.

[112] Giovanni Geraci, David Lopez-Perez, Mohamed Benzaghta, and Symeon Chatzinotas. **Integrating Terrestrial and Non-Terrestrial Networks: 3D Opportunities and Challenges**. *IEEE Communications Magazine* 61 (2022), 42–48. DOI: 10.1109/MCOM.002.2200366.

[113] H. Martikainen, M. Majamaa, and J. Puttonen. **Coordinated Dynamic Spectrum Sharing Between Terrestrial and Non-Terrestrial Networks in 5G and Beyond**. In: *2023 IEEE 24th International Symposium on a World of Wireless, Mobile and Multimedia Networks (WoWMoM)*. Los Alamitos, CA, USA: IEEE Computer Society, June 2023, 419–424. DOI: 10.1109/WoWMoM57956.2023.00074.

[114] Sophia Antipolis. **3GPP Technical Report: Study on channel model for frequencies from 0.5 to 100 GHz**. *3GPP TR* 38.901 (2020).

[115] B. Mondal et al. **3D channel model in 3GPP**. *IEEE Communications Magazine* 53 (March 2015), 16–23. DOI: 10.1109/MCOM.2015.7060514..

[116] J. Lyu, Y. Zeng, R. Zhang, and T. J. Lim. **Placement Optimization of UAV-Mounted Mobile Base Stations**. *IEEE Communications Letters* 21:3 (2017), 604–607. DOI: 10.1109/LCOMM.2016.2633248.

[117] O. Esrafilian, R. Gangula, and D. Gesbert. **Learning to Communicate in UAV-Aided Wireless Networks: Map-Based Approaches**. *IEEE Internet of Things Journal* 6:2 (2019), 1791–1802. DOI: 10.1109/JIOT.2018.2879682.

[118] H. Yang, J. Zhang, S. H. Song, and K. B. Lataief. **Connectivity-Aware UAV Path Planning with Aerial Coverage Maps**. In: *IEEE Wireless Communications and Networking Conference (WCNC)*. Marrakesh, Morocco, 2019, 1–6. DOI: 10.1109/WCNC.2019.8886129.

[119] S. Zhang and R. Zhang. **Radio Map Based Path Planning for Cellular-Connected UAV**. In: *IEEE Global Communications Conference (GLOBECOM)*. Ed. by IEEE. 2019, 1–6. DOI: 10.1109/GLOBECOM38437.2019.9013177.

[120] Bin Li, Zesong Fei, and Yan Zhang. **UAV Communications for 5G and Beyond: Recent Advances and Future Trends**. *IEEE Internet of Things Journal* 6:2 (2019), 2241–2263. DOI: 10.1109/JIOT.2018.2887086.

[121] Francesco Alessio Dicandia, Nelson J. G. Fonseca, Manlio Bacco, Sara Mugnaini, and Simone Genovesi. **Space-Air-Ground Integrated 6G Wireless Communication Networks: A Review of Antenna Technologies and Application Scenarios**. *Sensors* 22:9 (2022). ISSN: 1424-8220. DOI: 10.3390/s22093136. URL: https://www.mdpi.com/1424-8220/22/9/3136.

[122] W. Khawaja, I. Guvenc, D. W. Matolak, U. C. Fiebig, and N. Schneckenburger. **A Survey of Air-to-Ground Propagation Channel Modeling for Unmanned Aerial Vehicles**. *IEEE Communications Surveys and Tutorials* 21:3 (2019), 2361–2391. DOI: 10.1109/COMST.2019.2915069.

[123] A. AlHourani, S. Kandeepan, and A. Jamalipour. **Modeling air-to-ground path loss for low altitude platforms in urban environments**. In: *IEEE Global Communications Conference*. Ed. by IEEE. Austin, TX, USA, 2014, 2898–2904. DOI: 10.1109/GLOCOM.2014.7037248.

[124] G. Wolfle and F.M. Landstorfer. **Dominant paths for the field strength prediction**. In: *VTC '98. 48th IEEE Vehicular Technology Conference. Pathway to Global Wireless Revolution (Cat. No.98CH36151)*. Vol. 1. 1998, 552–556 vol.1. DOI: 10.1109/VETEC.1998.686635.

[125] Rene Wahl and Gerd Wolfle. **Combined urban and indoor network planning using the dominant path propagation model**. In: *2006 First European Conference on Antennas and Propagation*. 2006, 1–6. DOI: 10.1109/EUCAP.2006.4584790.

[126] G. Wolfle and F. M. Landstorfer. **Field strength prediction in indoor environments with neural networks**. In: *IEEE 47th Vehicular Technology Conference. Technology in Motion*. Ed. by IEEE. Phoenix, AZ, USA, 1997.

[127] W. Khawaja, I. Guvenc, and D. Matolak. **UWB Channel Sounding and Modeling for UAV Air-to-Ground Propagation Channels**. In: *IEEE Global Communications Conference (GLOBECOM)*. Ed. by IEEE. Washington, DC, USA, 2016, 1–7. DOI: 10.1109/GLOCOM.2016.7842372.

[128] Z. Cui, K. Guan, C. Briso-Rodríguez, B. Ai, Z. Zhong, and C. Oestges. *Channel Modeling for UAV Communications: State of the Art, Case Studies, and Future Directions*. 2021. DOI: 10.48550/arXiv.2012.06707.

[129] Phillip Isola, Jun-Yan Zhu, Tinghui Zhou, and Alexei A. Efros. **Image-to-Image Translation with Conditional Adversarial Networks**. In: *2017 IEEE Conference on Computer Vision and Pattern Recognition (CVPR)*. 2017, 5967–5976. DOI: 10.1109/CVPR.2017.632.

[130] Yingxue Pang, Jianxin Lin, Tao Qin, and Zhibo Chen. **Image-to-Image Translation: Methods and Applications**. *IEEE Transactions on Multimedia* 24 (2022), 3859–3881. DOI: 10.1109/TMM.2021.3109419.

[131] Chao Wang, Haiyong Zheng, Zhibin Yu, Ziqiang Zheng, Zhaorui Gu, and Bing Zheng. **Discriminative Region Proposal Adversarial Networks for High-Quality Image-to-Image Translation**. *Computer Vision* 8 (2018), 796–812. DOI: 10.1007/978-3-030-01246-5_47.

[132] Kyeorye Lee, Leonard Sunwoo, Tackeun Kim, and Kyong Joon Lee. **Spider U-Net: Incorporating Inter-Slice Connectivity Using LSTM for 3D Blood Vessel Segmentation**. *Applied Sciences* 11:5 (2021). DOI: 10.3390/app11052014.

[133] Ron Levie, Cagkan Yapar, Gitta Kutyniok, and Giuseppe Caire. **RadioUNet: Fast Radio Map Estimation With Convolutional Neural Networks**. *IEEE Transactions on Wireless Communications* 20:6 (2021), 4001–4015. DOI: 10.1109/TWC.2021.3054977.

[134] Ian J. Goodfellow, Jean Pouget-Abadie, Mehdi Mirza, Bing Xu, David Warde-Farley, Sherjil Ozair, Aaron Courville, and Yoshua Bengio. *Generative Adversarial Networks*. 2014. arXiv: 1406.2661 [stat.ML]. URL: https://arxiv.org/abs/1406.2661.

[135] Zhou Wang, A.C. Bovik, H.R. Sheikh, and E.P. Simoncelli. **Image quality assessment: from error visibility to structural similarity**. *IEEE Transactions on Image Processing* 13:4 (2004), 600–612. DOI: 10.1109/TIP.2003.819861.

[136] Yu Tian, Shuai Yuan, Weisheng Chen, and Naijin Liu. **Transformer based Radio Map Prediction Model for Dense Urban Environments**. In: *2021 13th International Symposium on Antennas, Propagation and EM Theory (ISAPE)*. Vol. Volume1. 2021, 1–3. DOI: 10.1109/ISAPE54070.2021.9753644.

[137] Yaxuan Xing, Hu An, and Yinghui Zhang. **Federated Learning-Based Space-Time Data Prediction on Edge Devices**. In: *2022 7th International Conference on Intelligent Computing and Signal Processing (ICSP)*. 2022, 737–741. DOI: 10.1109/ICSP54964.2022.9778747.

[138] Lukasz Kulacz and Adrian Kliks. **Federated Learning-Based Spectrum Occupancy Detection**. *Sensors* 23:14 (2023). ISSN: 1424-8220. DOI: 10.3390/s23146436. URL: https://www.mdpi.com/1424-8220/23/14/6436.

[139] Bouziane Brik, Adlen Ksentini, and Maha Bouaziz. **Federated Learning for UAVs-Enabled Wireless Networks: Use Cases, Challenges, and Open Problems**. *IEEE Access* 8 (2020), 53841–53849. DOI: 10.1109/ACCESS.2020.2981430.

[140] V. Mahalakshmi and B. Karthikeyan. **Edge Computing in Context Awareness: A Comprehensive Study**. *Engineering Proceedings* 62:1 (2024). ISSN: 2673-4591. DOI: 10.3390/engproc2024062017. URL: https://www.mdpi.com/2673-4591/62/1/17.

[141] Sizhuang Liu, Fang Yang, Changyong Pan, Chao Zhang, and Jian Song. **Federated Deep Reinforcement Learning-Based Spectrum Sharing and Power Allocation for Mobile Communication System**. *2023 International Conference on Electrical Engineering and Photonics (EExPolytech)* (2023), 155–158. URL: https://api.semanticscholar.org/CorpusID:265354529.

[142] L. Wang, J. Hu, R. Jiang, and Z. Chen. **A Deep Long-Term Joint Temporal-Spectral Network for Spectrum Prediction**. *Sensors (Basel)* 24:5 (2024). DOI: 10.3390/s24051498.